The Dissertation Committee for Avinash Kaur Gadok Certifies that this is the approved version of the following dissertation:

Overcoming the plasma membrane barrier to improve the efficiency of therapeutic delivery to the cellular cytoplasm

Committee:

Jeanne C. Stachowiak, Supervisor

Theresa O'Halloran

Hugh D. C. Smyth

Hsin-Chih (Tim) Yeh

Janet Zoldan

Overcoming the plasma membrane barrier to improve the efficiency of therapeutic delivery to the cellular cytoplasm

by

Avinash Kaur Gadok, BSEBE; MSE

Dissertation

Presented to the Faculty of the Graduate School of

The University of Texas at Austin

in Partial Fulfillment

of the Requirements

for the Degree of

Doctor of Philosophy

The University of Texas at Austin

May 2017

Acknowledgements

I am very grateful to my advisor, Dr. Jeanne Stachowiak, for giving me the opportunity to join her lab from its very beginning, and for giving me the chance to complete such an innovative and exciting project. I would like to thank her for tirelessly sharing her technical expertise, for patiently helping me to develop my public speaking and writing skills, and for serving as a never-ending source of encouragement and enthusiasm during times of disappointment. Most importantly, I thank her for teaching me how to think critically, solve problems, and never give up. These are invaluable lessons that I will carry with me for the rest of my life, no matter my career path.

I would also like to recognize the rest of my laboratory for their continued support and friendship over the last five years. In particular, I would like to especially thank our previous post-doctoral fellow, Dr. David Busch, for serving as an excellent mentor and source of inspiration to me throughout my graduate career. I am also very grateful to the senior scientist of the lab, Dr. Carl Hayden, for allowing me to conduct research with him in his laboratory at Sandia National Laboratories and for teaching me the art of optical design. I would also like to thank my partners in crime in the lab: Wilton Snead, for endlessly indulging in bizarre conversations with me; Chi Zhao, for reminding me that life is good; and Andre DeGroot, for eating lunch with me. I would also like to acknowledge the other past and present members of the laboratory, including Christine Scheve, Dr. Wade Zeno, Zachary Imam, Ryan Woodall, and Samuel Mihelic, who have all been tremendous sources of support over the years, and who have made our lab a safe and enjoyable workplace for me.

Further, I would also like to thank my undergraduate mentees, Katie Ha, Tu Cao, Brian Li, Tanner Rowley, and Amanda Meriwether, whose hard work and dedication

have been instrumental to the success of my project. I would also like to recognize my collaborators, Dr. Hugh Smyth, Dr. Silvia Ferrati, and Dr. Eileen Lafer, as well as the rest of my committee members, Dr. Theresa O'Halloran, Dr. Tim Yeh, and Dr. Janet Zoldan, for their support and guidance on my work.

I would also like to thank my friends outside of the lab, including Supreet Singh, Emily O'Toole, Dr. Maggie Rodgers, Dr. Rachel Buchanan, Salma Ayoub, and Daniela Santiesteban for their continued support, inspiration, and laughter over the years. Finally, I would like to thank my family, for encouraging the scientist within me from a very early age, for supporting me throughout the journey of graduate school, and for always believing in me.

Overcoming the plasma membrane barrier to improve the efficiency of therapeutic delivery to the cellular cytoplasm

Avinash Kaur Gadok, Ph.D.

The University of Texas at Austin, 2017

Supervisor: Jeanne C. Stachowiak

Difficulties in controlling endocytosis limit the success of many nanoparticle-based drug delivery strategies. Therefore, there is a need to both (i) introduce new mechanisms of therapeutic delivery that overcome the limitations of endocytic uptake, and (ii) gain better control of endocytosis by understanding its underlying mechanisms at a molecular level. Towards achieving efficient therapeutic delivery independently of endocytosis, I first report the development of targeted Connectosomes, cell-derived lipid vesicle materials that contain embedded connexons and are capable of forming functional gap junctions with cells. These materials encapsulated diverse molecular cargo, including dyes and drugs. These materials achieved efficient delivery of molecular cargo directly into the cytoplasm of specific populations of target cells, through interactions of embedded multi-functional, multi-domain transmembrane targeting proteins that target cell-specific receptors. By opening direct routes to the cytoplasm, targeted Connectosomes reduced the therapeutically effective dose (LD50) of doxorubicin for target cells by more than an order of magnitude in comparison to the unencapsulated drug, and by several orders of magnitude in comparison to conventional liposomal doxorubicin. These data illustrate the therapeutic importance of direct access to the cell

cytoplasm, and highlight the potential of gap junction-mediated cytoplasmic delivery to increase the effectiveness of diverse therapeutics. Towards furthering our basic biophysical understanding of the mechanisms that drive clathrin-mediated endocytosis, I then investigated the curvature sensing abilities of clathrin, a critical question limiting our understanding of how nanoparticles and other molecular cargo are internalized. In particular, my findings demonstrate that clathrin binds preferentially to highly curved membranes, suggesting a possible new explanation for clathrin's early participation in endocytic vesicle formation. In sum, this work represents key steps towards improving the success of nanoparticle-based drug delivery strategies from both applied and fundamental standpoints.

Table of Contents

List of Figures

Figure 2.4: **Connectosomes substantially reduced the cytotoxic dose of doxorubicin.** (a-c), Plasma membrane blebs were extracted from donor cells treated with doxorubicin to produce doxorubicin-loaded Connectosomes. (d), Schematic illustrating doxorubicin release from Connectosomes. (e), Average Connectosome fluorescence calculated from flow cytometry data. Connectosomes released significant amounts of doxorubicin within 5 minutes of calcium removal. The error bars represent the standard deviations of 3 independent trials, at least 800 Connectosomes analyzed per trial. (f),Schematic illustrating the 3 modes of drug delivery tested. (g), Percentage of nonviable HeLa cells after free doxorubicin treatment (blue), conventional liposomal doxorubicin treatment (purple), or doxorubicin-loaded Connectosome treatment (green). All points were measured using a 7-AAD viability assay, except for the free doxorubicin 10^5 nM point, which was measured using a trypan blue viability assay, owing to interference of doxorubicin in the 7-AAD measurement at this high doxorubicin concentration. The error bars represent the standard deviations of at least 3 independent trials, at least 4,000 cells (7-AAD assay) or 93 cells (trypan blue) analyzed per trial. (h), Flow cytometry histograms showing 7-AAD fluorescence for cells receiving doxorubicin-loaded Connectosomes at increasing equivalent free doxorubicin (dox) concentrations. The dotted line represents the threshold fluorescence value above which cells were considered nonviable. Each curve represents 3 independent, concatenated trials, at least 4,000 cells analyzed per trial. (i), Percentage of nonviable cells determined using both trypan blue (blue) and 7-AAD

Chapter 1: Introduction

How can therapeutics cross the plasma membrane barrier?

To reach intracellular targets in the cytoplasm, therapeutics must be membrane permeable. Specifically, therapeutics must maintain solubility as they journey from the aqueous extracellular space, through the hydrophobic membrane environment, to their final destination in the aqueous cytoplasm[1].

Unfortunately, these stringent restrictions limit the design of therapeutics, as only select, highly membrane permeable molecules are able to cross the plasma membrane. Despite high membrane permeability, transport of these compounds into the cytoplasm is limited, even for the most widely used drugs[2]. For example, in order for one highly membrane permeable chemotherapeutic drug, doxorubicin[3], to reach the cytoplasm, it must first associate with the outer leaflet of the plasma membrane, and then wait for a distinct trans-lipid bilayer flip-flop event to occur in order to reach the inner leaflet of the plasma membrane, before it can finally diffuse into the cytoplasm to reach its target[4]. In fact, *in vitro* studies have demonstrated that it takes on the order of several hours for doxorubicin to reach cytotoxic concentrations in the cytoplasm[2]. Further, increased membrane permeability also enhances association of therapeutics with multidrug efflux pumps. Therefore, the most highly membrane permeable drugs exhibit increased vulnerability to export by these pumps, limiting their accumulation inside the cell despite their ability to cross the plasma membrane barrier[5]. These hindrances necessitate large doses in order to achieve therapeutic efficacy, which in turn promote systemic toxicity toward healthy, off-target tissues[6].

The need for membrane permeability poses an even more substantially limit on the efficacy of highly hydrophilic drugs, which typically experience low rates of membrane transport. For example, nucleoside analogs such as gemcitabine and

cytarabine effectively inhibit DNA synthesis and are therefore promising cytotoxic agents. However, their therapeutic efficacy has been limited by insufficient cytoplasmic accumulation[7]. Similarly, the chemotherapeutic drug cisplatin also faces membrane solubility obstacles[8]. Therefore, the efficacy of each of these drugs could be improved by an efficient cytoplasmic delivery method.

Owing to these membrane permeability restrictions, a disproportionate number of existing drugs exploit cell-surface proteins, which are accessible from outside the cell, such as ion channels and G-protein coupled receptors[9]. In contrast, numerous intracellular targets remain undruggable[10]. Therefore, development of a strategy that bypasses the plasma membrane barrier could both enhance delivery of existing, membrane permeable drugs that are limited by inefficient cytoplasmic transport rates and export by multidrug efflux pumps, while also providing a new avenue for cytoplasmic delivery of entirely new types of therapeutic compounds, including membrane impermeable molecules.

Nanoparticles enable drugs to cross the plasma membrane barrier

In order to cross the plasma membrane barrier, therapeutics can be encapsulated within nanoparticles[11, 12]. For example, diverse membrane impermeable reagents can be encapsulated within the aqueous core of nanoparticle materials. Cells then internalize the nanoparticles via endocytosis[13], and in a way, intracellular delivery of the nanoparticles is achieved. However, the internalized nanoparticles largely remain trapped in endosomes, which are membrane-bound compartments responsible for molecular sorting of internalized cargo[14]. Unable to escape from endosomes, nanoparticles face eventual degradation or export[15]. Therefore, delivery of the therapeutic into the cytoplasm is

limited, and the drug concentration required for therapeutic efficacy actually increases[16, 17].

One of the first nanoparticles to be developed, doxorubicin loaded liposomes, best illustrates this dilemma. While these nanoparticles significantly reduced the systemic toxicity of doxorubicin[3], *in vitro* studies found that encapsulating this drug into liposomes actually increased the therapeutically effective dose, or the median lethal dose (LD50), by an order of magnitude, likely due to the inability of the drug to reach the cytoplasm[17]. More recent studies have also confirmed the inefficiencies of endocytosis for achieving cytoplasmic release. For example, less than 2% of lipid-based nanoparticles used for siRNA delivery escaped from the endosome within 6 hours[18], and more than 80% of mesoporous silica nanoparticles used for fluorescent dye delivery were exocytosed from cells after 6 hours[15]. Therefore, in sum, difficulties in controlling the endocytic process restrict the reliability of delivery strategies that rely upon this process for internalization[19].

Towards achieving cytoplasmic therapeutic delivery, diverse membrane-disrupting agents have been developed in order to facilitate the escape of nanoparticles from endosomes[20]. These compounds include pH-sensitive polymers, and fusiogenic peptides and lipids[20]. In theory, these compounds rely upon the acidic environment of the endosome for activation, triggering the nanoparticle's escape from the endosome and thereby facilitating cytoplasmic release[21]. For example, pH-sensitive polymers like poly(propyl acrylic acid) were used to efficiently disrupt eukaryotic membranes within narrowly defined pH ranges, suggesting promise as endosomal escape facilitators[22]. Further, the fusiogenic domain of hemagglutinin (HA), a virus fusion protein, and transactivator of transcription (TAT), the HIV fusion peptide, were used in combination to enhance *in vitro* intracellular protein delivery, providing proof-of-concept evidence of

the therapeutic potential of fusion peptides as endosomal escape agents[23]. Further, the fusiogenic lipid DOTAP was incorporated into synthetic liposomes also containing TAT to enhance delivery of DNA in A549 cells[24]. Finally, in some cases, incorporation similar of stimuli-responsive triggered-release compounds into nanoparticles[21, 25] has reduced the therapeutically effective dose of particle-encapsulated doxorubicin to concentrations equivalent to the free drug[21, 22, 25, 26].

However, cytosolic release from the endosome remains limited despite these developments[20, 27]. In particular, many of these endosomal escape strategies do not facilitate sufficient drug release, or fail when extended to other applications[20]. For example, in the above example where HA and TAT were used for intracellular protein delivery, more than 99% of the proteins remained trapped in endocytic vesicles, despite inclusion of the fusion peptides[20, 23] Additionally, the DOTAP liposomes discussed above failed to enhance delivery of DNA in other cell types[20, 24]. In light of these persistent limitations, a new delivery route that bypasses endocytic pathways entirely has the potential to dramatically improve therapeutic efficacy for both membrane permeable and impermeable drugs.

Gap junctions provide direct access to the cytoplasm

Cells naturally circumvent the plasma membrane barrier by relying upon gap junctions to deliver small molecules to each other. Gap junctions are formed from a family of 21 different connexin proteins, which range in molecular weight from 25 to 60 kDa[28]. Connexin proteins hexamerize into either homomeric or heteromeric connexon hemichannels, depending on the types of connexins involved[29]. Estimates for the connexon pore diameter based on atomic force microscopy and electron diffraction range

from 15 – 45 Å, while calculations based on the size of molecules known to be gap junction permeable approximate the pore diameter to be between 8 – 16 Å[30].

To form a complete gap junction, connexons present on the plasma membrane pair with connexons present on neighboring cell membranes, establishing a direct path that connects the cytoplasm of the cells. Cells use gap junctions to exchange diverse molecular cargo up to 1 kDa in size, including metabolites, second messengers, and peptides[31]. Gap junctions are expressed by nearly every cell type in the body, and the exchange of these molecules is critical for diverse cellular processes, including the maintenance of homeostasis, cell growth and differentiation, and coordination of electrical signaling that occurs in neurons, cardiac cells, and smooth muscle cells[28, 29, 32].

Gap junctions are emerging as a promising new therapeutic frontier

Although gap junctions are traditionally considered to be facilitators for exchange of signaling molecules between cells, they are emerging as a promising new frontier for therapeutic drug delivery. For example, in addition to their ability to transfer natural signaling molecules between cells, gap junctions also facilitate transfer of drugs, through a phenomenon known as the bystander effect. Through this effect, therapeutics which reach the cytoplasm of one cell are able to access the cytoplasm of neighboring cells through the gap junctions that connect the cells. Exchange of drugs through this phenomenon enhances the efficacy of numerous therapeutics, including paclitaxel, doxorubicin[33], gemcitabine[34], etoposide[33], and others[35], demonstrating the potential importance of gap junctions as therapeutic conveyers. Further, it has recently been demonstrated that the presence of gap junction channels in exosomes underlies their ability to deliver siRNA, further suggesting the therapeutic potential of gap junctions[36].

Taken together, these recent findings suggest that a therapeutic delivery approach that depends on gap junctions could provide an efficient new mode of drug transport. In particular, lipid vesicles that contain embedded gap junction hemichannels could come together with cellular hemichannles to form full gap junction channels with cells, opening a direct route to the cytoplasm that is independent of endocytosis. In this way, gap junction vesicles could both enhance delivery of existing, membrane soluble drugs, while also providing a new route for cytoplasmic delivery of hydrophilic molecules.

Plasma membrane blebbing enables production of gap junction vesicles

Despite the emerging evidence for gap junctions to act as therapeutic conveyers, gap junction vesicles have not been previously used for therapeutic delivery purposes. Although basic biological studies have demonstrated the formation of functional gap junctions between cells and synthetic vesicles containing reconstituted connexins[37], therapeutic application of these vesicles has been limited, due perhaps to challenges in purifying connexin proteins, and in inserting the connexin proteins into membranes in functional orientations.

However, plasma membrane blebs, also known as plasma membrane vesicles, are cell-derived materials that offer the potential to overcome these limitations. These vesicles are produced when the cytoskeleton's attachment to the plasma membrane is disrupted, and are produced naturally during certain cellular processes such as cell motility or cytokinesis[38], as well as a result of chemical induction[39].

In particular, biophysical studies on plasma membrane vesicles have shown that transmembrane proteins maintain their function and orientation when they are embedded in these vesicles[40]. Further, plasma membrane vesicles have recently emerged as potentially attractive therapeutic materials[41]. Exosomes, cell-derived vesicles that are

released from cells when multivesicular bodies fuse to the plasma membrane[42], are another type of cell-derived material with emerging therapeutic potential[43].

However, plasma membrane vesicles were used for these studies, due to several advantages arising from the differences in origin between these two types of vesicles. Primarily, since protein trafficking to the plasma membrane is well understood, expression of transmembrane proteins at the plasma membrane can be easily controlled. Therefore, incorporation of these transmembrane proteins into plasma membrane vesicles is relatively straightforward, since they are derived directly from the plasma membrane[39]. In contrast, exosomes are derived from cell's endosomal membrane system. Precise understanding of how proteins are sorted in endosomes in order to arrive in exosomes remains unclear[42], and because of this, controlled incorporation of specific proteins into exosomes remains a challenge.

Connectosomes for direct molecular delivery to the cellular cytoplasm

Inspired by the natural ability of gap junctions to directly access the cytoplasm, in Chapter One, I report the development of Connectosomes, cell-derived lipid vesicle materials that contain embedded connexons and are capable of forming complete gap junctions with cells[44]. Specifically, by harvesting plasma membrane blebs from donor cells that overexpressed connexin 43 proteins with a C-terminal YFP modification (Cx43-YFP), I produced cell-derived lipid vesicle materials with embedded connexin 43-YFP connexons, termed Connectosomes. These materials encapsulated diverse molecular cargo, including dye and drugs. By opening direct routes to the cytoplasm, Connectosomes achieved efficient delivery of molecular cargo to the cytoplasm in a gap junction-dependent manner. Further, I found that Connectosomes reduced the therapeutically effective dose (LD50) of doxorubicin by more than an order of magnitude

in comparison to the unencapsulated drug, and by several orders of magnitude in comparison to conventional liposomal doxorubicin. These data illustrate the therapeutic importance of direct access to the cell cytoplasm, and highlight the potential of gap junction-mediated cytoplasmic delivery to increase the effectiveness of diverse therapeutics.

Targeted delivery approaches increase the specificity of therapeutic delivery

While Connectosomes provide a promising new route for the delivery of therapeutics to the cytoplasm, the lack of specificity in this approach is a key roadblock limiting its therapeutic relevance. In particular, due to the ubiquitous[29] nature of connexin proteins, the translational potential of Connectosomes is restricted by the possibility of nonspecific drug interactions occurring between the vesicles and healthy, off-target tissues.

Towards achieving selective therapeutic delivery, targeting moieties have been incorporated into the surfaces of nanoparticles. By biochemically recognizing tumor-specific cell surface receptors, these targeting agents promote preferential interaction of the nanoparticles with target tumor cells. Diverse targeting ligands, including various antibodies, organic compounds, and peptides, have been employed to direct both synthetic and cell-derived nanoparticles to specific populations of target cells in this way[45-48].

Despite the increased specificity these approaches yield, their ability to direct nanoparticles to specific populations of target cells in more complex applications remains inherently limited due to their dependence on complex chemical conjugation processes that are often incompatible with the maintenance of transmembrane protein function. To work around these limitations, our group and others have developed alternative targeting

strategies, which employ the cell's own machinery to incorporate targeting ligands into cell-derived vesicles[49-54]. In particular, recent work from our group has harnessed the cell's ability to manufacture complex, sophisticated macromolecules, by engineering a set of multi-functional, multi-domain transmembrane targeting ligands, which selectively increase cell-derived vesicle binding to target cells[54].

Targeted Connectosomes achieve therapeutic delivery to specific cell populations

Towards achieving targeted, gap junction-mediated cytoplasmic therapeutic delivery, in Chapter Two, I report the development of targeted Connectosomes. Specifically, to enable delivery of therapeutic molecules directly into the cytoplasm of specific populations of target cells, I incorporated multi-functional, multi-domain transmembrane targeting proteins into the Connectosomes. In particular, by extracting plasma membrane blebs from engineered donor cells which co-express connexin 43-YFP and a targeting protein, we produced Connectosomes which also contained embedded copies of the targeting protein. I used a previously designed targeting protein that was comprised of five domains: the intracellular and transmembrane domains of transferrin receptor, an mRFP fluorophore domain, an intrinsically disordered linker domain comprised of the first 289 amino acids of AP180, and an affinity domain. Here, the affinity domain consisted of a single domain camelid GFP nanobody, which is a targeting ligand that specifically recognizes GFP, and can therefore be used to precisely target cells on the basis of their expression of GFP-tagged plasma membrane receptors. My results show that targeting selectively enhances Connectosome binding to target cells by more than an order of magnitude, compared to off-target cells. Targeted Connectosomes selectively deliver dye to the cytoplasm of target cells, three times as efficiently as to off-target cells. Further, using targeted Connectosomes to deliver doxorubicin reduces the

therapeutically effective dose (LD50) by a factor of 2 for target cells, compared to off-target cells. Illustrating the potential of targeted Connectosomes to serve as efficient vehicles for targeted molecular delivery of chemotherapeutics and other diverse drugs to the cell cytoplasm, this work represents a key step towards realizing the therapeutic potential of gap junction-mediated therapeutic delivery systems.

Clathrin-mediated endocytosis

While the majority of my thesis work has been focused on developing an alternate strategy that depends on gap junctions for therapeutic delivery rather than endocytosis, there is also value in approaching the problem of how to efficiently deliver drugs to the cytoplasm from a more fundamental standpoint. As mentioned above, difficulties in controlling endocytosis limit the success of many nanoparticle-based drug delivery strategies[19]. In order to effectively control and exploit endocytosis for optimal uptake of therapeutics, it is critical to first understand this process at a mechanistic level. Therefore, furthering our basic biophysical understanding of the mechanisms that drive clathrin-mediated endocytosis is important for guiding improved treatment of disease.

Membrane curvature sensing plays an important role in the nucleation of endocytic vesicles, which is the first step in endocytosis. In particular, by binding preferentially to curved regions of the plasma membrane, adaptor proteins involved in endocytic vesicle nucleation essentially determine where these vesicles will form, thereby controlling which cargo molecules are internalized by the cell. These adaptor proteins bind preferentially to regions of high membrane curvature in two ways: through (i) BAR domains, inherently curved domains which can scaffold curved membranes, and/or through (ii) amphipathic helices, which insert into lipid packing defects that are present on the surfaces of highly curved membranes[55-57].

Understanding which proteins sense curvature, and the length scale over which this sensitivity exists, is a critical for understanding the dynamics of endocytosis. For example, amphipathic helices and BAR domains enable proteins to sense curvature over nanometer-scale membrane regions, implying that this type of sensitivity is very important early in endocytosis[55-57]. However, if clathrin were to act as a curvature sensor, it could potentially sense curvature over tens-of-nanometer-scale membrane regions, which would imply that curvature sensing that occurs throughout the formation of endocytic vesicles.

Therefore, in Chapter Three, I investigate the curvature sensitivity of clathrin. Adaptor proteins, which bind to the membrane and to clathrin, are responsible for the biochemical recruitment of clathrin to endocytic structures. However, the physical cues that influence clathrin's recruitment remain debated. In particular, while both scaffolding adaptor proteins such as epsin, and endophilin, and amphiphysin bind preferentially to regions of high membrane curvature, it remains unknown whether clathrin triskelia themselves possess the ability to sense membrane curvature and bind preferentially to curved structures.

To address this question, I isolated clathrin's curvature sensing ability in the absence of adaptor proteins by using recombinant, histidine-tagged clathrin that is engineered to bind directly to Ni-NTA-containing membranes. To examine clathrin binding to these membranes, I used a quantitative fluorescence intensity-based approach in which vesicles were tethered to a passivated surface and incubated with clathrin triskelia at a specified concentration.

Using particle detection software and single-molecule calibrations to determine the brightness of each vesicle and the brightness of the protein colocalized to each vesicle, I quantified the curvature of each individual vesicle as well as the corresponding

number of bound clathrin triskelia. My results demonstrate that clathrin binds preferentially to membranes of higher curvature. Specifically, when incubated with the same concentration of clathrin triskelia, vesicles with an average diameter of 30 nm recruit ten times as many clathrin triskelia per membrane surface area in comparison to vesicles with an average diameter of 165 nm. Further, using the Boltzmann equation, we have determined how the binding energy released as clathrin triskelia bind to vesicles depends on vesicle curvature. Our ongoing work continues to map the distribution of bound triskelia over vesicles with a range of different curvatures and to improve the statistical model from which the curvature dependence of binding energy can be derived.

These findings provide fundamental insight into the process by which clathrin is recruited to highly curved membranes during clathrin-mediated endocytosis. In particular, it has previously been thought that only adaptor proteins sense curvature, while clathrin's role is simply to concentrate coated vesicle components and drive curvature[58]. However, our findings suggest that clathrin triskelia themselves are likely involved in sensing curvature. One possible role of clathrin as a curvature sensor could be to limit assembly of clathrin-coated vesicles only to groups of membrane-bound adaptor proteins located in regions of high membrane curvature.

More broadly, our data suggests that the highly sequential model of clathrin-coated vesicle assembly, in which adaptors arrive at membranes first and are then followed by clathrin, could be over simplified. Specifically, our findings suggest that recruiting a critical nucleus of clathrin triskelia could be an early event that depends on membrane curvature. This speculation is consistent with the recent finding by the Kirchhausen lab, which was based on studies in live cells and showed that recruitment of clathrin is one of the earliest events to occur in the formation of a clathrin-coated vesicle[59].

References

1. Lipinski, C. A.; Lombardo, F.; Dominy, B. W.; Feeney, P. J., Experimental and computational approaches to estimate solubility and permeability in drug discovery and development settings. Advanced Drug Delivery Reviews 1997, 23 (1-3), 3-25.
2. Durand, R. E.; Olive, P. L., FLOW-CYTOMETRY STUDIES OF INTRACELLULAR ADRIAMYCIN IN SINGLE CELLS-INVITRO. Cancer Research 1981, 41 (9), 3489-3494.
3. Barenholz, Y., Doxil (R) - The first FDA-approved nano-drug: Lessons learned. Journal of Controlled Release 2012, 160 (2), 117-134.
4. Eytan, G. D., Mechanism of multidrug resistance in relation to passive membrane permeation. Biomedicine & Pharmacotherapy 2005, 59 (3), 90-97.
5. Gottesman, M. M.; Fojo, T.; Bates, S. E., Multidrug resistance in cancer: Role of ATP-dependent transporters. Nature Reviews Cancer 2002, 2 (1), 48-58.
6. Ewer, M. S.; Ewer, S. M., Cardiotoxicity of anticancer treatments. Nature reviews. Cardiology 2015, 12 (9), 547-58.
7. Damaraju, V. L.; Damaraju, S.; Young, J. D.; Baldwin, S. A.; Mackey, J.; Sawyer, M. B.; Cass, C. E., Nucleoside anticancer drugs: the role of nucleoside transporters in resistance to cancer chemotherapy. Oncogene 2003, 22 (47), 7524-7536.
8. Barenholz, Y., Liposome application: problems and prospects. Current Opinion in Colloid & Interface Science 2001, 6 (1), 66-77.
9. Overington, J. P.; Al-Lazikani, B.; Hopkins, A. L., Opinion - How many drug targets are there? Nature Reviews Drug Discovery 2006, 5 (12), 993-996.

10. Mitragotri, S.; Burke, P. A.; Langer, R., Overcoming the challenges in administering biopharmaceuticals: formulation and delivery strategies. Nature Reviews Drug Discovery 2014, 13 (9), 655-672.

11. Phillips, M. A.; Gran, M. L.; Peppas, N. A., Targeted nanodelivery of drugs and diagnostics. Nano Today 2010, 5 (2), 143-159.

12. Peer, D.; Karp, J. M.; Hong, S.; FaroKhzad, O. C.; Margalit, R.; Langer, R., Nanocarriers as an emerging platform for cancer therapy. Nature Nanotechnology 2007, 2 (12), 751-760.

13. Sahay, G.; Alakhova, D. Y.; Kabanov, A. V., Endocytosis of nanomedicines. Journal of Controlled Release 2010, 145 (3), 182-195.

14. Thevenin, D.; An, M.; Engelman, D. M., pHLIP-Mediated Translocation of Membrane-Impermeable Molecules into Cells. Chemistry & Biology 2009, 16 (7), 754-762.

15. Yanes, R. E.; Tarn, D.; Hwang, A. A.; Ferris, D. P.; Sherman, S. P.; Thomas, C. R.; Lu, J.; Pyle, A. D.; Zink, J. I.; Tamanoi, F., Involvement of Lysosomal Exocytosis in the Excretion of Mesoporous Silica Nanoparticles and Enhancement of the Drug Delivery Effect by Exocytosis Inhibition. Small 2013, 9 (5), 697-704.

16. Bareford, L. A.; Swaan, P. W., Endocytic mechanisms for targeted drug delivery. Advanced Drug Delivery Reviews 2007, 59 (8), 748-758.

17. Horowitz, A. T.; Barenholz, Y.; Gabizon, A. A., INVITRO CYTOTOXICITY OF LIPOSOME-ENCAPSULATED DOXORUBICIN - DEPENDENCE ON LIPOSOME COMPOSITION AND DRUG RELEASE. Biochimica Et Biophysica Acta 1992, 1109 (2), 203-209.

18. Gilleron, J.; Querbes, W.; Zeigerer, A.; Borodovsky, A.; Marsico, G.; Schubert, U.; Manygoats, K.; Seifert, S.; Andree, C.; Stoter, M.; Epstein-Barash, H.; Zhang, L. G.; Koteliansky, V.; Fitzgerald, K.; Fava, E.; Bickle, M.; Kalaidzidis, Y.; Akinc, A.; Maier,

M.; Zerial, M., Image-based analysis of lipid nanoparticle-mediated siRNA delivery, intracellular trafficking and endosomal escape. Nature Biotechnology 2013, 31 (7), 638-U102.

19. Sakhtianchi, R.; Minchin, R. F.; Lee, K. B.; Alkilany, A. M.; Serpooshan, V.; Mahmoudi, M., Exocytosis of nanoparticles from cells: Role in cellular retention and toxicity. Advances in Colloid and Interface Science 2013, 201, 18-29.

20. El-Sayed, A.; Futaki, S.; Harashima, H., Delivery of Macromolecules Using Arginine-Rich Cell-Penetrating Peptides: Ways to Overcome Endosomal Entrapment. Aaps Journal 2009, 11 (1), 13-22.

21. Mura, S.; Nicolas, J.; Couvreur, P., Stimuli-responsive nanocarriers for drug delivery. Nature Materials 2013, 12 (11), 991-1003.

22. Murthy, N.; Robichaud, J. R.; Tirrell, D. A.; Stayton, P. S.; Hoffman, A. S., The design and synthesis of polymers for eukaryotic membrane disruption. Journal of Controlled Release 1999, 61 (1-2), 137-143.

23. Wadia, J. S.; Stan, R. V.; Dowdy, S. F., Transducible TAT-HA fusogenic peptide enhances escape of TAT-fusion proteins after lipid raft macropinocytosis. Nature Medicine 2004, 10 (3), 310-315.

24. Hyndman, L.; Lemoine, J. L.; Huang, L.; Porteous, D. J.; Boyd, A. C.; Nan, X. S., HIV-1 Tat protein transduction domain peptide facilitates gene transfer in combination with cationic liposomes. Journal of Controlled Release 2004, 99 (3), 435-444.

25. Ganta, S.; Devalapally, H.; Shahiwala, A.; Amiji, M., A review of stimuli-responsive nanocarriers for drug and gene delivery. Journal of Controlled Release 2008, 126 (3), 187-204.

26. Caldorera-Moore, M.; Guimard, N.; Shi, L.; Roy, K., Designer nanoparticles: incorporating size, shape and triggered release into nanoscale drug carriers. Expert Opinion on Drug Delivery 2010, 7 (4), 479-495.

27. Erazo-Oliveras, A.; Muthukrishnan, N.; Baker, R.; Wang, T.-Y.; Pellois, J.-P., Improving the endosomal escape of cell-penetrating peptides and their cargos: strategies and challenges. Pharmaceuticals (Basel, Switzerland) 2012, 5 (11), 1177-209.

28. Harris, A. L., Emerging issues of connexin channels: biophysics fills the gap. Quarterly Reviews of Biophysics 2001, 34 (3), 325-472.

29. Goodenough, D. A.; Paul, D. L., Gap Junctions. Cold Spring Harbor Perspectives in Biology 2009, 1 (1), 19.

30. Weber, P. A.; Chang, H. C.; Spaeth, K. E.; Nitsche, J. M.; Nicholson, B. J., The permeability of gap junction channels to probes of different size is dependent on connexin composition and permeant-pore affinities. Biophysical Journal 2004, 87 (2), 958-973.

31. Neijssen, J.; Herberts, C.; Drijfhout, J. W.; Reits, E.; Janssen, L.; Neefjes, J., Cross-presentation by intercellular peptide transfer through gap junctions. Nature 2005, 434 (7029), 83-88.

32. Mese, G.; Richard, G.; White, T. W., Gap junctions: Basic structure and function. Journal of Investigative Dermatology 2007, 127 (11), 2516-2524.

33. Huang, R. P.; Hossain, M. Z.; Huang, R.; Gano, J.; Fan, Y.; Boynton, A. L., Connexin 43 (cx43) enhances chemotherapy-induced apoptosis in human glioblastoma cells. International Journal of Cancer 2001, 92 (1), 130-138.

34. Garcia-Rodriguez, L.; Perez-Torras, S.; Carrio, M.; Cascante, A.; Garcia-Ribas, I.; Mazo, A.; Fillat, C., Connexin-26 Is a Key Factor Mediating Gemcitabine Bystander Effect. Molecular Cancer Therapeutics 2011, 10 (3), 505-517.

35. Mesnil, M.; Piccoli, C.; Tiraby, G.; Willecke, K.; Yamasaki, H., Bystander killing of cancer cells by herpes simplex virus thymidine kinase gene is mediated by connexins. Proceedings of the National Academy of Sciences of the United States of America 1996, 93 (5), 1831-1835.

36. Soares, A. R.; Martins-Marques, T.; Ribeiro-Rodrigues, T.; Ferreira, J. V.; Catarino, S.; Pinho, M. J.; Zuzarte, M.; Anjo, S. I.; Manadas, B.; Sluijter, J. P. G.; Pereira, P.; Girao, H., Gap junctional protein Cx43 is involved in the communication between extracellular vesicles and mammalian cells. Scientific Reports 2015, 5, 13.

37. Kaneda, M.; Nomura, S. M.; Ichinose, S.; Kondo, S.; Nakahama, K.; Akiyoshi, K.; Morita, I., Direct formation of proteo-liposomes by in vitro synthesis and cellular cytosolic delivery with connexin-expressing liposomes. Biomaterials 2009, 30 (23-24), 3971-3977.

38. Charras, G.; Paluch, E., Blebs lead the way: how to migrate without lamellipodia. Nature Reviews Molecular Cell Biology 2008, 9 (9), 730-736.

39. Sezgin, E.; Kaiser, H. J.; Baumgart, T.; Schwille, P.; Simons, K.; Levental, I., Elucidating membrane structure and protein behavior using giant plasma membrane vesicles. Nature Protocols 2012, 7 (6), 1042-1051.

40. Chen, L. R.; Novicky, L.; Merzlyakov, M.; Hristov, T.; Hristova, K., Measuring the Energetics of Membrane Protein Dimerization in Mammalian Membranes. Journal of the American Chemical Society 2010, 132 (10), 3628-3635.

41. Costello, D. A.; Hsia, C. Y.; Millet, J. K.; Porri, T.; Daniel, S., Membrane Fusion-Competent Virus-Like Proteoliposomes and Proteinaceous Supported Bilayers Made Directly from Cell Plasma Membranes. Langmuir 2013, 29 (21), 6409-6419.

42. Simons, M.; Raposo, G., Exosomes - vesicular carriers for intercellular communication. Current Opinion in Cell Biology 2009, 21 (4), 575-581.

43. El Andaloussi, S.; Maeger, I.; Breakefield, X. O.; Wood, M. J. A., Extracellular vesicles: biology and emerging therapeutic opportunities. Nature Reviews Drug Discovery 2013, 12 (5), 348-358.

44. Gadok, A. K.; Busch, D. J.; Ferrati, S.; Li, B.; Smyth, H. D. C.; Stachowiak, J. C., Connectosomes for Direct Molecular Delivery to the Cellular Cytoplasm. Journal of the American Chemical Society 2016, 138 (39), 12833-12840.

45. Allen, T. M., Ligand-targeted therapeutics in anticancer therapy. Nature Reviews Cancer 2002, 2 (10), 750-763.

46. Ren, Y.; Wong, S. M.; Lim, L. Y., Folic acid-conjugated protein cages of a plant virus: A novel delivery platform for doxorubicin. Bioconjugate Chemistry 2007, 18 (3), 836-843.

47. Mukthavaram, R.; Shi, G. X.; Kesari, S.; Simberg, D., Targeting and depletion of circulating leukocytes and cancer cells by lipophilic antibody-modified erythrocytes. Journal of Controlled Release 2014, 183, 146-153.

48. Zhang, W.; Yu, Z. L.; Wu, M.; Ren, J. G.; Xia, H. F.; Sa, G. L.; Zhu, J. Y.; Pang, D. W.; Zhao, Y. F.; Chen, G., Magnetic and Folate Functionalization Enables Rapid Isolation and Enhanced Tumor-Targeting of Cell-Derived Microvesicles. Acs Nano 2017, 11 (1), 277-290.

49. Johnsen, K. B.; Gudbergsson, J. M.; Skov, M. N.; Pilgaard, L.; Moos, T.; Duroux, M., A comprehensive overview of exosomes as drug delivery vehicles - Endogenous nanocarriers for targeted cancer therapy. Biochimica Et Biophysica Acta-Reviews on Cancer 2014, 1846 (1), 75-87.

50. Alvarez-Erviti, L.; Seow, Y. Q.; Yin, H. F.; Betts, C.; Lakhal, S.; Wood, M. J. A., Delivery of siRNA to the mouse brain by systemic injection of targeted exosomes. Nature Biotechnology 2011, 29 (4), 341-U179.

51. Ohno, S.; Takanashi, M.; Sudo, K.; Ueda, S.; Ishikawa, A.; Matsuyama, N.; Fujita, K.; Mizutani, T.; Ohgi, T.; Ochiya, T.; Gotoh, N.; Kuroda, M., Systemically Injected Exosomes Targeted to EGFR Deliver Antitumor MicroRNA to Breast Cancer Cells. Molecular Therapy 2013, 21 (1), 185-191.

52. Tian, Y. H.; Li, S. P.; Song, J.; Ji, T. J.; Zhu, M. T.; Anderson, G. J.; Wei, J. Y.; Nie, G. J., A doxorubicin delivery platform using engineered natural membrane vesicle exosomes for targeted tumor therapy. Biomaterials 2014, 35 (7), 2383-2390.

53. Bronshtein, T.; Toledano, N.; Danino, D.; Pollack, S.; Machluf, M., Cell derived liposomes expressing CCR5 as a new targeted drug-delivery system for HIV infected cells. Journal of Controlled Release 2011, 151 (2), 139-148.

54. Zhao, C.; Busch, D. J.; Vershel, C. P.; Stachowiak, J. C., Multifunctional Transmembrane Protein Ligands for Cell-Specific Targeting of Plasma Membrane-Derived Vesicles. Small 2016, 12 (28), 3837-3848.

55. Peter, B. J.; Kent, H. M.; Mills, I. G.; Vallis, Y.; Butler, P. J. G.; Evans, P. R.; McMahon, H. T., BAR domains as sensors of membrane curvature: The amphiphysin BAR structure. Science 2004, 303 (5657), 495-499.

56. Bhatia, V. K.; Madsen, K. L.; Bolinger, P. Y.; Kunding, A.; Hedegard, P.; Gether, U.; Stamou, D., Amphipathic motifs in BAR domains are essential for membrane curvature sensing. Embo Journal 2009, 28 (21), 3303-3314.

57. Hatzakis, N. S.; Bhatia, V. K.; Larsen, J.; Madsen, K. L.; Bolinger, P. Y.; Kunding, A. H.; Castillo, J.; Gether, U.; Hedegard, P.; Stamou, D., How curved membranes recruit amphipathic helices and protein anchoring motifs. Nature Chemical Biology 2009, 5 (11), 835-841.

58. McMahon, H. T.; Boucrot, E., Molecular mechanism and physiological functions of clathrin-mediated endocytosis. Nature Reviews Molecular Cell Biology 2011, 12 (8), 517-533.

59. Cocucci, E.; Aguet, F.; Boulant, S.; Kirchhausen, T., The First Five Seconds in the Life of a Clathrin-Coated Pit. Cell 2012, 150 (3), 495-507.

Chapter 2: Connectosomes for Direct Molecular Delivery to the Cellular Cytoplasm[1]

Abstract

Transport of biomolecules, drugs, and other reagents across the cell's plasma membrane barrier is an inefficient and poorly controlled process, despite its fundamental importance to biotechnology, cell biology, and pharmaceutics. In particular, insufficient membrane permeability frequently limits the accumulation of drugs and reagents in the cytoplasm, undermining their efficacy. While encapsulating drugs in particles increases uptake by cells, inefficient release of drugs from these particles into the cytoplasm ultimately limits drug efficacy. In contrast, gap junctions provide a direct route to the cytoplasm that bypasses the plasma membrane. As transmembrane channels that physically connect the cytoplasm of adjacent cells, gap junctions permit transport of a diverse range of molecules, from ions and metabolites to siRNA, peptides, and chemotherapeutics. To utilize gap junctions for molecular delivery we have developed Connectosomes, cell-derived lipid vesicles that contain functional gap junction channels and encapsulate molecular cargoes. Here we show that these vesicles form gap junction channels with cells, opening a direct and efficient route for the delivery of molecular cargo to the cellular cytoplasm. Specifically, we demonstrate that using gap junctions to deliver the chemotherapeutic doxorubicin reduces the therapeutically effective dose of the drug by more than an order of magnitude. Delivering drugs through gap junctions has

[1] This chapter is adapted from the publication: A. K. Gadok, D. J. Busch, S. Ferrati, B. Li, H. D. C. Smyth, J. C. Stachowiak, "Connectosomes for Direct Molecular Delivery to the Cellular Cytoplasm," 2016, Journal of the American Chemical Society. 138(39), 12833-12840. I performed all of the experiments and wrote the manuscript.

the potential to boost the effectiveness of existing drugs such as chemotherapeutics, while simultaneously enabling the delivery of membrane-impermeable drugs and reagents.

Introduction

Membrane permeability is a fundamental requirement for biomolecules, drugs, and reagents that act on intracellular targets. To cross the plasma membrane, molecules must be soluble in both the hydrophobic membrane environment and in the aqueous cytosol[1]. Meeting these requirements while maintaining activity frequently over-constrains molecular design. For example, the effectiveness of chemotherapeutic drugs with marginal membrane permeability, such as gemcitabine, cytarabine[2], or cisplatin[3], is limited by poor accumulation in the cytoplasm. Even highly membrane permeable drugs, such as doxorubicin[4], have limited transport rates across the plasma membrane[5], such that therapeutically effective doses are large, promoting systemic toxicity[6]. Further, increasing the membrane permeability of drugs also frequently increases their vulnerability to export by multidrug efflux pumps[7], restricting their accumulation in the cytoplasm. In sum, crossing the plasma membrane is a substantial challenge that limits the performance of even the most successful drugs. This challenge is among the primary reasons that easily accessible cell-surface proteins, such as G-protein coupled receptors and ion channels, are the targets of the majority of existing drugs[8], while many potentially valuable intracellular targets have not been successfully exploited[9].

Towards overcoming the challenge of crossing the plasma membrane, drugs are frequently encapsulated within nanoparticle materials[10,11]. Loading doxorubicin into liposomes was one of the earliest uses of nanoparticles for drug delivery. This approach substantially reduced the drug's systemic toxicity[4], illustrating the potential of nanoparticles to improve drug delivery. However, upon reaching tumor cells,

nanoparticles enter cells through endocytosis,[12] frequently becoming trapped in the endosomal lumen, which is topologically equivalent to the extracellular milieu[13]. Inefficient endosomal escape leads to nanoparticle degradation and export[14], limiting the efficiency of cytoplasmic delivery[15] and increasing the drug concentration required to kill cancer cells[16]. For example, in *in vitro* studies the therapeutically effective dose, i.e. the median lethal dose (LD50), of doxorubicin increases by an order of magnitude when the drug is encapsulated within liposomes[16].

To facilitate endosomal escape, several strategies have been developed that incorporate pH-sensitive polymers[17], peptides[18], and other compounds[19] into nanoparticles. These membrane-disrupting agents are activated by the acidic endosomal environment, leading to intracellular release of encapsulated drugs[20]. Along with other triggered-release strategies[21], these advancements have reduced the therapeutically effective dose of particle-encapsulated doxorubicin to concentrations equivalent to the free drug[17,19-21]. Further, in some cases, endosomal release strategies have helped to overcome multidrug efflux processes[22], and coupling endosomal release to materials with high drug-carrying capacities, such as silica protocells[23,24] or laponite disks[25], has further reduced the therapeutically effective dose of particle-encapsulated doxorubicin to levels below that of the free drug.

Despite these substantial advancements, delivery approaches that rely upon endocytosis to achieve intracellular release remain constrained by the difficulty of controlling the process[26] and by the variability of the endosomal environment, which frequently limits release[27,28]. For example, more than 80% of mesoporous silica nanoparticles are exocytosed from cells after 6 hours[14], leaving a limited window of time for intracellular drug release. In addition, less than 2% of lipid nanoparticles taken up by endocytosis escape from the endosome within 6 hours[29]. In light of these persistent

limitations, a new delivery route that bypasses endocytic pathways entirely has the potential to dramatically improve therapeutic efficacy.

By providing direct access to the cytoplasm, the cellular gap junction network suggests a means of circumventing the plasma membrane barrier. Cells exchange molecular cargo including metabolites, second messengers, peptides[30], and siRNA with their neighbors using gap junctions[31]. The proteins that form gap junctions, connexins, assemble into connexons. These hexameric pores are present on the cellular plasma membrane. When connexons from two neighboring cells meet, they form a complete gap junction channel, enabling molecules to move from the cytoplasm of one cell to the next by diffusing through the channel. Through a phenomenon known as the bystander effect, cells share drugs via gap junctions. This effect enables drug penetration in tumors[32] and promotes the efficacy of diverse chemotherapeutics, including doxorubicin[33], etoposide[33], paclitaxel[33], gemcitabine[34], and others[35]. Inspired by the ability of gap junctions to directly access the cytoplasm, here we report the development of Connectosomes, connexon-containing cell-derived lipid vesicle materials that form functional gap junctions with cells. Using these materials, we demonstrate gap junction-dependent delivery of molecular cargo into the cytoplasm. Our results indicate that this approach reduces the therapeutically effective dose (LD50) of doxorubicin by more than an order of magnitude in comparison to the free drug, and by multiple orders of magnitude in comparison to liposomal doxorubicin. These results demonstrate the potential of gap junction-mediated intracellular delivery to enhance the effectiveness of diverse therapeutics.

Results and Discussion

Connectosome formation and loading

Connexons have previously been reconstituted in synthetic vesicles for basic biological studies, demonstrating formation of functional junctions between vesicles and cells[36]. However, these vesicles have not been pursued for therapeutic purposes, likely due to technical difficulties including (i) purifying sufficient quantities of transmembrane proteins, (ii) inserting the proteins into vesicles, and (iii) controlling their orientation in the membrane. To overcome these limitations, we used the process of plasma membrane blebbing to harvest Connectosomes directly from donor cells that overexpressed gap junctions. Plasma membrane blebs, also known as plasma membrane vesicles, form when attachments between the plasma membrane and the cytoskeleton are disrupted[37] during cellular processes including cell motility and cytokinesis[37], and maintain the directional insertion and function of transmembrane proteins[38]. Plasma membrane blebs have frequently been used as biophysical models, and have recently emerged as potentially attractive materials for therapeutic applications[39,40]. Notably, exosomes, which are cell-derived vesicles released from cells by fusion of multivesicular bodies to the plasma membrane[41] have also recently emerged as potential drug delivery vehicles[42] Plasma membrane blebs and exosomes differ in several significant ways including the membrane system they originate from and the extent to which their transmembrane protein content can be controlled. Specifically, blebs are derived directly from the plasma membrane system, while exosomes are derived from the cell's endosomal membrane system. Since protein traffic to the plasma membrane is well understood, conventional protocols can be used to express proteins at the plasma membrane surface, resulting in their incorporation into blebs[43]. In contrast, understanding of how protein sorting in the endosomal system leads to selection of proteins by the exosomal pathway is still emerging[41] making the

incorporation of specific protein constituents in exosomes difficult to predict and control. Nonetheless, a recent report suggests that connexins may contribute to the ability of exosomes to transfer their native internal contents to cells[44] While this study did not investigate the use of connexins to deliver drugs, these findings are consistent with the idea that cell-derived particles with well-controlled connexin expression could provide an effective new mode of drug delivery. By extracting blebs from donor cells that overexpressed connexin 43 proteins with a C-terminal YFP modification (Cx43-YFP), we produced cell-derived lipid vesicle materials with embedded connexin 43-YFP (Figure 2.1a-e). Over 90% of these Connectosomes contained connexin 43-YFP at levels detectable by fluorescence imaging. The Connectosomes ranged in diameter from 4 to more than 20 μm, with an average diameter of 10 μm (Figure 2.1j). Notably, Connectosomes can be extruded to reduce their diameter to around 100 nanometers. Based on quantitative measurements of YFP fluorescence, we determined that the average Connectosome contained over 400,000 connexons, which cumulatively covered nearly 10% of the vesicle surface (Figure 2.1k).

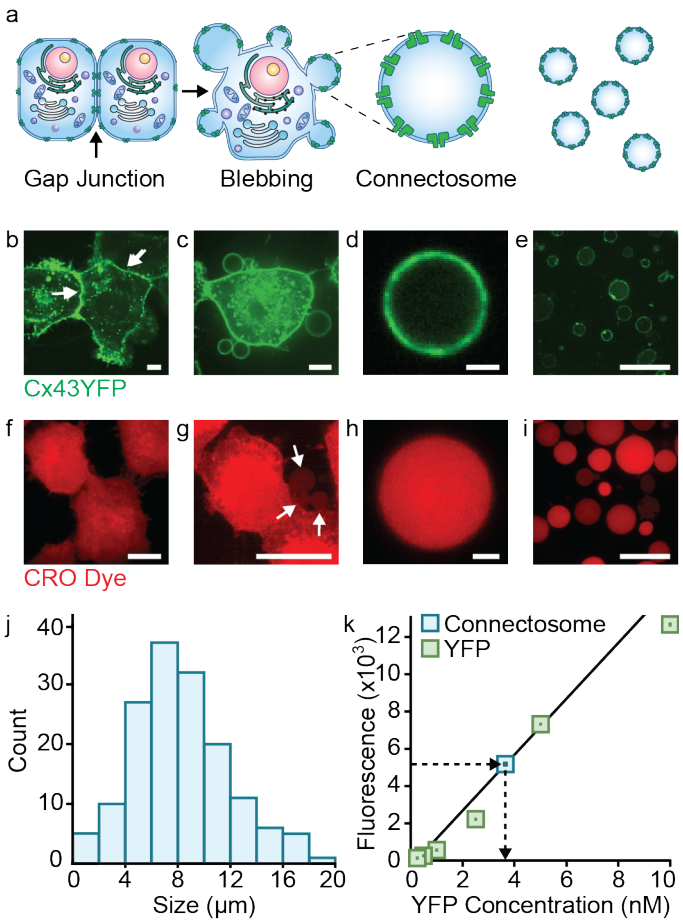

Figure 2.1: **Connectosomes loaded with molecular cargo were harvested from donor cells.** Confocal fluorescence images. (a), Schematic of the Connectosome production process. (b-d), Plasma membrane blebs were extracted from donor cells overexpressing connexin 43-YFP (arrows) to produce Connectosomes, cell-derived lipid vesicle materials with embedded connexin 43-YFP connexons. (e), Multiple Connectosomes in a single field of view. (f-h), Plasma membrane blebs (arrows) were extracted from donor cells treated with CRO dye to produce CRO dye-loaded Connectosomes. (i), Multiple CRO dye-loaded Connectosomes in a single field of view. (j), Histogram of Connectosome diameters. 154 Connectosomes were measured. (k), A calibration curve of YFP fluorescence was generated to determine the YFP content of the Connectosomes. All scale bars 20 μm except for (d) and (h), which are 2 μm. Images in (c) and (g) intentionally saturated to show Connectosome formation.

Connectosomes contained functional gap junction channels

To test the functionality of connexon channels embedded in Connectosomes, we examined the ability of the channels to open and close in the absence and presence of calcium. Specifically, it is well established that calcium causes unpaired connexons to close, obstructing the passage of molecules[45-47]. However, in the absence of calcium, connexons undergo a conformational change that causes them to open, allowing small molecules to diffuse through them[45]. We began by examining the ability of connexons to open upon calcium removal, releasing dye encapsulated within the Connectosomes. To load Connectosomes with the dye we treated the donor cells with calcein red-orange (CRO) acetomethoxy (AM) prior to extracting membrane blebs (Figure 2.1f-i). CRO AM diffuses freely across the plasma membrane. However, when the dye reaches the cytoplasm, intracellular esterases hydrolyze the acetomethoxy group. The resulting CRO dye molecule is membrane impermeable, trapped inside of the cell and permeable only to gap junctions (Figure 2.1f)[48]. In the presence of calcium, the Connectosomes retained the CRO dye (Figure 2.2a, top). However, when calcium was removed by addition of EGTA and EDTA chelators, the dye was released from 87% of the Connectosomes and retained by only 13%, demonstrating that the connexons opened (Figure 2.2a, bottom; b-c).

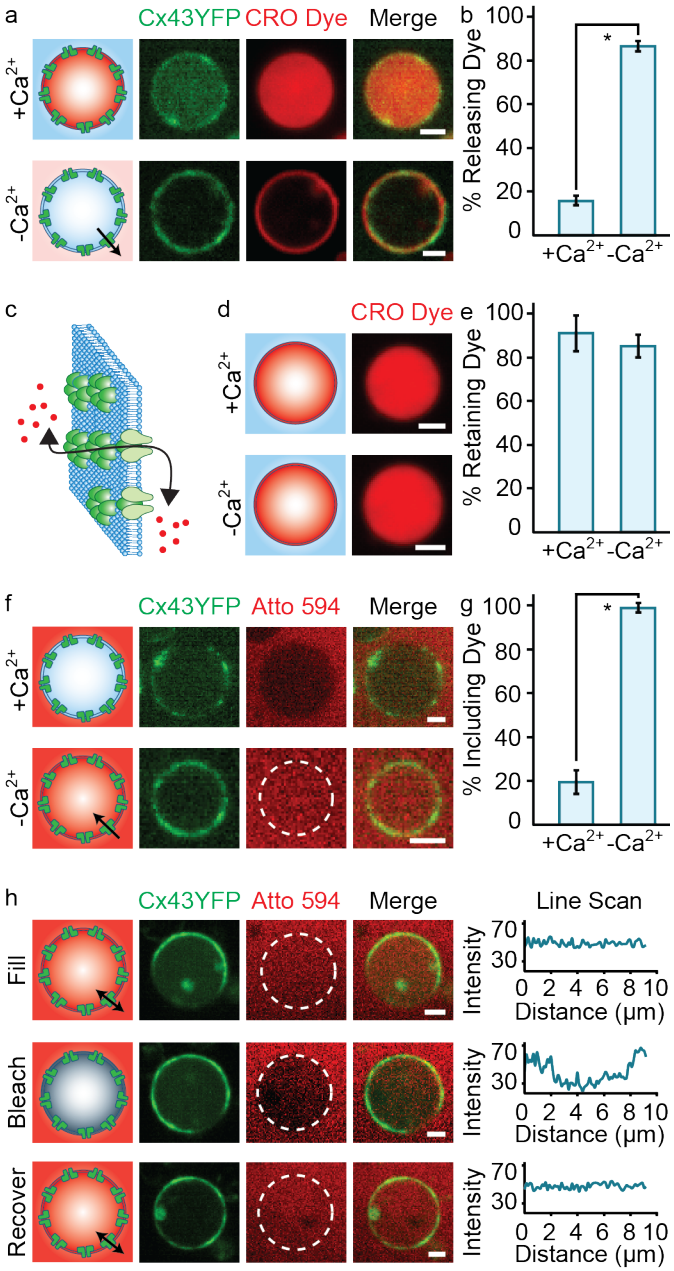

Figure 2.2: Continued on next page.

Figure 2.2: **Connectosomes contained functional connexons. Confocal fluorescence images.** (a), Connectosomes retained CRO dye in a solution of 2 mM Ca^{2+} (top), but released dye when Ca^{2+} was removed (bottom). (b), Percentage of Connectosomes releasing dye +/- Ca^{2+}. The error bars represent the standard deviations of 3 independent trials; at least 54 Connectosomes analyzed per trial. (c), Schematic illustrating connexon-dependent molecular exchange. (d), Plasma membrane blebs derived from MDA-MB-231 cells retained CRO dye in a solution of 2mM Ca^{2+} (top), as well as when Ca^{2+} was removed (bottom). (e), Percentage of MDA-MB-231 GPMVs releasing dye +/- Ca^{2+}. The error bars represent the standard deviations of 3 independent trials, at least 36 Connectosomes analyzed per trial. (f), Connectosomes excluded Atto 594 in 2 mM Ca^{2+} (top), but filled with dye when Ca^{2+} was removed (bottom). (g), Percentage of Connectosomes including dye +/- Ca^{2+}. The error bars represent the standard deviations of 3 independent trials, at least 51 Connectosomes analyzed per trial. (h), The Atto 594 dye within Connectosomes (top) was photobleached (middle) in the absence of Ca^{2+}. The Connectosomes refilled with dye within 75 seconds after the laser illumination was stopped (bottom). Scale bars: 2μm. Asterisks represent statistically significant differences (two-tailed t-test, $p < 0.001$).

To further illustrate the dependence of dye release on the presence of functional connexons in the Connectosomes, we formed CRO dye-loaded plasma membrane blebs from MDA-MB-231 donor cells. MDA-MB-231 cells express low levels of connexin 43 and exhibit defective connexin trafficking and gap junction formation, resulting in substantially reduced gap junction intercellular communication[49]. In the presence of calcium, 91% of MDA-MB-231 blebs retained the dye (Figure 2.2d, top). When calcium was removed by addition of EGTA and EDTA chelators, 85% of the MDA-MB-231 blebs continued to retain the dye, in comparison to only 13% of Connectosomes, demonstrating that the dye release was dependent on the presence of functional connexons (Figure 2.2d, bottom; e).

Next, we developed an exogenous method of loading, in which molecular cargo was encapsulated after Connectosome formation. Specifically, we added a water-soluble dye with little or no membrane permeability, Atto 594, to the solution surrounding pre-formed Connectosomes. In the presence of calcium, the Connectosomes excluded the dye, demonstrating that connexons remained closed (Figure 2.2f, top). However, when calcium was removed by addition of EGTA and EDTA chelators, 99% of the Connectosomes filled with dye, demonstrating that the connexons opened (Figure 2.2f,

bottom; g). Similar results were also obtained for Connectosomes loaded with Atto 488 dye using an identical protocol (Supporting Information Figure 2.5). Atto 488 has been reported to have no significant interaction with membranes[50], making the dye almost perfectly membrane impermeable.

Finally, to probe the timescale of diffusion through open connexons, we photobleached Atto 594 dye loaded within the Connectosomes. In the absence of calcium, the Connectosomes refilled with dye within 75 seconds after photobleaching (Figure 2.2h). Together, these results demonstrate two distinct modes of loading Connectosomes and demonstrate that Connectosomes contain multiple functional connexons, capable of opening and closing to enable rapid molecular exchange with the external environment. Further, comparison to MDA-MB-231 blebs suggests that molecular exchange is connexon-dependent.

Connectosomes delivered molecular cargo to the cellular cytoplasm

Having established the functionality of the connexons, we next examined the ability of the Connectosomes to deliver molecular cargo into the cellular cytoplasm (Figure 2.3a). While the presence of calcium keeps unpaired connexons closed[45], complete channels form and open when two unpaired connexons on the surfaces of neighboring cells meet, even in the presence of physiological levels of extracellular calicium[51,52]. To test the ability of Connectosomes to form gap junctions with cells, we prepared a confluent monolayer of recipient HeLa cells. CRO dye-loaded Connectosomes were prepared as described above (Figure 2.1f-i) and incubated with the recipient cells. Imaging the recipient cells after 2 hours revealed the intracellular accumulation of dye (Figure 2.3b, Supporting Information Figure 2.6). To quantify the CRO dye delivery, we measured the relative fluorescence intensity of the cell populations using flow cytometry

(Figure 2.3c-e). Exposure to CRO dye-loaded Connectosomes increased the average fluorescence of the recipient cells by a factor of 6, in comparison to background fluorescence from untreated cells (Figure 2.3d, Supporting Information Figure 2.6). Additionally, we drew a threshold at the peak of the fluorescence histogram for cells receiving dye-loaded Connectosomes (Figure 2.3c). The average percentage of cells with fluorescence greater than this threshold increased from less than 4% for untreated cells to over 51% for cells exposed to dye-loaded Connectosomes (Figure 2.3e). To demonstrate that the CRO dye delivery was gap junction-dependent, we used carbenoxolone[53] (CBX), a drug which blocks the coupling of connexons, to inhibit the formation of gap junctions between Connectosomes and recipient HeLa cells. Repeating the dye delivery experiment in the presence of this gap junction inhibitor significantly decreased the average recipient cell fluorescence, illustrating that dye delivery was dependent on the assembly of gap junction channels between the Connectosomes and the cells (Figure 2.3c-e, Supporting Information Figure 2.6). CBX treatment did not completely eliminate the increase in fluorescence of the recipient cells upon exposure to dye-loaded Connectosomes, likely because CBX is not a complete inhibitor of gap junction communication[53] and because CBX itself somewhat increases the fluorescence of the recipient cells, in the absence of Connectosome treatment (Figure 2.3c-e, Supporting Information Figure 2.7).

To further demonstrate the gap junction-dependence of the CRO dye delivery, we repeated the same experiment as above, using plasma membrane vesicles that lacked a significant concentration of functional connexons (Supporting Information Figure 2.8). Specifically, we formed CRO dye-loaded plasma membrane vesicles from A549 cells, which are known to have low levels of connexin expression and gap junctional communication[54]. We incubated these connexon-lacking plasma membrane vesicles with recipient HeLa cells, and measured the relative recipient cell fluorescence using flow

cytometry (Supporting Information Figure 2.8). We found that the fluorescence signal from cells exposed to CRO dye-loaded A549 vesicles was more than an order of magnitude less than the average fluorescence signal from cells exposed to Connectosomes. Collectively, these results demonstrate gap junction-dependent delivery of molecular cargo using Connectosomes.

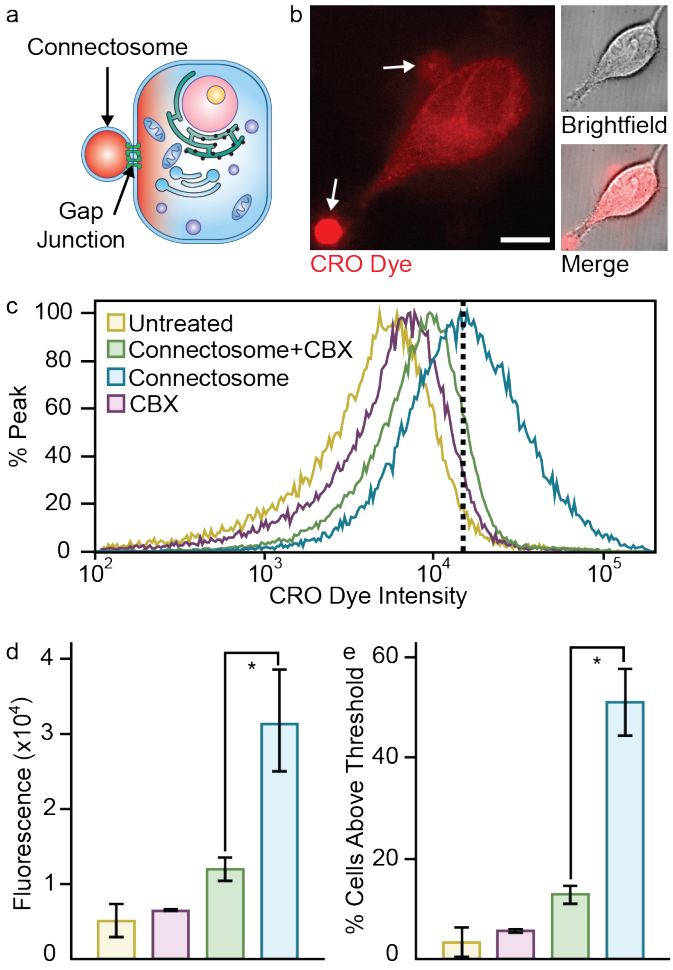

Figure 2.3: **Connectosomes delivered dye to the cellular cytoplasm. Brightfield and confocal fluorescence images.** (a), Schematic. (b), Two Connectosomes (arrows) delivering CRO dye to the cellular cytoplasm. (c), Flow cytometry histograms showing CRO dye fluorescence for each recipient cell condition. The dotted line, drawn at the peak of the fluorescence histogram for cells receiving CRO dye-loaded Connectosomes, is used as a threshold in (e). Each curve represents 3 independent, concatenated trials, 10,000 cells analyzed per trial. (d), Average recipient cell fluorescence for each condition. The error bars represent the standard deviations of 3 independent trials, 10,000 cells analyzed per trial. (e), Percentage of cells with fluorescence values above the threshold drawn in (c). The error bars represent the standard deviations of 3 independent trials, 10,000 cells analyzed per trial. Legend in (c) applies to (d-e). Scale bar: 10 μm. Asterisks represent statistically significant differences (two-tailed t-test, $p < 0.04$ (d) and $p < 0.01$ (e)). Image of Connectosome in (b) intentionally saturated to show intracellular dye accumulation.

Connectosomes increased the therapeutic efficacy of doxorubicin

Next, we investigated the use of Connectosomes to deliver the chemotherapeutic doxorubicin to the cellular cytoplasm. We began with doxorubicin because its inherent fluorescence allowed us to visualize its encapsulation within Connectosomes. We note that doxorubicin may not be an ideal candidate for delivery via Connectosomes, owing to its cardiotoxicity and the importance of connexins in heart tissue. However, any small molecule drug or biomolecule can in principle be encapsulated within Connectosomes, and nanoparticles in general have not been observed to accumulate in the heart[55,56]. Further, incorporation of targeting ligands has recently been demonstrated to dramatically increase binding specificity of cell derived vesicles to target cells overexpressing biomarkers such as the epidermal growth factor receptor (EGFR)[57].

To encapsulate doxorubicin within Connectosomes, we treated donor cells with doxorubicin (Figure 2.4a), such that the plasma membrane blebs derived from these cells contained the drug (Figure 2.4b-c). Notably, chemotherapeutics such as doxorubicin require 2-3 days to substantially impact cell viability[16], while harvesting Connectosomes requires only a few hours (see methods). Therefore, loss of donor cell viability owing to drug loading was found to be insignificant during the Connectosome production process. Additionally, it is important to note that doxorubicin could be encapsulated within Connectosomes either by loading the cells with the semi-membrane permeable drug, or by opening and subsequently closing the connexons of preformed Connectosomes in the presence of a solution of the drug. Loading of the cells prior to Connectosome extraction was found to slightly increase the concentration of encapsulated drug and the overall material yield (ie. Connectosomes per donor cell) and was therefore used to produce the Connectosomes for the doxorubicin studies presented here.

We quantified the doxorubicin content of the Connectosomes by measuring their fluorescence emission after resuspending them in fresh solution (Supporting Information Figure 2.9). The native fluorescence of empty Connectosomes was measured and determined negligible. Based on the peak fluorescence emission of each Connectosome sample and a calibration curve of free doxorubicin fluorescence emission, we were able to determine that the average concentration of doxorubicin in each Connectosome sample was in the micromolar range. Based on this value as well as the average diameter and number of Connectosomes per volume, we estimated that the concentration of doxorubicin within Connectosomes was approximately 1 mM. Notably, this concentration could be further increased by crystalizing doxorubicin within vesicles, as is done in the preparation of conventional liposomal formulations[4].

We then investigated the timescale of doxorubicin release from Connectosomes (Figure 2.4d). To begin, we measured the fluorescence of doxorubicin-loaded Connectosomes using flow cytometry (Figure 2.4e). After addition of EGTA and EDTA chelators to remove residual calcium and open connexons, the average doxorubicin fluorescence of the Connectosomes decreased significantly within 5 minutes. These results demonstrate the potential for rapid drug release upon connexon opening. In contrast, when chelators were not added, the vesicles retained their content throughout the time course of all experiments.

Next, we conducted a control study in which the viability of a confluent monolayer of HeLa cells was measured 24 hours after free doxorubicin was added directly to the cell media at increasing concentrations from 100 nM to 100 μM (Figure 2.4f-g, i, Supporting Information Figure 2.10). The cytotoxic dose of doxorubicin for HeLa cells after 24 hours of exposure is approximately 10 μM[58]. We evaluated cell viability using both trypan blue and 7-AAD cell permeability assays on at least 3

independent populations of cells per condition per stain. As expected, we found a trend of decreasing cell viability with increasing doxorubicin concentration. Specifically, while a dose of 100 nM was not significantly cytotoxic (9% trypan blue / 10% 7-AAD), the percentage of nonviable cells increased with increasing doxorubicin dose at 1 μM (21% trypan blue / 9% 7-AAD), 10 μM (44% trypan blue / 45% 7-AAD), and 100 μM (87% trypan blue) (Figure 2.4g, i). Cells receiving 100 μM doxorubicin were outside the range of sensitivity for the 7-AAD assay, therefore, the percentage of nonviable cells at this concentration measured using the trypan blue assay was used in Figure 2.4g.

Then, we conducted a study in which the viability of a confluent monolayer of HeLa cells was measured 24 hours after conventional, commercially sourced liposomal doxorubicin was added directly to the cell media at increasing doxorubicin concentrations from 10 nM to 1 mM (Figure 2.4f-g, i, Supporting Information Figure 2.10). These experimental parameters are consistent with the systemic infusions used to administer liposomal doxorubicin in the clinical setting. We evaluated cell viability using both trypan blue and 7-AAD cell permeability assays on at least 3 independent populations of cells per condition per stain. We found that the LD50 of liposomal doxorubicin was more than an order of magnitude greater than the LD50 of free doxorubicin (Figure 2.4g,i). This result confirms previous reports, and likely arises from the inhibited release of doxorubicin when encapsulated within a liposome[16].

Finally, we exposed confluent HeLa cell monolayers to doxorubicin-loaded Connectosomes for 2 hours (Figure 2.4f). Independent cell samples were exposed to increasing concentrations of Connectosomes, which were equivalent in terms of total doxorubicin content to free doxorubicin concentrations of 15 nM, 150 nM, 400 nM, and 1.5 μM. As discussed above, these concentrations were determined by measuring the doxorubicin fluorescence emission for each sample (Supporting Information Figure 2.9).

While the 15 nM Connectosome dose was not significantly cytotoxic (7% 7-AAD), the percentage of nonviable cells increased with increasing Connectosome concentration at 150 nM (18% 7-AAD), 400 nM (74% 7-AAD), and 1.5 μM (75% 7-AAD) (Figure 2.4g-h, Supporting Information Figure 2.11). To confirm our results, we repeated the experiment with doxorubicin-loaded Connectosomes at the lowest effective dose, 400 nM, measuring viability using the trypan blue assay (Figure 2.4i). The results of this study were comparable to the results of the 7-AAD assay.

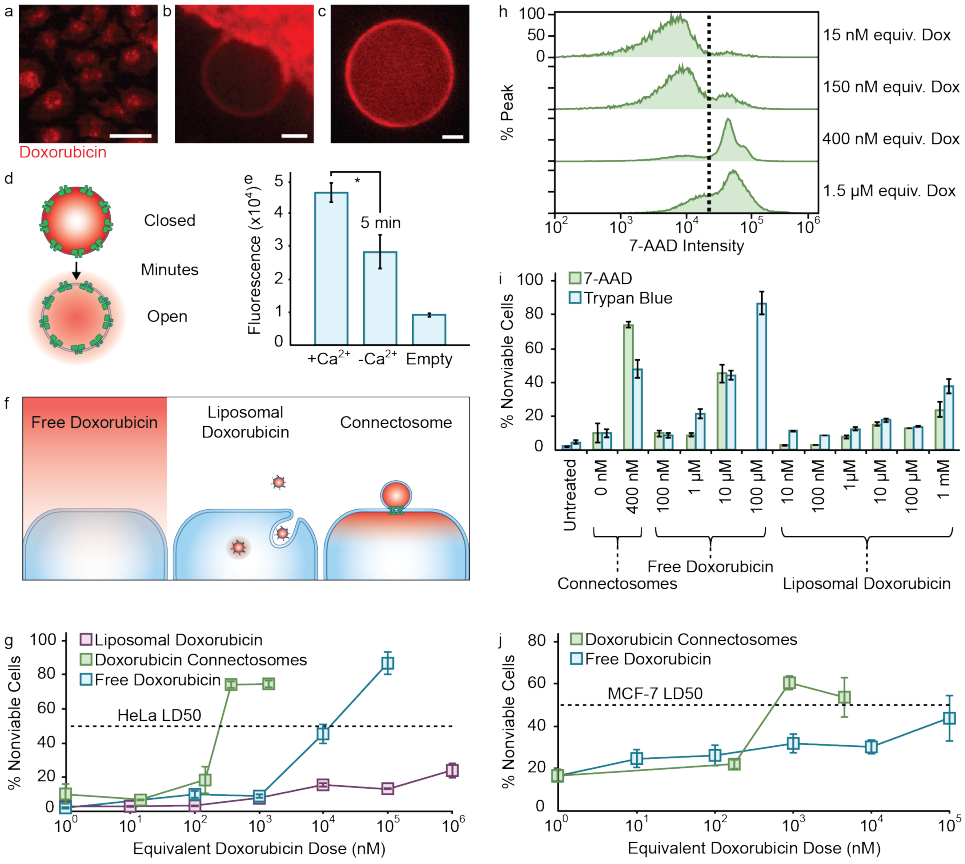

Figure 2.4: Continued on next page.

Figure 2.4: **Connectosomes substantially reduced the cytotoxic dose of doxorubicin.** (a-c), Plasma membrane blebs were extracted from donor cells treated with doxorubicin to produce doxorubicin-loaded Connectosomes. (d), Schematic illustrating doxorubicin release from Connectosomes. (e), Average Connectosome fluorescence calculated from flow cytometry data. Connectosomes released significant amounts of doxorubicin within 5 minutes of calcium removal. The error bars represent the standard deviations of 3 independent trials, at least 800 Connectosomes analyzed per trial. (f),Schematic illustrating the 3 modes of drug delivery tested. (g), Percentage of nonviable HeLa cells after free doxorubicin treatment (blue), conventional liposomal doxorubicin treatment (purple), or doxorubicin-loaded Connectosome treatment (green). All points were measured using a 7-AAD viability assay, except for the free doxorubicin 10^5 nM point, which was measured using a trypan blue viability assay, owing to interference of doxorubicin in the 7-AAD measurement at this high doxorubicin concentration. The error bars represent the standard deviations of at least 3 independent trials, at least 4,000 cells (7-AAD assay) or 93 cells (trypan blue) analyzed per trial. (h), Flow cytometry histograms showing 7-AAD fluorescence for cells receiving doxorubicin-loaded Connectosomes at increasing equivalent free doxorubicin (dox) concentrations. The dotted line represents the threshold fluorescence value above which cells were considered nonviable. Each curve represents 3 independent, concatenated trials, at least 4,000 cells analyzed per trial. (i), Percentage of nonviable cells determined using both trypan blue (blue) and 7-AAD (green) viability assays. The error bars represent the standard deviations of at least 3 independent trials, at least 4,000 cells (7-AAD assay) or 93 cells (trypan blue assay) analyzed per trial. (j), Percentage of nonviable MCF-7 cells after free doxorubicin treatment (blue) or doxorubicin-loaded Connectosome treatment (green). All points were measured using a trypan blue viability assay. The error bars represent the standard deviations of 3 independent trials, at least 166 cells analyzed per trial. Scale bars: 2 μM. Asterisks represent statistically significant differences (two-tailed t-test, $p < 0.02$). Image in (b) intentionally saturated to show doxorubicin-loaded Connectosome formation.

To test Connectosomes in a second model cell line, we repeated our assay using recipient MCF-7 cells. MCF-7 cells are human breast adenocarcinoma cells that have been used frequently in studies of drug delivery materials[59]. First, we conducted a control study in which the viability of a confluent monolayer of MCF-7 cells was measured 48 hours after free doxorubicin was added directly to the cell media at increasing concentrations from 10 nM to 100 μM (Figure 2.4j). Next, we exposed independent cell samples to increasing concentrations of Connectosomes, which were equivalent in terms of total doxorubicin content to free doxorubicin concentrations of 180 nM, 900 nM, and 4.5 μM. While the majority of cells treated with Connectosomes at an equivalent doxorubicin concentration of 900 nM were nonviable (61% 7-AAD trypan blue), the majority of cells treated with free doxorubicin remained viable even at a concentration of 100 μM (44% trypan blue), consistent with literature reports[60] (Figure 2.4j).

As illustrated by these collective results, the therapeutically effective dose (LD50) of doxorubicin increases by more than an order of magnitude when the drug is encapsulated within a conventional liposome, rather than administered to cells as a free drug in solution. This result, which is in agreement with the original literature on liposomal doxorubicin *in vitro*[16], points to a key limitation of liposomal formulations that has prevented their broad clinical adoption to date. Specifically, their ability to concentrate drugs is largely negated by a corresponding reduction in the availability of the encapsulated drug to the cellular cytoplasm. In contrast, the LD50 for doxorubicin-loaded Connectosomes is more than an order of magnitude less than the LD50 for free doxorubicin and several orders of magnitude less than the LD50 for liposomal doxorubicin. These results illustrate the ability of Connectosomes to dramatically increase the efficiency of drug delivery to the cellular cytoplasm, removing a key limitation of liposomal formulations[4].

Conclusion

Here we report the development of Connectosomes, a cell-derived material that efficiently delivers molecular cargoes across the plasma membrane barrier. By utilizing gap junction channels, Connectosomes make it possible to sequester reagents and drugs in a particle, yet release them rapidly and efficiently into the cellular cytoplasm. By combining these two capabilities, Connectosomes represent a key step toward realizing the long-anticipated advantages of particle-based drug delivery materials. In particular, this bio-inspired delivery approach has led to a remarkable decrease in the therapeutically effective dose of doxorubicin, which has the potential to address long-standing problems associated with chemotherapy, such as dose-limiting toxicity. Further, this result implies

the ability to rapidly increase the drug concentration within the cytoplasm, suggesting the potential to outpace cellular efflux pumps, a key mechanism of multidrug resistance.

The focus of this work has been on fundamental development of Connectosomes as liposomal materials that utilize gap junctions to create a new molecular delivery route to the cytoplasm. However, in the future, these materials could create a path forward for efficient intracellular delivery of hydrophilic drugs and small biologics, including peptides, siRNA, and other compounds with intracellular targets[31]. As evidence of this potential, in Figure 2.2c, a hydrophilic dye, Atto 594, passed through the connexon channels of Connectosomes. In drug design, lack of membrane permeability is currently considered a severe disadvantage that immediately eliminates compounds from drug candidate libraries. However, gap junction-based delivery could remove this requirement, substantially expanding the chemical diversity of drug candidates to include those with high polarity and significant negative charge[1]. For example, this approach could improve the cytoplasmic delivery of drugs that have not been successful in liposomal formulations because they lack membrane permeability, such as cisplatin[3]. Ultimately, by dramatically improving molecular transport across the plasma membrane barrier, Connectosomes have the potential to improve the performance of existing drugs and enable the design of new therapeutics and biochemical reagents that reach a broader class of cytoplasmic targets.

Supporting Information

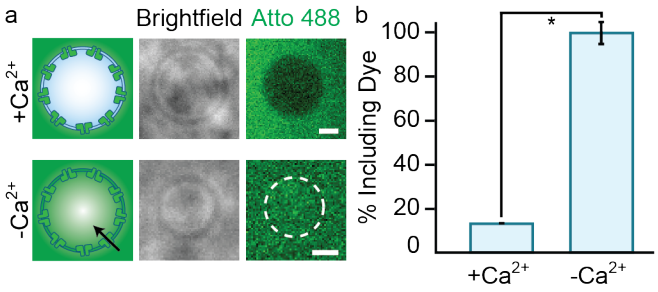

Figure 2.5: **Exogenously-loaded Connectosomes encapsulated a membrane impermeable dye.** (a), Connectosomes excluded CRO dye in a solution of 2 mM Ca^{2+} (top), but filled with dye when Ca^{2+} was removed (bottom). (b), Percentage of Connectosomes including dye +/- Ca^{2+}. The error bars represent the standard deviations of 3 independent trials; at least 39 Connectosomes analyzed per trial. Scale bars: 2 μm. Asterisk represents statistically significant differences (two-tailed t-test, $p < 0.002$).

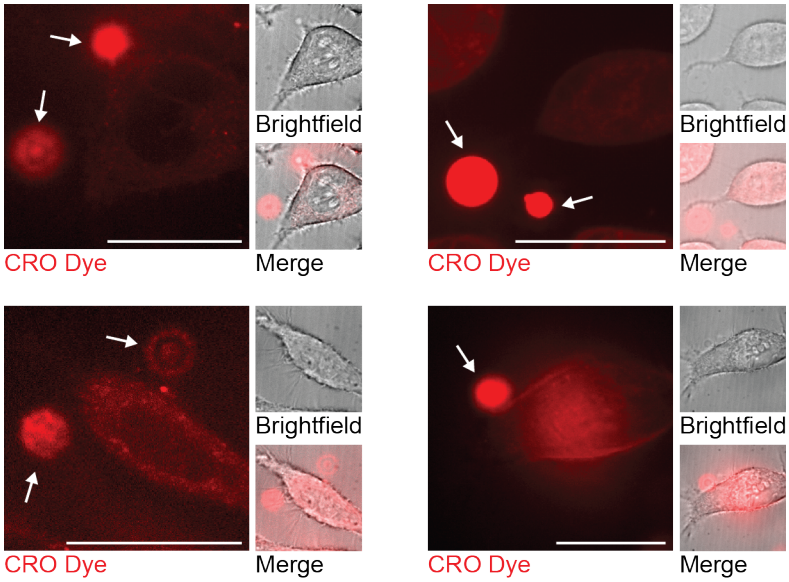

Figure 2.6: **Connectosomes (arrows) delivered dye to the cytoplasm.** Brightfield and confocal fluorescence images. Scale bars: 20 μm. Connectosomes intentionally saturated to show intracellular dye accumulation.

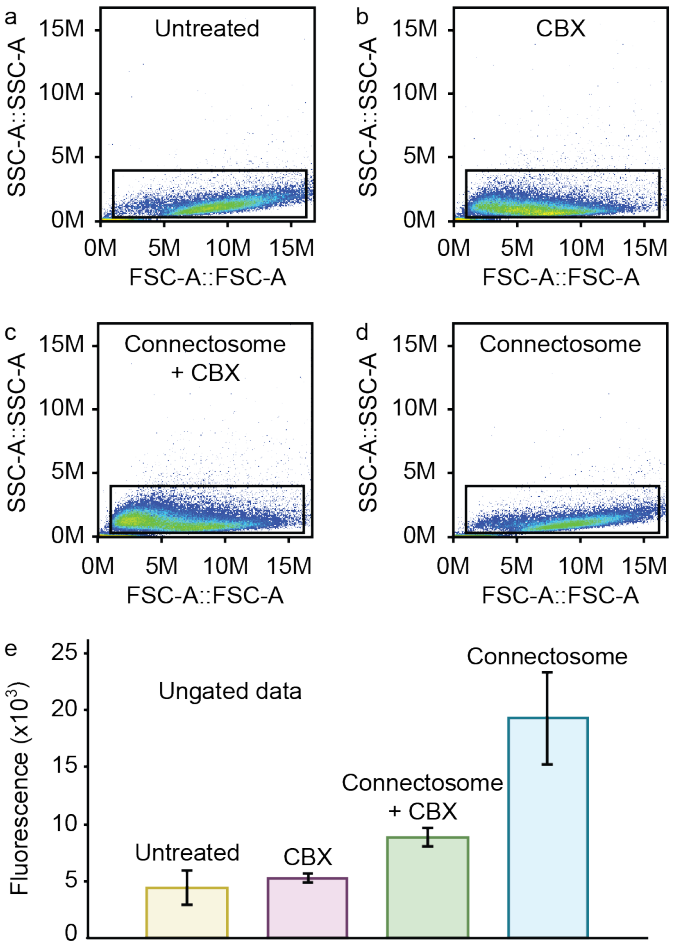

Figure 2.7: **Connectosomes delivered CRO dye to the cytoplasm.** (a-d), Side-scatter versus forward-scatter plots showing all events detected in 3 independent, concatenated trials for untreated cells (a) and cells treated with carbenoxolone (b), carbenoxolone + CRO dye-loaded Connectosomes (d), and CRO dye-loaded Connectosomes (d). The gate shown was used for analysis in Fig. 3. (e), Average recipient cell fluorescence for the ungated samples for each condition. These results show approximately the same trend and relative magnitudes as the data in Fig. 3, demonstrating that the result of the experiment does not depend on the choice of the gate. For each trial, at least 17,000 events were detected. At least 10,000 of these events fell within the gate and were analyzed in Fig. 3. The error bars represent standard deviations of 3 independent trials. M stands for million.

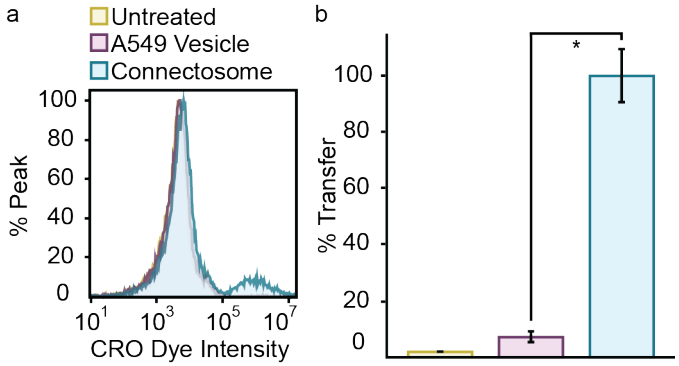

Figure 2.8: **Dye delivery is dependent on gap junction assembly.** (a), Flow cytometry histograms showing CRO dye fluorescence for each recipient cell condition: (i) untreated cells, (ii) cells treated with CRO-loaded blebs from A549 cells lacking connexin expression, (iii) Connectosomes derived from HeLa cells stably expressing Cx43. Each curve represents 3 independent, concatenated trials, at least 10,000 cells analyzed per trial. The population of highly fluorescent cells (centered around 10^6), which is only present for cells exposed to Connectosomes, represents the fraction of cells that received a substantial dose of CRO dye. In contrast, cells treated with CRO-loaded blebs derived from A549 cells do not have significantly greater fluorescence than untreated cells. (b), Average recipient cell fluorescence for each condition, normalized to the average recipient cell fluorescence for cells treated with Connectosomes. The error bars represent the standard deviations of 3 independent trials, at least 10,000 cells analyzed per trial. Legend in (a) applies to (b). Asterisk represents statistically significant differences (two-tailed t-test, $p < 0.003$).

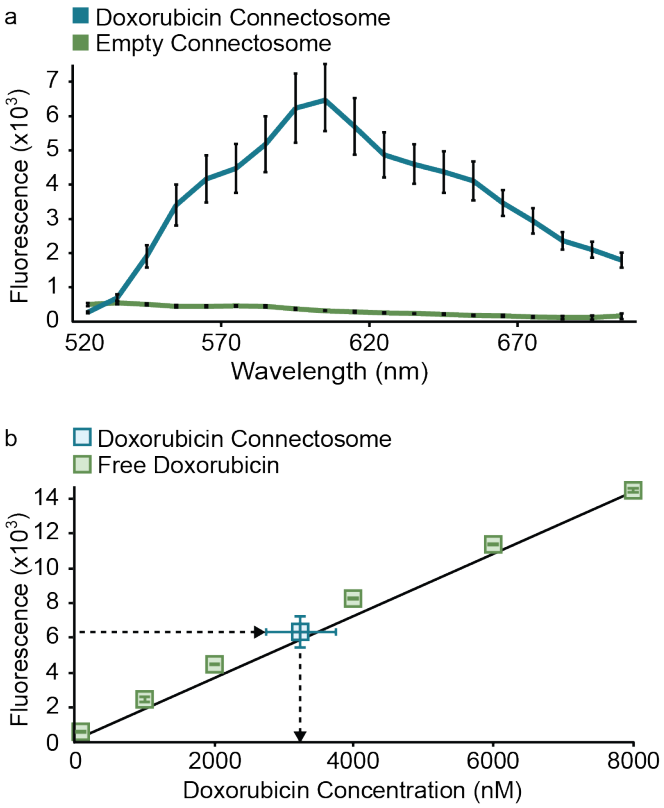

Figure 2.9: **Connectosomes contained doxorubicin.** (a), A representative fluorescence spectrum of doxorubicin-loaded Connectosomes (blue), compared to empty Connectosomes (green). Connectosomes were washed to remove free doxorubicin from solution. (b), A calibration curve of doxorubicin fluorescence in solution (green) was generated by plotting the peak of the fluorescence spectrum for each concentration of doxorubicin dissolved in aqueous solution. A line was fit to this curve and the doxorubicin content of the Connectosomes (blue) was estimated by calculating the doxorubicin concentration corresponding to the measured fluorescence. The error bars represent the standard deviations of 3 independent trials.

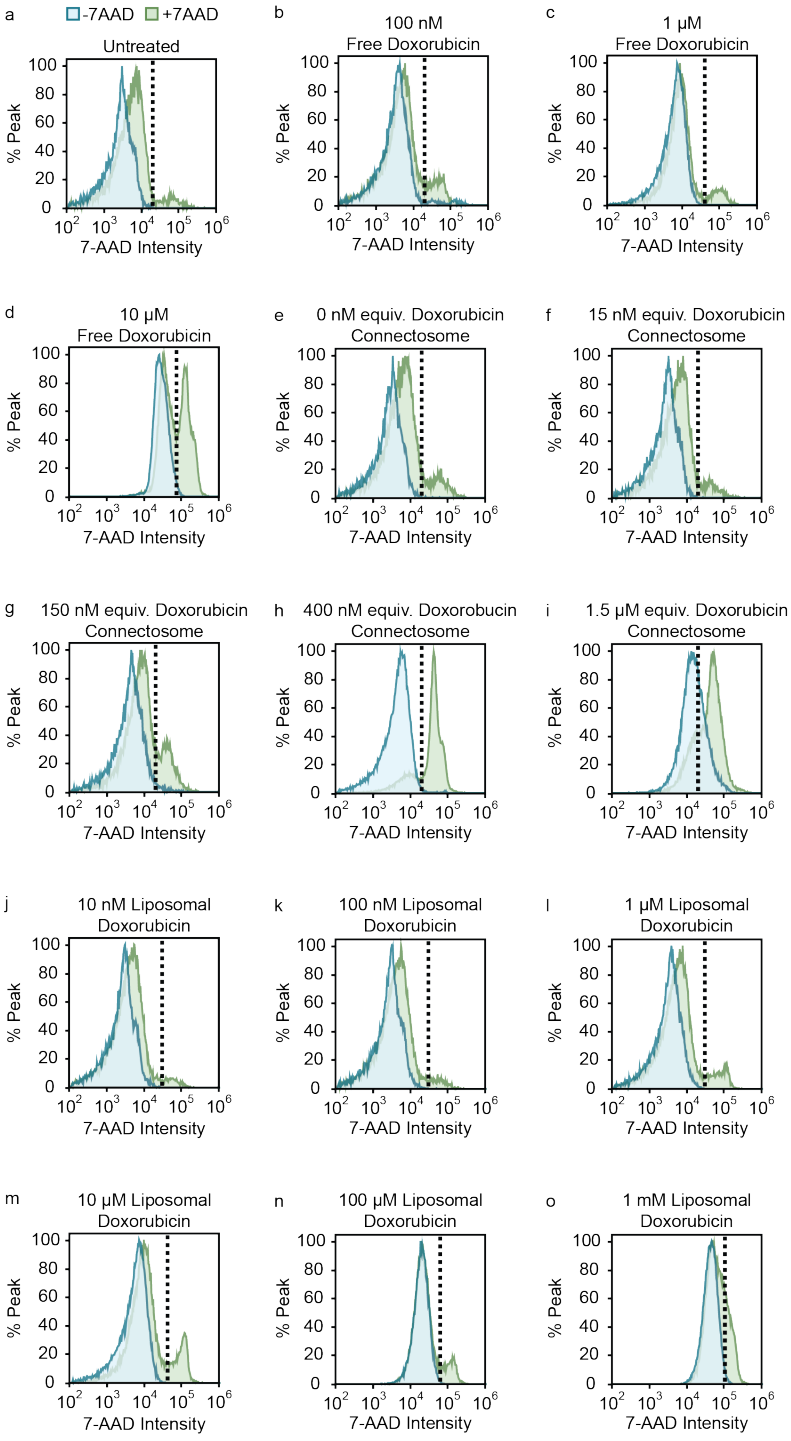

Figure 2.10: Continued on next page

Figure 2.10: **Thresholds for 7-AAD viability assay.** (a-o), Flow cytometry histograms showing 7-AAD fluorescence histograms for cells with and without 7-AAD for each condition. Legend in (a) applies to (b-o). The dotted line represents the threshold fluorescence value above which cells were considered nonviable, for untreated cells (a), and for cells treated with 100 nM (b), 1μM (c), and 10 μM (d) free doxorubicin, for cells treated with empty Connectosomes (e) and doxorubicin-loaded Connectosomes at equivalent doxorubicin concentrations of 15 nM (f), 150 nM (g), 400 nM (h), and 1.5 μM (i), and for cells treated with liposomal doxorubicin at equivalent doxorubicin concentrations of 10 nM (j), 100 nM (k), 1 μM (l), 10 μM (m), 100 μM (n), and 1 mM (o). Each curve represents 3 independent, concatenated trials, at least 4,000 cells analyzed per trial.

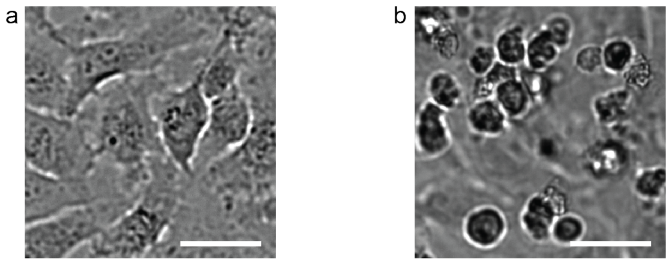

Figure 2.11: **Doxorubicin-loaded Connectosomes were cytotoxic to HeLa cells.** Brightfield images. (a), Untreated, control HeLa cells. (b), Cells after treatment with doxorubicin-loaded Connectosomes at an equivalent doxorubicin dose of 400 nM. Scale bars: 200 μm.

Materials and Methods

Chemical reagents. CellTrace Calcein Red-Orange AM and trypan blue were purchased from Life Technologies. Sodium phosphate, DTT (dithiothreitol), PFA (paraformaldehyde), doxycycline, glycine, Atto 594-NHS ester, imidazole, NaCl, $CaCl_2$, EGTA (ethylene glycol tetraacetic acid), EDTA (ethylenediaminetetraacetic acid), HEPES (4-(2-hydroxyethyl)-1-piperazineethanesulfonic acid), DMSO (dimethyl sulfoxide) and doxorubicin were purchased from Sigma-Aldrich. Fetal bovine serum (FBS), trypsin, penicillin, streptomycin, L-glutamine, PBS (phosphate buffered saline), and DMEM (Dulbecco's modified Eagle medium) were purchased from GE Healthcare. Puromyocin was purchased from Clontech. Geneticin (G418) was purchased from Corning. Leupeptin and pepstatin were purchased from Roche. PMSF (phenylmethanesulfonyl fluoride), β-ME (β-mercaptoethanol) were purchased from Fisher Scientific. 7-AAD (7-amino-actinomycin D) was purchased from Affymetrix eBioscience. Conventional liposomal doxorubicin (Dox-NP) was purchased from Avanti Polar Lipids. All chemical reagents were used without further purification.

Cell culture. Stably transfected, inducible tet-on cells expressing connexin 43 with a C terminal YFP modification were a gift from Matthias Falk[52,53]. These cells were cultured in Dulbecco's Modified Eagle Medium (DMEM) supplemented with 10% Fetal Bovine Serum (FBS), 1% penicillin, 1% streptomycin, 1% L-glutamine (PSLG), 100 μg/ml geneticin and 0.4 μg/ml puromycin. To induce Cx43YFP expression, cells were incubated with 1 μg/mL doxycycline. Wild type HeLa, MCF-7, and MD-MB-231 cells were cultured in DMEM supplemented with 10% FBS and 1% PSLG. Cell media was changed every 48-72 hours. Cells were incubated at 37 °C with 5% CO_2. All studies were conducted on the fifth day after plating.

Optical microscopy. Fluorescence and brightfield images have been optimized for contrast and brightness. A Zeiss AxioObserver microscope with 10x and 20x objectives was used for widefield imaging. A Zeiss AxioObserver Spinning Disk Confocal microscope with 100x oil immersion (numerical aperture, 1.4) and 63x oil immersion (numerical aperture, 1.4) objectives was used for both fluorescence and brightfield imaging. Three filters were used: an emission filter centered at 525 nm with a 50nm width, an emission filter centered at 629 nm with a 62 nm width, and a triple pass dichroic mirror designed to reflect laser illumination at 405 nm, 488nm, and 561 nm excitation wavelengths. For spinning disk confocal and brightfield imaging, cells were cultured on 35 mm collagen-coated glass bottom dishes (MatTek).

Flow cytometry. A BD Accuri C6 Flow Cytometer was used for all flow cytometry studies and all flow cytometry data was analyzed using FlowJo software. Flow cytometry data was collected at a speed of 35 events per second. Gates were drawn to include at least 30% of the detected events. In each experiment, once the appropriate gate was determined it was applied to all trials and all experimental conditions without modification.

Connectosome formation. Following established protocols for making giant plasma membrane vesicles (GPMVs)[54], Connectosomes were formed by rinsing donor connexin 43-YFP HeLa cells twice with GPMV buffer (10 mM HEPES, pH 7.4, 2 mM $CaCl_2$, 150 mM NaCl) and once with active buffer (10 mM HEPES, pH 7.4, 2 mM $CaCl_2$, 150 mM NaCl, 25 mM PFA, 2 mM DTT, 125 mM glycine). Then, the cells were incubated for 6 hours in active buffer, and the active buffer containing the Connectosomes was collected from the cells. To concentrate the Connectosomes, the sample was centrifuged at 17,000 x g for 20-30 minutes at 4 °C. Finally, the Connectosome pellet was resuspended in fresh GPMV buffer. To determine the average

Connectosome diameter, the diameters of 154 Connectosomes were measured from brightfield images. To determine the average percentage of Connectosomes containing connexin 43-YFP embedded in the membrane, confocal spinning disk and brightfield images of 3 independent samples of Connectosomes were analyzed for fluorescence in the membrane. At least 37 Connectosomes were analyzed per trial.

MDA-MB-231 plasma membrane bleb formation. MDA-MB-231 plasma membrane blebs were formed from MDA-MB-231 donor cells as described above.

YFP purification. The pET28a-HisYFP-Sp100 plasmid was generously shared by the lab of Frauke Melchior (Addgene plasmid #53141)[55]. Following the provider's protocol[55], hisYFP-Sp100 was expressed in BL21(DE3)pLysS cells for 1 hour at 18 °C and then 5 hours at 30 °C.

Bacterial extracts were made by lysing the cells in 50 mM Na_3PO_4, pH 8.0, 300 mM NaCl, 20 mM imidazole, 1 mM β-ME, and 1 μg/mL each of leupeptin, pepstatin, and PMSF. HisYFP-Sp100 was purified by incubating with Ni-NTA agarose beads. After washing with 50 mM Na_3PO_4, pH 8.0, 300 mM NaCl, 20 mM imidazole, 1 mM β-ME, and 1 μg/mL each of leupeptin, pepstatin, and PMSF, proteins were eluted in 250 mM imidazole. Eluted proteins were concentrated and dialyzed in 50 mM Na_3PO_4, pH 8.0, 300mM NaCl, 1 mM β-ME at 4 °C overnight followed by a second 2 hour dialysis at 4 °C. The final protein concentration was calculated from the absorbance spectrum measured on a Nanodrop 2000 spectrophotometer (Thermo Scientific).

Quantification of connexon density on Connectosome surfaces. Purified SP100-YFP was serially diluted to generate a calibration curve of protein concentration. The YFP fluorescence of the calibration curve and a sample of 8.9 x 10^6 Connectosomes were measured in a BioTek Cytation 3 fluorimeter to calculate the average molar concentration of YFP molecules in the Connectosome sample. The molar concentration was converted

to number of YFP molecules and divided by the number of Connectosomes per sample to achieve an average number of connexin 43-YFP molecules per Connectosome. Finally, the surface area per Connectosome was calculated from the average diameter described above to determine a density of connexons per Connectosome. The percentage of the Connectosome surface covered by connexons was estimated using the approximate membrane area per connexon channel in cellular connexin plaques[38], 70 nm^2.

Calcein red-orange loading. A stock solution of calcein red-orange (CRO) acetomethoxy (AM) dye in DMSO was prepared at a concentration of 1.7 mg/mL and diluted to a final concentration of 17 ng/μL in GPMV buffer. To form CRO dye-loaded Connectosomes or MD-MB-231 plasma membrane blebs, donor cells were incubated in the CRO AM dye solution for 30 minutes immediately before extraction of membrane blebs.

Connexon function study. For the CRO dye release study, Connectosomes containing CRO dye were formed from donor cells as described above. Connexon channels were opened by removing calcium from the solution by adding EGTA and EDTA to a final concentration of 5 mM at pH greater than 8.5. Three independent samples of Connectosomes were imaged within 2 hours of EGTA and EDTA addition, and examined for luminal fluorescence above the background level. At least 54 Connectosomes were analyzed for each trial.

To demonstrate the connexon-dependence of the dye release, MDA-MB-231 plasma membrane blebs containing CRO dye were formed from MDA-MB-231 donor cells as described above. Connexon channels were opened by removing calcium from the solution by adding EGTA and EDTA to a final concentration of 5 mM. Three independent samples of MDA-MB-231 plasma membrane blebs were imaged within 2 hours of EGTA and EDTA addition, and examined for luminal fluorescence above the

background level. At least 36 MDA-MB-231 plasma membrane blebs were analyzed for each trial.

For the Atto 594 and Atto 488 studies, a 10 μM stock solution of Atto 594-NHS Ester (with NHS ester hydrolyzed) or Atto 488-NHS Ester (with NHS ester hydrolyzed) was prepared in GPMV buffer. Atto 594 was added to preformed Connectosomes in GPMV buffer at a final concentration of 20 nM, and Atto 488 was added to preformed Connectosomes at a final concentration of 200 nM. To remove calcium from solution, EGTA and EDTA were added to the Connectosomes as described above. Three independent samples of Connectosomes were imaged within 1 hour of EGTA and EDTA addition, and examined for luminal fluorescence above the background level. At least 51 Connectosomes were analyzed for each trial for the Atto 594 study, and at least 39 Connectosomes were analyzed for each trial for the Atto 488 study.

For the photobleaching study, Atto 594 dye within Connectosomes was bleached using a 561 nm laser on the spinning disk confocal microscope described above. Then, laser illumination was stopped and images were taken every 15 seconds for 75 seconds.

Dye delivery study. Recipient HeLa cells were plated in a 12 well plate at a density of 25,000 cells per well and a total media volume of 2 mL per well. Seven hours before addition of the Connectosomes, the recipient cells received fresh media. The media for the blocked condition was supplemented with 300 μM carbenoxolone, prepared from a 100 mM stock in water. Just before addition of the Connectosomes, the recipient cells were rinsed once with 2 mL PBS and then incubated in 500 μL fresh PBS. Recipient cells for the blocked condition were incubated in PBS supplemented with 300 μM carbenoxolone. For each trial, an independent sample of CRO dye-loaded Connectosomes was formed using GPMV buffer without calcium. Concentrated Connectosomes were resuspended in fresh GPMV buffer without calcium and counted

with a hemocytometer. Connectosomes were added to recipient cells at a ratio of approximately 1 Connectosome per 2 recipient cells and incubated in the dark at 37 °C and 5% CO_2 for 2 hours. This ratio was estimated based on hemocytometer counts of the number of collected Connectosomes and of the number of recipient cells in a single well of a 12 well plate. After incubation, the recipient cells were rinsed with 2 mL PBS to remove the Connectosomes and then imaged or prepared for flow cytometry. For flow cytometry, the recipient cells were trypsinized with 500 μL trypsin for 5 minutes at 37 °C, 5% CO_2 and then quenched with 1500 μL media and centrifuged for 5 minutes at 300 x g. The cell pellet was resuspended in 100 μL PBS before flow cytometry. At least 10,000 cells were analyzed for each trial. In a separate experiment, CRO dye-loaded plasma membrane vesicles derived from A549 cells were incubated with recipient HeLa cells plated in a 96 well plate at 6,000 cells per well for one hour before being analyzed using flow cytometry as described above. An equivalent number of CRO dye-loaded Connectosomes were incubated with a separate population of recipient HeLa cells.

Doxorubicin loading. A 10 mM stock solution of doxorubicin was prepared in DMSO. To form doxorubicin-loaded Connectosomes, donor cells were incubated in a 1 mM doxorubicin solution in active buffer without calcium for 30 minutes immediately before Connectosome formation. After 30 minutes, the doxorubicin was diluted to a final concentration of 200 μM in active buffer without calcium and remained throughout the duration of blebbing. After formation, doxorubicin-loaded Connectosomes were collected as described above and then washed with 1 mL fresh GPMV buffer without calcium. Connectosomes were then resuspended in fresh GPMV buffer without calcium.

Doxorubicin encapsulation measurement. To estimate the amount of doxorubicin encapsulated within the Connectosomes, free doxorubicin was serially diluted to generate a calibration concentration curve (n=3). The doxorubicin fluorescence

of the calibration curve, 3 independent samples of 3 x 10^5 doxorubicin-loaded Connectosomes, and 3 independent samples of 3 x 10^5 empty Connectosomes was measured in a BioTek Cytation 3 fluorimeter to determine the average molar doxorubicin concentration of the Connectosome samples. This molar concentration was converted to moles of doxorubicin and divided by the approximate total volume of all Connectosomes (based on the number of Connectosomes in the sample and the average diameter of Connectosomes) present in the sample to estimate the concentration of doxorubicin inside the Connectosomes.

Doxorubicin release study. Doxorubicin-loaded Connectosomes were formed as described above. The initial doxorubicin content of the Connectosomes was measured using flow cytometry. EGTA and EDTA were added to the Connectosome solution as described above in the connexon function studies in order to open the connexon channels. Using flow cytometry, the final doxorubicin content of the Connectosomes was then measured 5 minutes after EGTA and EDTA addition. Three independent Connectosome samples were analyzed for each condition, and at least 800 Connectosomes were analyzed for each trial.

Doxorubicin cytotoxicity study. Recipient HeLa cells were plated in a 12 well plate at a density of 25,000 cells per well and a total media volume of 2 mL media per well. Recipient MCF-7 cells were plated in a 48 well plate at a density of 100,000 cells per well and a total media volume of 2mL media per well. Seven hours before addition of the Connectosomes, recipient cells received fresh media. Just before addition of the Connectosomes, the recipient HeLa cells were rinsed once with 2 mL PBS and then incubated in 500 μL fresh PBS, while the recipient MCF-7 cells were rinsed once with 2mL media and then incubated in 500 μL fresh media. For each trial, a sample of doxorubicin-loaded Connectosomes was formed as described above. Concentrated

Connectosomes were resuspended in fresh GPMV buffer without calcium and counted using a hemocytometer. The doxorubicin encapsulated within each sample of Connectosomes was determined as described above. Connectosomes were added to recipient cells at increasing equivalent doxorubicin doses and incubated in the dark at 37 °C with 5% CO_2 for 2 hours (recipient HeLa cells) or 48 hours (recipient MCF-7 cells). After incubation, the recipient cells were rinsed with 2 mL media and then incubated in 2 mL fresh media at 37 °C with 5% CO_2. After 24 hours, HeLa cell viability was analyzed using a trypan blue or 7-AAD assay. MCF-7 cell viability was analyzed directly after Connectosome incubation using a trypan blue assay.

For the trypan blue assay, the cells were detached with 500 μL trypsin for 5 minutes at 37 °C, 5% CO_2. Trypsinized cells were then quenched with 1.5 mL media and pelleted for 5 minutes at 300 x g. The cell pellet was resuspended in 200 μL media, and trypan blue was added to the cells at a volume ratio of 1:1. At least 93 cells were counted for each trial using a hemocytometer. Cells including the trypan blue stain were considered non-viable and cells excluding the trypan blue were considered viable.

For the 7-AAD assay, the cells were trypsinized with 500 μL trypsin for 5 minutes at 37 °C, 5% CO_2. Trypsinized cells were then quenched with 1.5 mL media and centrifuged for 5 minutes at 300 x g. The cell pellet was resuspended in 100 μL PBS. Five μL of 7-AAD was added to 45 μL of the resuspended cells, and analyzed using flow cytometry three minutes after 7-AAD addition. At least 5,000 cells were analyzed for each trial. To determine the percentage of non-viable cells in each sample, a threshold was drawn on the flow cytometry fluorescence histograms at the minimum point between the population of cells excluding the dye and the population of cells including the dye (See fig. S4). The percentage of cells with fluorescence above these thresholds were considered non-viable.

The relationship between the concentration of doxorubicin added via solution and cell viability was determined by incubating recipient HeLa cells in the specified doxorubicin concentration diluted in media from a 10 mM stock in DMSO for 24 hours. Cell viability was measured using both viability assays as described above.

The relationship between the concentration of doxorubicin added via conventional liposomal doxorubicin (Dox-NPs) and cell viability was determined by incubating recipient HeLa cells in the specified doxorubicin concentration diluted in media for 24 hours. Cell viability was measured using both viability assays as described above. The concentration of doxorubicin within DOX-NPs was provided by the manufacturer.

***Statistical analysis*.** As noted throughout the main text and methods sections, at least three independent trials are reported for all experimental results. In each case where a statistically significant comparison is reported based on this data (Figs. 2B, 2G, 3D-E, 4E), an unpaired, two-tailed student's t-test, with unequal sample variance, was performed and yielded a probability value no greater than 5%.

References

1. Lipinski, C. A.; Lombardo, F.; Dominy, B. W.; Feeney, P. J., Experimental and computational approaches to estimate solubility and permeability in drug discovery and development settings. Advanced Drug Delivery Reviews 1997, 23 (1-3), 3-25.
2. Damaraju, V. L.; Damaraju, S.; Young, J. D.; Baldwin, S. A.; Mackey, J.; Sawyer, M. B.; Cass, C. E., Nucleoside anticancer drugs: the role of nucleoside transporters in resistance to cancer chemotherapy. Oncogene 2003, 22 (47), 7524-7536.
3. Barenholz, Y., Liposome application: problems and prospects. Curr Opin Colloid In 2001, 6 (1), 66-77.
4. Barenholz, Y., Doxil (R) - The first FDA-approved nano-drug: Lessons learned. Journal of Controlled Release 2012, 160 (2), 117-134.
5. Durand, R. E.; Olive, P. L., FLOW-CYTOMETRY STUDIES OF INTRACELLULAR ADRIAMYCIN IN SINGLE CELLS-INVITRO. Cancer Research 1981, 41 (9), 3489-3494.
6. Ewer, M. S.; Ewer, S. M., Cardiotoxicity of anticancer treatments. Nature reviews. Cardiology 2015, 12 (9), 547-58.
7. Gottesman, M. M.; Fojo, T.; Bates, S. E., Multidrug resistance in cancer: role of ATP-dependent transporters. Nat Rev Cancer 2002, 2 (1), 48-58.
8. Overington, J. P.; Al-Lazikani, B.; Hopkins, A. L., Opinion - How many drug targets are there? Nature Reviews Drug Discovery 2006, 5 (12), 993-996.

9. Mitragotri, S.; Burke, P. A.; Langer, R., Overcoming the challenges in administering biopharmaceuticals: formulation and delivery strategies. Nature Reviews Drug Discovery 2014, 13 (9), 655-672.

10. Phillips, M. A.; Gran, M. L.; Peppas, N. A., Targeted nanodelivery of drugs and diagnostics. Nano Today 2010, 5 (2), 143-159.

11. Peer, D.; Karp, J. M.; Hong, S.; FaroKhzad, O. C.; Margalit, R.; Langer, R., Nanocarriers as an emerging platform for cancer therapy. Nat Nanotechnol 2007, 2 (12), 751-760.

12. Sahay, G.; Alakhova, D. Y.; Kabanov, A. V., Endocytosis of nanomedicines. Journal of Controlled Release 2010, 145 (3), 182-195.

13. Thevenin, D.; An, M.; Engelman, D. M., pHLIP-Mediated Translocation of Membrane-Impermeable Molecules into Cells. Chemistry & Biology 2009, 16 (7), 754-762.

14. Yanes, R. E.; Tarn, D.; Hwang, A. A.; Ferris, D. P.; Sherman, S. P.; Thomas, C. R.; Lu, J.; Pyle, A. D.; Zink, J. I.; Tamanoi, F., Involvement of lysosomal exocytosis in the excretion of mesoporous silica nanoparticles and enhancement of the drug delivery effect by exocytosis inhibition. Small 2013, 9 (5), 697-704.

15. Bareford, L. A.; Swaan, P. W., Endocytic mechanisms for targeted drug delivery. Advanced Drug Delivery Reviews 2007, 59 (8), 748-758.

16. Horowitz, A. T.; Barenholz, Y.; Gabizon, A. A., INVITRO CYTOTOXICITY OF LIPOSOME-ENCAPSULATED DOXORUBICIN - DEPENDENCE ON LIPOSOME COMPOSITION AND DRUG RELEASE. Biochimica Et Biophysica Acta 1992, 1109 (2), 203-209.

17. Murthy, N.; Robichaud, J. R.; Tirrell, D. A.; Stayton, P. S.; Hoffman, A. S., The design and synthesis of polymers for eukaryotic membrane disruption. Journal of Controlled Release 1999, 61 (1-2), 137-143.

18. Li, M.; Tao, Y.; Shu, Y.; LaRochelle, J. R.; Steinauer, A.; Thompson, D.; Schepartz, A.; Chen, Z. Y.; Liu, D. R., Discovery and characterization of a peptide that enhances endosomal escape of delivered proteins in vitro and in vivo. Journal of the American Chemical Society 2015, 137 (44), 14084-93.

19. Ganta, S.; Devalapally, H.; Shahiwala, A.; Amiji, M., A review of stimuli-responsive nanocarriers for drug and gene delivery. Journal of Controlled Release 2008, 126 (3), 187-204.

20. Mura, S.; Nicolas, J.; Couvreur, P., Stimuli-responsive nanocarriers for drug delivery. Nature Materials 2013, 12 (11), 991-1003.

21. Caldorera-Moore, M.; Guimard, N.; Shi, L.; Roy, K., Designer nanoparticles: incorporating size, shape and triggered release into nanoscale drug carriers. Expert Opin Drug Deliv 2010, 7 (4), 479-495.

22. Lee, E. S.; Na, K.; Bae, Y. H., Doxorubicin loaded pH-sensitive polymeric micelles for reversal of resistant MCF-7 tumor. Journal of Controlled Release 2005, 103 (2), 405-418.

23. Ashley, C. E.; Carnes, E. C.; Phillips, G. K.; Padilla, D.; Durfee, P. N.; Brown, P. A.; Hanna, T. N.; Liu, J. W.; Phillips, B.; Carter, M. B.; Carroll, N. J.; Jiang, X. M.; Dunphy, D. R.; Willman, C. L.; Petsev, D. N.; Evans, D. G.; Parikh, A. N.; Chackerian, B.; Wharton, W.; Peabody, D. S.; Brinker, C. J., The targeted delivery of multicomponent cargos to cancer cells by nanoporous particle-supported lipid bilayers. Nature Materials 2011, 10 (5), 389-397.

24. Park, J. H.; Gu, L.; von Maltzahn, G.; Ruoslahti, E.; Bhatia, S. N.; Sailor, M. J., Biodegradable luminescent porous silicon nanoparticles for in vivo applications. Nature Materials 2009, 8 (4), 331-336.

25. Wang, S. G.; Wu, Y. L.; Guo, R.; Huang, Y. P.; Wen, S. H.; Shen, M. W.; Wang, J. H.; Shi, X. Y., Laponite Nanodisks as an Efficient Platform for Doxorubicin Delivery to Cancer Cells. Langmuir 2013, 29 (16), 5030-5036.

26. Sakhtianchi, R.; Minchin, R. F.; Lee, K. B.; Alkilany, A. M.; Serpooshan, V.; Mahmoudi, M., Exocytosis of nanoparticles from cells: role in cellular retention and toxicity. Adv Colloid Interface Sci 2013, 201-202, 18-29.

27. El-Sayed, A.; Futaki, S.; Harashima, H., Delivery of Macromolecules Using Arginine-Rich Cell-Penetrating Peptides: Ways to Overcome Endosomal Entrapment. Aaps Journal 2009, 11 (1), 13-22.

28. Erazo-Oliveras, A.; Muthukrishnan, N.; Baker, R.; Wang, T. Y.; Pellois, J. P., Improving the endosomal escape of cell-penetrating peptides and their cargos: strategies and challenges. Pharmaceuticals (Basel) 2012, 5 (11), 1177-209.

29. Gilleron, J.; Querbes, W.; Zeigerer, A.; Borodovsky, A.; Marsico, G.; Schubert, U.; Manygoats, K.; Seifert, S.; Andree, C.; Stoter, M.; Epstein-Barash, H.; Zhang, L.; Koteliansky, V.; Fitzgerald, K.; Fava, E.; Bickle, M.; Kalaidzidis, Y.; Akinc, A.; Maier, M.; Zerial, M., Image-based analysis of lipid nanoparticle-mediated siRNA delivery, intracellular trafficking and endosomal escape. Nature biotechnology 2013, 31 (7), 638-46.

30. Neijssen, J.; Herberts, C.; Drijfhout, J. W.; Reits, E.; Janssen, L.; Neefjes, J., Cross-presentation by intercellular peptide transfer through gap junctions. Nature 2005, 434 (7029), 83-88.

31. Evans, W. H.; Martin, P. E. M., Gap junctions: structure and function (Review). Molecular Membrane Biology 2002, 19 (2), 121-136.

32. Yamasaki, H.; Krutovskikh, V.; Mesnil, M.; Tanaka, T.; Zaidan-Dagli, M. L.; Omori, Y., Role of connexin (gap junction) genes in cell growth control and carcinogenesis. C R Acad Sci III 1999, 322 (2-3), 151-9.

33. Huang, R. P.; Hossain, M. Z.; Huang, R.; Gano, J.; Fan, Y.; Boynton, A. L., Connexin 43 (cx43) enhances chemotherapy-induced apoptosis in human glioblastoma cells. International Journal of Cancer 2001, 92 (1), 130-138.

34. Garcia-Rodriguez, L.; Perez-Torras, S.; Carrio, M.; Cascante, A.; Garcia-Ribas, I.; Mazo, A.; Fillat, C., Connexin-26 is a key factor mediating gemcitabine bystander effect. Mol Cancer Ther 2011, 10 (3), 505-17.

35. Mesnil, M.; Piccoli, C.; Tiraby, G.; Willecke, K.; Yamasaki, H., Bystander killing of cancer cells by herpes simplex virus thymidine kinase gene is mediated by connexins. P Natl Acad Sci USA 1996, 93 (5), 1831-5.

36. Kaneda, M.; Nomura, S. M.; Ichinose, S.; Kondo, S.; Nakahama, K.; Akiyoshi, K.; Morita, I., Direct formation of proteo-liposomes by in vitro synthesis and cellular cytosolic delivery with connexin-expressing liposomes. Biomaterials 2009, 30 (23-24), 3971-7.

37. Charras, G.; Paluch, E., Blebs lead the way: how to migrate without lamellipodia. Nature Reviews Molecular Cell Biology 2008, 9 (9), 730-736.

38. Chen, L.; Novicky, L.; Merzlyakov, M.; Hristov, T.; Hristova, K., Measuring the energetics of membrane protein dimerization in mammalian membranes. Journal of the American Chemical Society 2010, 132 (10), 3628-35.

39. Costello, D. A.; Hsia, C. Y.; Millet, J. K.; Porri, T.; Daniel, S., Membrane fusion-competent virus-like proteoliposomes and proteinaceous supported bilayers made

directly from cell plasma membranes. Langmuir : the ACS journal of surfaces and colloids 2013, 29 (21), 6409-19.

40. Zhao, C.; Busch, D. J.; Vershel, C. P.; Stachowiak, J. C., Multifunctional Transmembrane Protein Ligands for Cell-Specific Targeting of Plasma Membrane-Derived Vesicles. Small 2016, 12 (28), 3837-48.

41. Simons, M.; Raposo, G., Exosomes--vesicular carriers for intercellular communication. Current opinion in cell biology 2009, 21 (4), 575-81.

42. S, E. L. A.; Mager, I.; Breakefield, X. O.; Wood, M. J., Extracellular vesicles: biology and emerging therapeutic opportunities. Nature reviews. Drug discovery 2013, 12 (5), 347-57.

43. Sezgin, E.; Kaiser, H.-J.; Baumgart, T.; Schwille, P.; Simons, K.; Levental, I., Elucidating membrane structure and protein behavior using giant plasma membrane vesicles. Nature Protocols 2012, 7 (6), 1042-1051.

44. Soares, A. R.; Martins-Marques, T.; Ribeiro-Rodrigues, T.; Ferreira, J. V.; Catarino, S.; Pinho, M. G.; Zuzarte, M.; Anjo, S. I.; Manadas, B.; Sluijter, J. P. G.; Pereira, P.; Girao, H., Gap junctional protein Cx43 is involved in the communication between extracellular vesicles and mammalian cells. Scientific Reports 2015, 5, 13.

45. Allen, M. J.; Gemel, J.; Beyer, E. C.; Lal, R., Atomic force microscopy of Connexin40 gap junction hemichannels reveals calcium-dependent three-dimensional molecular topography and open-closed conformations of both the extracellular and cytoplasmic faces. The Journal of biological chemistry 2011, 286 (25), 22139-46.

46. Thimm, J.; Mechler, A.; Lin, H.; Rhee, S.; Lal, R., Calcium-dependent open/closed conformations and interfacial energy maps of reconstituted hemichannels. Journal of Biological Chemistry 2005, 280 (11), 10646-10654.

47. Muller, D. J.; Hand, G. M.; Engel, A.; Sosinsky, G. E., Conformational changes in surface structures of isolated connexin 26 gap junctions. Embo Journal 2002, 21 (14), 3598-3607.

48. Elzarrad, M. K.; Haroon, A.; Willecke, K.; Dobrowolski, R.; Gillespie, M. N.; Al-Mehdi, A. B., Connexin-43 upregulation in micrometastases and tumor vasculature and its role in tumor cell attachment to pulmonary endothelium. BMC Med 2008, 6, 20.

49. Qin, H.; Shao, Q.; Curtis, H.; Galipeau, J.; Belliveau, D. J.; Wang, T.; Alaoui-Jamali, M. A.; Laird, D. W., Retroviral delivery of connexin genes to human breast tumor cells inhibits in vivo tumor growth by a mechanism that is independent of significant gap junctional intercellular communication. The Journal of biological chemistry 2002, 277 (32), 29132-8.

50. Hughes, L. D.; Rawle, R. J.; Boxer, S. G., Choose your label wisely: water-soluble fluorophores often interact with lipid bilayers. PLoS One 2014, 9 (2), e87649.

51. Preus, D.; Johnson, R.; Sheridan, J.; Meyer, R., ANALYSIS OF GAP-JUNCTIONS AND FORMATION PLAQUES BETWEEN REAGGREGATING NOVIKOFF HEPATOMA-CELLS. Journal of Ultrastructure Research 1981, 77 (3), 263-276.

52. Segretain, D.; Falk, M. A., Regulation of connexin biosynthesis, assembly, gap junction formation, and removal. Biochim. Biophys. Acta-Biomembr. 2004, 1662 (1-2), 3-21.

53. Connors, B. W., Tales of a dirty drug: carbenoxolone, gap junctions, and seizures. Epilepsy Curr 2012, 12 (2), 66-8.

54. Hada, S.; Sato, H.; Virgona, N.; Hagiwara, H.; Saito, T.; Suzuki, K.; Asano, R.; Yano, T., Connexin 32 expression reduces malignant phenotype in human A549 adenocarcinoma cells: Implication of Src involvement. Oncol Rep 2006, 16 (5), 1149-54.

55. Maeda, H.; Wu, J.; Sawa, T.; Matsumura, Y.; Hori, K., Tumor vascular permeability and the EPR effect in macromolecular therapeutics: a review. Journal of Controlled Release 2000, 65 (1-2), 271-284.

56. Safra, T.; Muggia, F.; Jeffers, S.; Tsao-Wei, D. D.; Groshen, S.; Lyass, O.; Henderson, R.; Berry, G.; Gabizon, A., Pegylated liposomal doxorubicin (doxil): Reduced clinical cardiotoxicity in patients reaching or exceeding cumulative doses of 500 mg/m(2). Annals of Oncology 2000, 11 (8), 1029-1033.

57. Ohno, S.-i.; Takanashi, M.; Sudo, K.; Ueda, S.; Ishikawa, A.; Matsuyama, N.; Fujita, K.; Mizutani, T.; Ohgi, T.; Ochiya, T.; Gotoh, N.; Kuroda, M., Systemically Injected Exosomes Targeted to EGFR Deliver Antitumor MicroRNA to Breast Cancer Cells. Molecular Therapy 2013, 21 (1), 185-191.

58. Nurcahyanti, A. D.; Wink, M., L-Canavanine potentiates the cytotoxicity of doxorubicin and cisplatin in arginine deprived human cancer cells. PeerJ 2016, 4, e1542.

59. Kirpotin, D. B.; Drummond, D. C.; Shao, Y.; Shalaby, M. R.; Hong, K.; Nielsen, U. B.; Marks, J. D.; Benz, C. C.; Park, J. W., Antibody targeting of long-circulating lipidic nanoparticles does not increase tumor localization but does increase internalization in animal models. Cancer Res 2006, 66 (13), 6732-40.

60. Kamba, A. S.; Ismail, M.; Ibrahim, T. A.; Zakaria, Z. A.; Gusau, L. H., In vitro ultrastructural changes of MCF-7 for metastasise bone cancer and induction of apoptosis via mitochondrial cytochrome C released by CaCO3/Dox nanocrystals. Biomed Res Int 2014, 2014, 391869.

Chapter 3: Connectosomes for Direct and Specific Molecular Delivery to the Cellular Cytoplasm

Abstract

Gap junctions are a promising new frontier for therapeutic delivery. Connectosomes, an emerging technology, are cell-derived vesicles that are capable of forming gap junctions with cells and delivering their encapsulated cargo directly to the cytoplasm. Remarkably, by using gap junctions to create a direct route for molecular transport that bypasses the plasma membrane barrier, these materials dramatically increase the effectiveness of chemotherapeutic drugs. However, nonspecific interactions of these particles with healthy tissues is a major obstacle that limits their potential as relevant therapeutic vehicles. To achieve directed cytoplasmic delivery, we have developed targeted Connectosomes. Specifically, by embedding multi-functional, multi-domain targeting proteins into the membrane surfaces of Connectosomes, we demonstrate their ability to selectively interact with target cells on the basis of cell-surface receptor expression. Here we show that targeting enhances Connectosome binding to target cells, and selectively increases the efficiency of cytoplasmic transport. Further, using targeted Connectosomes to deliver the chemotherapeutic drug doxorubicin reduces the therapeutically effective dose of the drug by a factor of two for target cells. More generally, our approach has the potential to boost cytoplasmic delivery of diverse therapeutic molecules to specific cell populations while protecting off-target cells, a critical step toward realizing the therapeutic potential of gap junctions.

Introduction

Gap junctions, transmembrane channels that connect the cytoplasm of adjacent cells, are emerging as a promising new route for therapeutic drug delivery[1-4]. Formed from hexameric connexin proteins, gap junctions are traditionally considered to be facilitators for exchange of metabolites, ions, second messengers and other signaling molecules between cells[5]. However, gap junctions also enable drug transfer between cells through the bystander effect[6], in which therapeutics permeate tissues by using gap junctions to pass from the cytoplasm of one cell to its neighbors. Through this intriguing phenomenon, gap junctions enhance the efficacy of numerous therapeutics, including paclitaxel[7], doxorubicin[7], gemcitabine[8], etoposide[7], and others[9], demonstrating the potential importance of gap junctions as therapeutic conveyers. Further, it has recently been proposed that the presence of gap junction channels in exosomes underlies their ability to deliver siRNA, further suggesting their therapeutic potential[2].

Inspired by the natural ability of cells to transfer chemotherapeutics between gap junctions, we recently developed Connectosomes, cell-derived lipid vesicles that contain functional, embedded gap junction channels[1]. Capable of forming complete gap junctions with cells, Connectosomes increase the efficacy of doxorubicin delivery by several orders of magnitude compared to traditional liposomal formulations of doxorubicin, illustrating the therapeutic importance of direct access to the cell cytoplasm. By creating a new avenue for molecular transport that bypasses the plasma membrane barrier, Connectosomes and other gap junction vesicles[4] create a path forward for efficient cytoplasmic delivery of diverse molecules, such as existing therapeutics as well as membrane-impermeable drugs and reagents. However, since connexin proteins are found ubiquitously in cells throughout the tissue of the body[10], nonspecific drug interactions with healthy tissues could limit the translational relevance of these vesicles. Therefore,

development of a chemotherapeutic delivery system that can both efficiently and selectively kill diseased cells while protecting healthy, off-target tissue is an important step in the realization of gap junction-based therapeutic delivery approaches.

To precisely target tumor cells, biochemical moieties that recognize tumor-specific cell surface receptors can be incorporated onto the surfaces of therapeutic delivery particles[11]. By promoting preferential interaction of the particles with tumor cells that overexpress specific receptors, these targeting ligands improve the specificity of drug delivery. The advantages of targeting have been well-documented for synthetic nanoparticles, as ligands including antibodies[12-14], organic compounds[15, 16], and peptides[17] have been used to direct therapeutics to a diverse range of specific cell populations[18]. These approaches have also been extended to cell-derived materials. For example, folic acid has been conjugated to virus-like particles for doxorubicin delivery to ovarian cancer cells[19], anti-CD43 antibodies have been conjugated to red blood cells to target CD43 positive leukocytes[20], and iron oxide nanoparticles have been conjugated to cell-derived microvesicles to deliver doxorubicin to target tissues via an external magnetic field[21].

However, chemical conjugation of targeting moieties to nanoparticles inherently limits the complexity of these approaches. More recently, several groups have harnessed the cell's own machinery to incorporate targeting peptides into cell-derived vesicles[22]. For example, RVG peptide has been used to target exosomes to acetylcholine receptors in the brain for siRNA delivery[23], GE11 peptide has been used to target exosomes to EGFR receptors in breast cancer cells for miRNA delivery[24], iRGD peptide has been used to target exosomes to integrin breast cancer cells for doxorubicin delivery[25], and CCR5 has been used to target cell-derived liposomes to HIV-infected cells for EDTA delivery[26]. Inspired by this work but desiring a more tunable system, capable of fully harnessing the cell's ability to manufacture complex, sophisticated macromolecules, our group recently

engineered a set of multi-functional, multi-domain transmembrane targeting ligands, which selectively increase vesicle binding by a ratio of 50:1[27].

Towards designing a targeted drug delivery system which can deliver therapeutic molecules directly into the cytoplasm of a specific population of target cells, here we have incorporated previously designed multi-functional, multi-domain transmembrane targeting proteins[27] into Connectosomes. Specifically, we have engineered a mammalian cell line which co-expresses connexin 43-YFP and a targeting protein, comprised of a transmembrane anchor domain and a multi-functional extracellular domain. Here, the multi-functional extracellular domain includes a fluorophore domain for visualization, an intrinsically disordered linker domain to prevent steric inhibition, and an affinity domain comprised of a single domain camelid antibody against enhanced green fluorescent protein (eGFP). Our results show that targeting selectively enhances Connectosome binding to target cells by thirty times compared to off-target cells. Additionally, targeting selectively increases the efficiency of dye transport to the cytoplasm of target cells by five times. Further, using targeted Connectosomes to deliver doxorubicin reduces the therapeutically effective dose (LD50) by a factor of 2 for target cells, compared to off-target cells. Taken together, these data illustrate the potential of targeted Connectosomes to serve as efficient vehicles for targeted molecular delivery of chemotherapeutics and other diverse drugs to the cell cytoplasm.

Results and Discussion

Targeted Connectosome development

To achieve targeted cytoplasmic delivery, we began by incorporating a chimeric targeting protein into the surfaces of the Connectosomes. To demonstrate this general targeting strategy, we utilized a previously developed multifunctional targeting protein

engineered to selectively bind to any plasma membrane receptor with an eGFP modification in its extracellular domain[27]. Notably, the targeting protein could be restructured to selectively bind to other, disease-relevant receptors, such as the epidermal growth factor receptor (EGFR), which is a popular target for therapeutic delivery systems[28]. However, in this study, we targeted eGFP-tagged receptors in order to isolate the absolute binding specificity of the targeted Connectosomes, as cells do not endogenously express these fluorescently-tagged receptors.

Our targeting protein was comprised of five domains: the intracellular and transmembrane domains of transferrin receptor, an mRFP fluorophore domain, an intrinsically disordered linker domain comprised of the first 289 amino acids of AP180, and an affinity domain. Here, the affinity domain consisted of a single domain camelid antibody against eGFP, a nanobody targeting ligand that specifically recognizes eGFP and can therefore be used to precisely target cells on the basis of their expression of eGFP-tagged plasma membrane receptors[27, 29].

To produce targeted Connectosomes, we co-expressed the eGFP nanobody targeting protein (GFPnb-mRFP) in donor HeLa cells that also expressed a fluorescently tagged connexin protein (Cx43-YFP) (Figure 3.1a-d). By inducing these donor HeLa cells to bleb using established protocols[1, 27, 30], we extracted targeted Connectosomes, plasma membrane vesicles that contained both connexin and targeting proteins embedded in their surfaces (Figure 3.1a-d). Plasma membrane blebbing occurs when the cytoskeleton's attachments to the plasma membrane are disrupted, which can occur naturally during cellular processes such as cell motility or cytokinesis[31], or as a result of chemical induction[30]. Transmembrane proteins embedded in the plasma membrane vesicles that form during blebbing maintain their function and orientation in the membrane[32], and ours and other groups have recently harnessed this ability in order to

develop therapeutic materials that depend on the functionality of embedded transmembrane proteins[1, 27, 33]. Exosomes are similar cell-derived materials with emerging therapeutic potential[34]. However, because protein trafficking to the plasma membrane is well understood compared to our understanding of how proteins arrive in exosomal membranes[35], controlled incorporation of transmembrane proteins into plasma membrane vesicles through blebbing is relatively simpler. Therefore, blebbing was used to produce targeted Connectosomes for these studies.

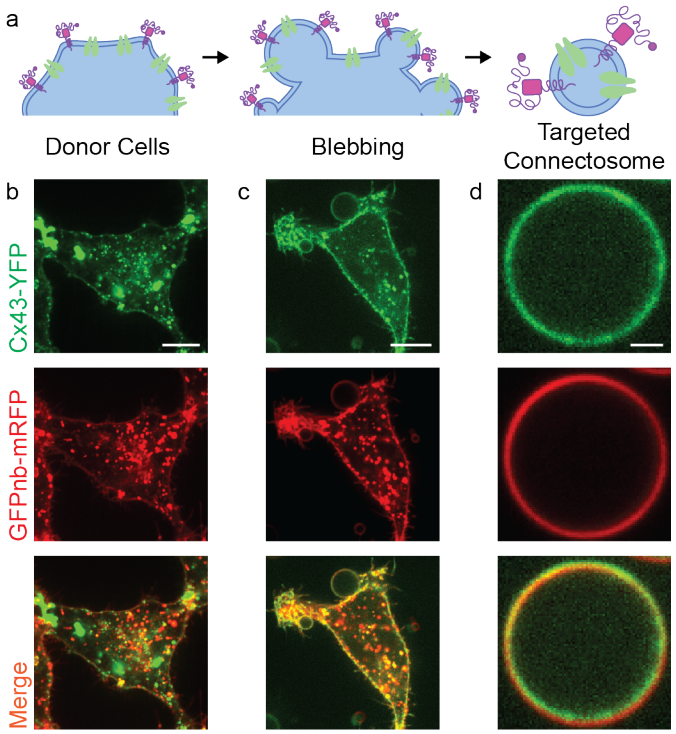

Figure 3.1: **Targeted Connectosomes were harvested from donor cells.** Confocal fluorescence images. (a), Schematic of the targeted Connectosome formation process. (b-d), Giant plasma membrane vesicles were harvested from donor cells co-expressing connexin 43-YFP (green) and an RFP-tagged GFP nanobody targeting protein (red) to produce targeted Connectosomes. Scale bar in (b) and (c), 10 μm. Scale bar in (d), 2 μm. Images intentionally saturated to show membrane expression of the connexin and targeting proteins.

To test the accessibility and functionality of the eGFP nanobody embedded in the targeted Connectosomes, we first exposed HeLa cells expressing the targeting protein to soluble eGFP. To enable detection of eGFP binding to the cells, it was necessary here to use cells without fluorescent connexin proteins, as the fluorescent signatures of YFP and eGFP are difficult to distinguish. Fluorescence imaging revealed that soluble eGFP bound significantly to cells expressing the eGFP nanobody, but did not bind to cells lacking expression of the targeting protein (Figure 3.2a-b). Then, to investigate whether the targeting protein retained its ability to bind eGFP throughout the blebbing process, we exposed cells in the process of blebbing to soluble eGFP. Blebbing cells also recruited the fluorophore, as did vesicles incubated with soluble eGFP, demonstrating that the targeting protein retained its accessibility and functionality throughout the process of vesicle formation (Figure 3.2a). Further, fluorescence intensity comparisons of the eGFP and mRFP fluorophores revealed that the amount of eGFP bound to each vesicle increased with the amount of targeting protein present on the vesicle surface, similarly to previous studies on vesicles containing the same targeting protein but derived from a different cell line[27] (Figure 3.2c). Taken together, these data demonstrate that the targeted Connectosomes contain accessible, functional targeting proteins capable of binding to eGFP.

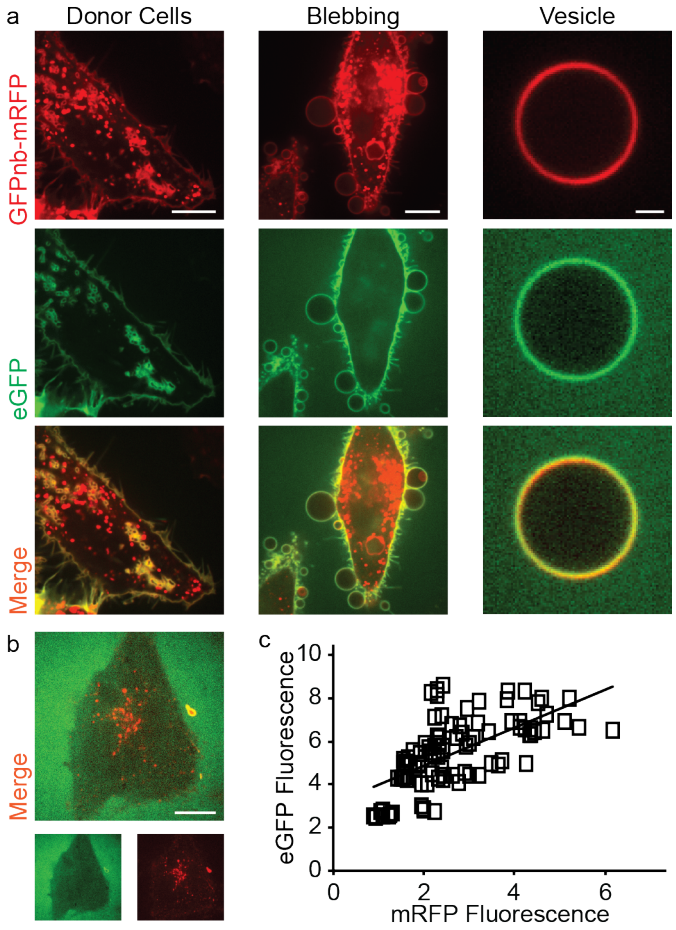

Figure 3.2: **Soluble eGFP recruitment depends on targeting protein expression.** (a), Soluble eGFP (green) is recruited to cells expressing the targeting protein at each stage of the Connectosome formation process. Scale bars in left and middle column 10 μm, right column 5 μm. (b) Soluble eGFP is not recruited to cells lacking significant targeting protein expression at the plasma membrane. Scale bar 10 μm. (c), Binding of soluble eGFP is positvely correlated with targeting protein expression. 45 vesicles analyzed in two membrane regions, each represented by a single point on the plot. Images intentionally saturated to show membrane expression of the targeting proteins.

Targeting selectively enhanced Connectosome binding to target cells

Having demonstrated the functionality of the targeting ligands, we next examined the ability of the targeted Connectosomes to bind target cells. Unprocessed Connectosomes have an average diameter of approximately 10 μm[1], but to minimize gravitational settling[27] and increase therapeutic relevance, targeted Connectosomes were extruded using a 1 μm filter for this study. To measure the baseline level of nonspecific interactions of the targeted Connectosomes with off-target cells, extruded, targeted Connectosomes were incubated with confluent monolayers of recipient HeLa cells, as these cells lack eGFP expression. Using established flow cytometry protocols[27], binding was quantified by measuring the increase in mRFP fluorescence of the recipient cells four hours after addition of the vesicles (Figure 3.3a, left). Addition of the targeted Connectosomes increased the average mRFP fluorescence of the recipient off-target cells by less than 3000 (a.u.) (Figure 3.3b-c). Then, to investigate the ability of targeted Connectosomes to bind to target cells, extruded, targeted Connectosomes were incubated with confluent monolayers of HeLa cells expressing a chimeric transmembrane eGFP receptor protein (eGFPr). The eGFP receptor was comprised of the intracellular and transmembrane domains of the transferrin receptor, and an eGFP ectodomain. Addition of the targeted Connectosomes increased the average mRFP fluorescence of the recipient target cells by nearly 32,000 (a.u.) (Figure 3.3a, bottom; b-c). This ten-fold increase in the shift in average mRFP fluorescence upon vesicle addition demonstrates that the incorporation of the targeting protein in the Connectosomes enhances target cell binding substantially. Fluorescence imaging of these cells further confirmed that targeted Connectosomes bound extensively to the surfaces of target cells, and bound minimally to off-target cells (Figure 3.3d-e). Taken together, these data suggest that targeting selectively enhances Connectosome binding to target cells.

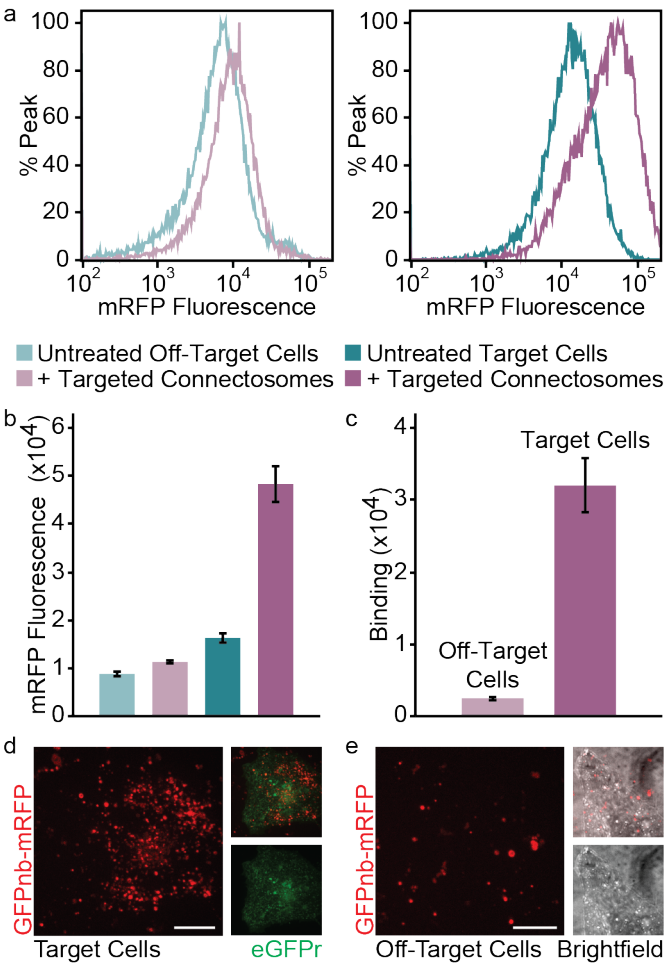

Figure 3.3: **Targeting enhanced Connectosome binding to target cells.** (a) Flow cytometry histograms showing mRFP fluorescence for recipient off-target (left) and target (right) cells before (blue) and after (purple) incubation with extruded, targeted Connectosomes. Each curve represents 3 independent, concatenated trials, 5,000 cells analyzed per trial. (b), Average recipient cell mRFP fluorescence for each condition. The error bars represent the standard deviations of 3 independent trials, 5,000 cells analyzed per trial. (c), Average increase in mRFP fluorescence after incubation with targeted Connectosomes for off-target and target cells represents the extent to which binding occurred. The error bars represent the standard deviations of 3 independent trials, 5,000 cells analyzed per trial. (d), Confocal fluorescence image showing targeted Connectosomes bound to target cells. (e), Confocal fluorescence image showing that off-target cells recruit targeted Connectosomes much less significantly. All scale bars 10 μm. Legend in (a) applies to (b) and (c).

To further demonstrate the dependence of targeted Connectosome binding on eGFP receptor expression, we then analyzed the relationship between binding and the eGFP receptor expression level of the target cells. Specifically, using the eGFP fluorescence of the untreated target cells as an indicator for eGFP receptor expression level, target cells were equally distributed between five cell groups with increasing eGFP receptor expression, such that each group contained 20% of the total cell population (Figure 3.4a). The average eGFP fluorescence for these groups increased from 150,000 (a.u.) for the group with the lowest eGFP receptor expression, to 2,750,000 (a.u.) for the group with the highest eGFP receptor expression (Figure 3.4b). For each cell group, binding was quantified by measuring the increase in average mRFP fluorescence after incubation with targeted Connectosomes (Figure 3.4c-e). As expected, we found that Connectosome binding increased with increasing eGFP receptor expression. For example, the group of target cells with the lowest eGFP receptor expression had an increase in mRFP fluorescence of only 6,000 (a.u.) after incubation with targeted Connectosomes. However, for the group of target cells with the highest eGFP receptor expression, the increase in mRFP fluorescence after addition of the targeted Connectosomes was 65,000 (a.u.). Further, as the eGFP receptor expression increases, the increase in mRFP fluorescence begins to plateau, indicating that the binding is saturated, and perhaps suggesting that if more targeted Connectosomes were added to the cells the mRFP fluorescence for group with the highest eGFP receptor expression would increase further (Figure 3.4e).

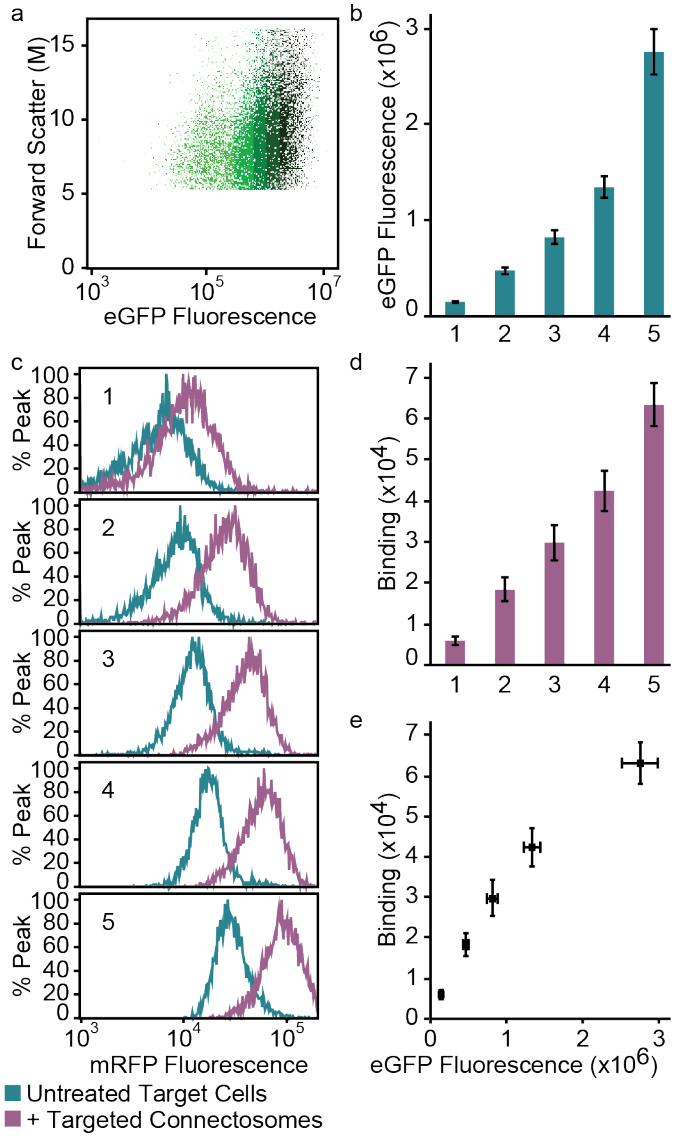

Figure 3.4: Continued on next page.

Figure 3.4: **Targeted Connectosome binding is correlated with eGFP receptor expression.** (a), Example scatterplot from flow cytometry analysis showing the five gates used to analyze recipient target cells based on their eGFP receptor expression, as indicated by their eGFP fluorescence. (b) Average recipient cell eGFP fluorescence for each group. The error bars represent the standard deviations of 3 independent trials, 5,000 total cells analyzed per trial. (c), Flow cytometry histograms showing mRFP fluorescence for each group of recipient target cells before (blue) and after (purple) incubation with extruded, targeted Connectosomes. Each curve represents 3 independent, concatenated trials, 5,000 total cells analyzed per trial. (d), Average increase in mRFP fluorescence after incubation with targeted Connectosomes for each cell group. The error bars represent the standard deviations of 3 independent trials, 5,000 total cells analyzed per trial. (e), Targeted Connectosome binding as a function of GFP receptor expression.

Next, to confirm the binding selectivity of the targeted Connectosomes, we completed a competitive binding study. Specifically, confluent monolayers of recipient target and off-target cells co-cultured in the same dish were incubated with targeted Connectosomes at the same concentration as the above experiments. After incubation, the recipient cells were washed to remove unbound vesicles, and binding was quantified using flow cytometry (Figure 3.5a-d). Target cells were separated from off-target cells based on their eGFP fluorescence intensity, so that binding for each cell type could be analyzed separately (Figure 3.5a). As expected, the average mRFP fluorescence of off-target cells increased slightly, by less than 2,000 (a.u.) (Figure 3.5b-d). However, the average mRFP fluorescence of target cells increased dramatically, by almost 50,000 (a.u.) (Figure 3.5b-d). Interestingly, this data illustrates that in a competitive scenario, targeting selectively enhances Connectosome binding to target cells by nearly 30 times, almost triple the extent to which targeting enhances binding when the target and off-target cells are cultured separately as in the previous experiment. This finding implies that the interactions of Connectosomes with cells maybe somewhat transient, and that Connectosomes likely sample the surfaces of multiple cells in order to find the ones to which they bind most strongly.

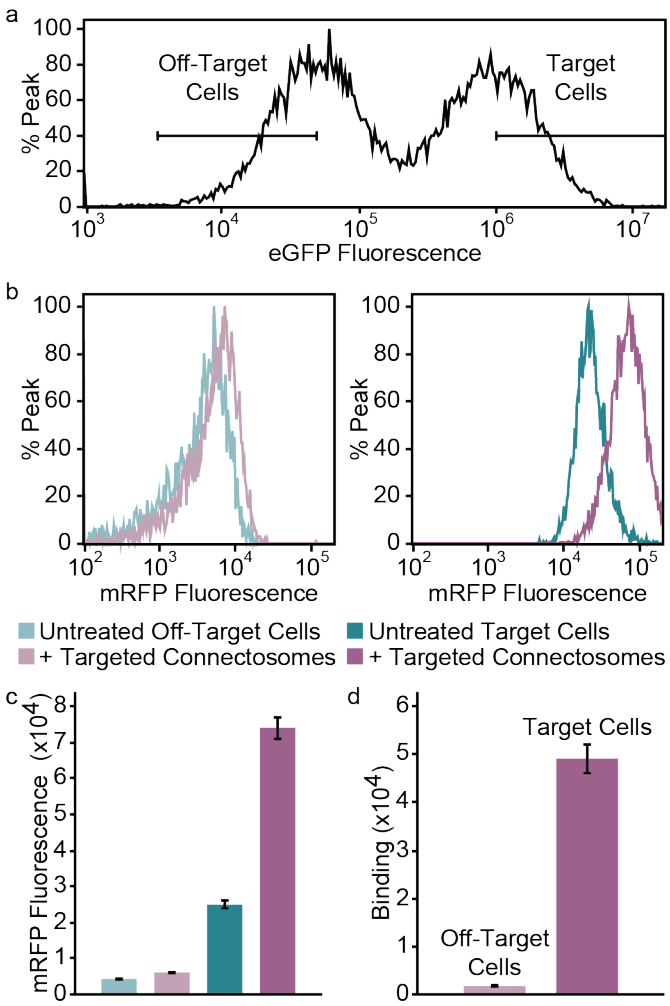

Figure 3.5: **Targeted Connectosomes bound selectively to target cells.** (a) Flow cytometry histogram showing eGFP fluorescence for co-cultured target and off-target cells. Gates shown were used to analyze each group of cells separately. The curve represents 3 independent, concatenated trials, 2,000 total cells analyzed per trial. (b), Flow cytometry histograms showing mRFP fluorescence for recipient off-target cells before (blue) and after (purple) incubation with extruded, targeted Connectosomes (left) and for recipient target cells (right) before (blue) and after (purple) incubation with extruded, targeted Connectosomes. Each curve represents 3 independent, concatenated trials, 2,000 cells analyzed per trial. (c), Average recipient cell mRFP fluorescence for each condition. The error bars represent the standard deviations of 3 independent trials, 2,000 cells analyzed per trial. (d), Average increase in mRFP fluorescence for off-target and target cells after incubation with targeted Connectosomes. The error bars represent the standard deviations of 3 independent trials, 2,000 cells analyzed per trial. Legend in (b) applies to (c) and (d).

Targeting selectively enhanced cytoplasmic dye delivery to target cells

Having established the selectivity of targeted Connectosome binding, we next investigated how enhanced target cell binding affects molecular delivery (Figure 3.6). Specifically, targeted Connectosomes were loaded with calcein red orange (CRO) dye using established protocols[1]. Briefly, donor cells were treated with CRO-acetomethoxy (CRO-AM) dye prior to Connectosome production. The AM group renders the CRO-AM dye membrane permeable, but as the CRO-AM dye accumulates in the cytoplasm, the AM group is metabolized by intracellular esterases. The resulting CRO dye is membrane impermeable, and therefore trapped in the cytoplasm and permeable only to gap junctions[36]. Previous studies using untargeted Connectosomes to deliver CRO dye to cells established that delivery was both cytoplasmic and gap junction-dependent[1]. In particular, dye transfer was significantly reduced when cells were treated with carbenoxolone, a gap junction inhibitor[37] that prevents junctions from forming between Connectosomes and cells, before incubation with dye-loaded Connectosomes.

Therefore, to demonstrate the ability of targeting to enhance selective delivery of molecular cargo to the cytoplasm, we conducted a competitive dye delivery study (Figure 3.6). Specifically, confluent monolayers of co-cultured recipient target and off-target cells were incubated with either targeted or untargeted Connectosomes. Dye delivery was quantified by using flow cytometry to measure the increase in mRFP fluorescence after a 45-minute incubation with the vesicles. Target cells were separated from off-target cells based on their eGFP fluorescence intensity, so that delivery for each cell type could be analyzed separately (Figure 3.6a). There was no significant difference in the increase in the average mRFP fluorescence for both target and off-target cells treated with untargeted Connectosomes, or for target cells treated with untargeted Connectosomes (Figure 3.6b-e). However, the average mRFP fluorescence for target cells incubated with targeted

Connectosomes increased by 27,000, a nearly five-fold increase in delivery compared to untargeted Connectosomes. This data illustrates the ability of targeting to enhance selective delivery of molecular cargo to the cytoplasm of specific populations of target cells.

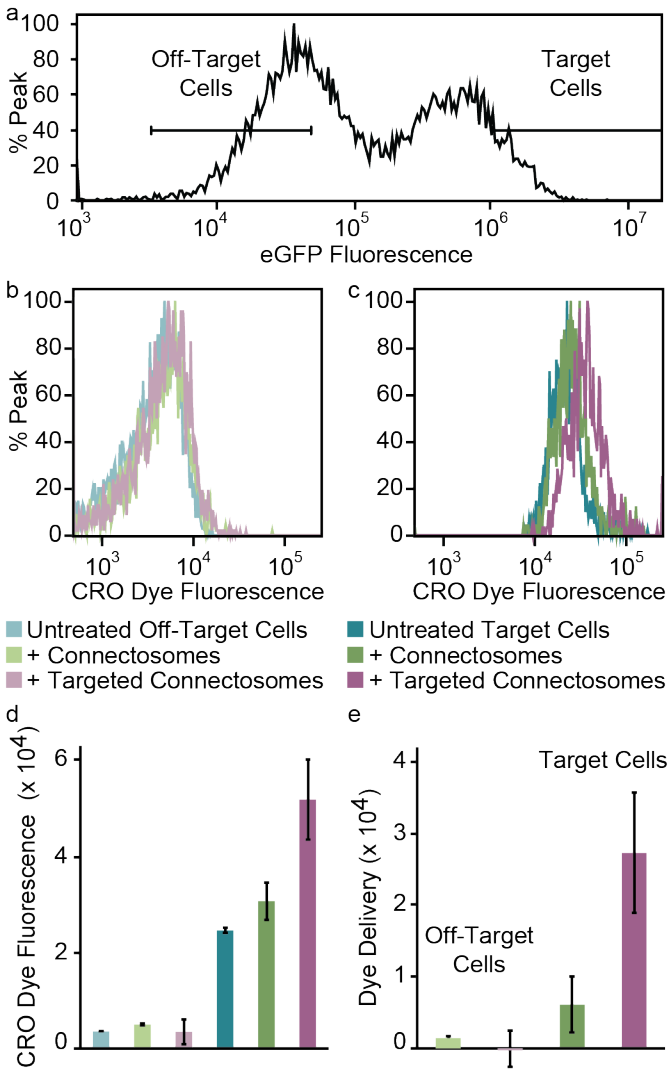

Figure 3.6: Continued on next page.

Figure 3.6: **Targeting enhances dye delivery to the cellular cytoplasm.** (a), Flow cytometry histogram showing eGFP fluorescence for co-cultured target and off-target cells. Gates shown were used to analyze each group of cells separately. The curve represents 3 independent, concatenated trials, 2,000 total cells analyzed per trial. (b), Flow cytometry histograms showing mRFP fluorescence for recipient off-target cells before (blue) and after incubation with either untargeted (green) or targeted (purple) Connectosomes. Each curve represents 3 independent, concatenated trials, 2,000 cells analyzed per trial. (c), Flow cytometry histograms showing mRFP fluorescence for recipient target cells before (blue) and after incubation with either untargeted (green) or targeted (purple) Connectosomes. Each curve represents 3 independent, concatenated trials, 2,000 cells analyzed per trial. (d), Average recipient cell mRFP fluorescence for each condition. The error bars represent the standard deviations of 3 independent trials, 2,000 cells analyzed per trial. (e), Average increase in mRFP fluorescence after incubation with either untargeted or targeted Connectosomes for off-target and target cells. The error bars represent the standard deviations of 3 independent trials, 2,000 cells analyzed per trial. Legend in (b) applies to (c) and (d).

Targeted Connectosomes selectively delivered chemotherapeutics to target cells

Having established the ability of targeting to enhance the selective delivery of molecular cargo to the cytoplasm, we then sought to understand the effects of targeting on the delivery and efficacy of the chemotherapeutic drug doxorubicin. Previously, untargeted Connectosomes were used to reduce the therapeutically effective dose of this drug by more than an order of magnitude compared to free doxorubicin, and by several orders of magnitude compared to conventional liposomal doxorubicin[1]. However, we wanted to test whether targeting would simultaneously enable the selectivity of delivery while also enhancing the efficacy of delivery to target cells.

We formed doxorubicin-loaded targeted Connectosomes by extruding unprocessed Connectosomes in cell media containing 300 μM doxorubicin using a 1 μm filter. The loaded, extruded, targeted Connectosomes were pelleted and washed to remove the unencapsulated doxorubicin. Then, the Connectosomes were resuspended in fresh media, and their doxorubicin content was quantified using established protocols[1] based on measuring the doxorubicin fluorescence emission of the vesicles. The targeted Connectosomes were then incubated with co-cultured target and off-target cells at equivalent doxorubicin doses increasing from 125 nM to 500 nM. After two hours, the Connectosomes were washed away. After 24 hours, cell viability was measured using a

7AAD viability stain (Figure 3.7a-c). As expected, for both target and off-target cells, the viability decreased with increasing doxorubicin dose. However, we found that at each equivalent doxorubicin dose, target cells were significantly less viable than off-target cells. For example, at 250 nM doxorubicin, only 3% of off-target cells were nonviable, while almost 23% of target cells were nonviable. Further, at 500 nM doxorubicin, only 9% of off-target cells were nonviable, while target cells were more than six times less viable, at 62% nonviable.

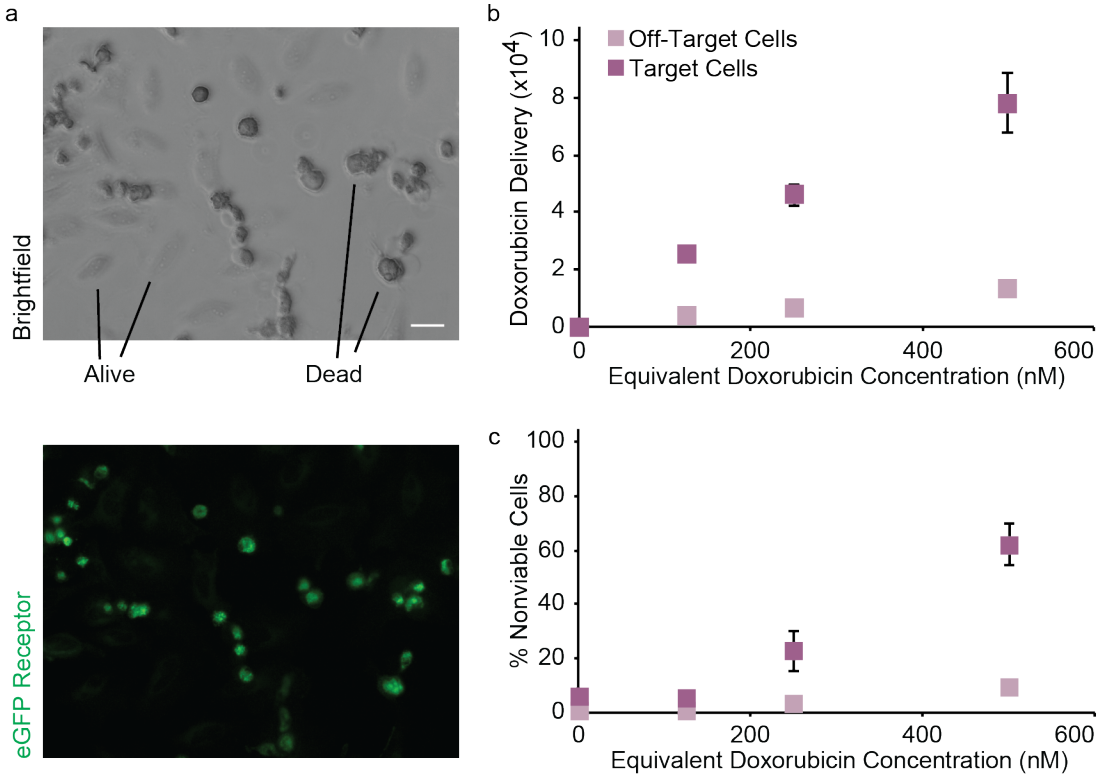

Figure 3.7: **Targeted Connectosomes enhance doxorubicin delivery to target cells.** (a), Percentage of nonviable off-target cells(light purple) and nonviable target cells (dark purple) treatment with doxorubicin-loaded targeted Connectosomes. All points were measured using a 7-AAD viability assay, except for the 500 nM point, which was measured using a trypan blue viability assay. The error bars represent the standard deviations of 3 independent trials, 1,000 cells analyzed per trial. (b), Brightfield and fluorescence image showing that most dead cells are target cells. (c), Doxorubicin delivery to target and off-target cells after treatment with targeted Connectosomes at an equivalent doxorubicin dose of 250 nM, based on average doxorubicin fluorescence. The error bars represent the standard deviations of 3 independent trials, 1,000 cells analyzed per trial. Legend in (a) applies to (c). Scale bar 250 μm.

To verify that this increase in nonviability was due to increased doxorubicin delivery to target cells, we examined the increase in doxorubicin fluorescence for both target and off-target cells after treatment with targeted Connectosomes (Figure 3.7b). We found that at each equivalent doxorubicin dose, significantly more doxorubicin was delivered to the target cells than to the off-target cells, confirming that the enhanced efficacy of treatment with targeted Connectosomes is indeed due to increased doxorubicin delivery.

It is important to note that the increase in therapeutic efficacy observed for target cells is not necessarily expected to precisely match the increase in doxorubicin delivery to target cells, due to the fact that the bystander effect promotes transfer of drugs between cells. Specifically, cells that receive doxorubicin from targeted Connectosomes may transfer some doxorubicin to neighboring cells through gap junctions, perhaps increasing the therapeutic efficacy beyond the extent to which doxorubicin delivery itself was increased. Further, increased doxorubicin delivery may enhance the effects of the bystander effect. Additionally, the factor by which targeting increased the delivery of doxorubicin is not expected to precisely match the factor by which targeting increased in delivery of dye as discussed in Figure 3.6, due to the differences in timescales of these experiments, as well as differences in transport rates of these molecules through gap junctions.

From this data, the therapeutically effective dose (LD50) of targeted Connectosomes for off-target cells can be estimated to be greater than 600 nM. While previous studies using untargeted Connectosomes to deliver doxorubicin to HeLa cells estimate the LD50 for this treatment to be around 500 nM[1], the small difference we report here is expected due to the fact that extruded Connectosomes were used for the current studies, while intact Connectosomes were used for the previous studies. Extrusion is

expected to increase the LD50 of particles by reducing gravitational settling[27], which results in reduced non-specific interactions with cells

However, the LD50 for target cells was approximately 300 nM, demonstrating that targeting selectively increases the efficacy of chemotherapeutic delivery to target cells by approximately two-fold. This data demonstrates that targeting further reduces the LD50 of doxorubicin-loaded Connectosomes to a concentration that is more than an order of magnitude lower than the LD50 for free doxorubicin, which is approximately 10 μM[1], and more than several orders of magnitude lower than the LD50 for conventional liposomal doxorubicin, which is greater than 1 mM[1]. In sum, these findings demonstrate the ability of targeting to selectively enhance the therapeutic efficacy of doxorubicin delivery via Connectosomes to specific populations of cells while protecting off-target cells cultured in the same dish, removing the limitations of non-specificity restricting the therapeutic potential of gap junction-based drug delivery strategies.

Conclusion

Connectosomes were previously established as promising therapeutic materials capable of efficiently transporting therapeutics to the cytoplasm through gap junctions[1]. These materials reduced the LD50 of doxorubicin by an order of magnitude compared to free doxorubicin, and by several orders of magnitude compared to conventional liposomal doxorubicin. However, their translational relevance was limited by the inherent lack of specificity in gap junction-based delivery approaches. Towards addressing this issue, here we report the development of targeted Connectosomes, cell-derived particles that use gap junctions and targeting proteins to selectively transport molecular cargoes to the cytoplasm of specific populations of cells.

Incorporating targeting proteins into Connectosomes selectively enhanced binding to target cells by 30 times compared to off-target cells, which is comparable to increases in binding exhibited by synthetic targeted particles[12]. Further, our data demonstrated that targeting selectively enhanced delivery of both dyes and drugs to target cells. In particular, targeting reduced the therapeutically effective dose of doxorubicin-loaded Connectosomes for target cells by 2 times compared to off-target cells, a similar increase in therapeutic efficacy compared to other targeting strategies[38]. In sum, this data demonstrates that harnessing the cell's machinery to display multi-functional targeting molecules on the surfaces of cell-derived membrane particles is a promising strategy for overcoming issues of non-specific therapeutic delivery by Connectosomes.

Further, our multi-functional targeting approach enables the incorporation of desirable features into the targeting protein, which may be difficult to include through chemical conjugation or other synthetic targeting strategies. For example, our approach could allow for incorporation of multiple, distinct targeting ligands in the targeting protein, in order to enable targeting of multiple receptors. Increasing the specificity and sophistication of the targeting system in this way could be useful for addressing challenge of delivery to heterogeneous tumors[39].

Ultimately, the development of a chemotherapeutic delivery system that both efficiently and selectively kills diseased cells represents a critical step towards realizing the therapeutic potential of Connectosomes and other particles which employ gap junctions for delivery. In the future, our targeting strategy could be utilized to target Connectosomes to a broad range of cell types. In this way, targeted Connectosomes could be used to deliver a range of membrane impermeable drugs and reagents, such as siRNA, peptides, and other macromolecules, to diverse populations of target cells.

Materials and Methods

Plasmid constructs. The Tf-RΔEcto-mRFP AP180 CTD plasmid was first constructed by excising eGFP from the Tf-RΔEcto-eGFP AP180 CTD plasmid above with BamH1 and SalI digestion and inserting the PCR amplified mRFP (Addgene plasmid #13032, pcDNA3 backbone), a generous gift from Dr. Douglas Golenbock (University of Massachusetts Medical School). The pOPINE GFP nanobody sequence, a gift from Brett Collins (Addgene plasmid #49172), was PCR amplified and restriction cloned into Tf-RΔEcto-mRFP AP180 CTD using primers containing MluI sites. All constructs were confirmed by DNA sequencing.

The chimaeric Tf-RΔEcto-GFP (GFP cargo) was made by modifying the Tf-R-GFP construct (pEGFP-N1 backbone), kindly provided by Dr Tomas Kirchhausen (Harvard medical school), where the entire Tf-R sequence was excised by digesting with EcoRI and BamHI, and inserting only the PCR amplified intracellular and transmembrane domains of Tf-R adjacent to the GFP fluorophore with EcoRI and BamHI sites. An intermediate construct lacking a stop codon was made by digesting Tf-RΔEcto-GFP with BamHI and NotI to remove GFP, and inserting a mutated PCR amplified GFP with the stop codon (TAA) replaced by a glycine (GGA).

Stable cell line production. The GFP expressing HeLa cells were produced via lentiviral transfection. The GFP-tagged receptor gene sequence was subcloned onto pLJM1 viral transfer vector (addgene #19319) with NheI and EcoRI sites. Lentiviruses were generated by co-transfecting the transfer plasmid, packaging plasmid Δ8.9 and the envelope plasmid VSVG into 293T packaging cells with FuGENE. 48 hours after the transfection, virus-containing supernatant was collected, filtered and added to HeLa cells

with 8 ug/mL of polybrene. Transduced HeLa cells were selected with 2 ug/mL puromycin for 7 days.

eGFP purification. The pRSET vector containing the nondimeriz- able hexa-his-tagged eGFP (hisGFP A206K) was generously shared by Dr. Adam Arkin (University of California, Berkeley). Following published purification protocols[40, 41], his-eGFP was expressed in BL21(DE3) pLysS cells overnight at 18 °C and purified from bacterial extracts by incubating with Ni-NTA agarose beads in 25 mM HEPES, 150 mM NaCl, 1 mM imidazole, 1 mM β-mercaptoethanol, pH 7.4. After extensive washing with 25 mM HEPES, 150-300 mM NaCl, 1-5 mM imidazole, 1 mM β-mercaptoethanol, pH 7.4, proteins were eluted via a gradient imidazole wash to a final concentration of 250 mM. Eluted proteins were concentrated and dialyzed in 2 L 25 mM HEPES, 150 mM NaCl, 1 mM EDTA, and 1 mM β-mercaptoethanol, pH 7.4, at 4 °C overnight and again for 2 h in fresh buffer at 4 °C.

Targeting Protein Expression and Function. Soluble eGFP binding—HeLa cells stably expressing the GFPnb targeting protein were co-incubated with 250 nM soluble eGFP for 5 min at 37 °C, and then imaged. To test the expression and functionality of the GFPnb targeting protein, plasma membrane vesicles collected from the GFPnb cell line were incubated with 250 nM purified eGFP. Images were taken after 5 min of incubation at 37 °C. Expression and binding correlation analysis—A line was drawn across the GPMVs bound to soluble eGFP and the fluorescence intensity maximum in the eGFP and the mRFP channels were recorded. A total of 45 vesicles were analyzed with two distinct points per vesicle. All images were taken under the same camera settings.

Binding studies. Off-target HeLa and/or target HeLa GFPr cells were plated in 96 well plates at a density of 5,000 total cells per well. Targeted, intact Connectosomes were collected and extruded to 1.0 μm. The media was aspirated away from confluent cells and

the vesicles were added to the wells for 4 h at 37 °C. At the end of the incubation, recipient cell samples were then either imaged on the spinning disc confocal microscope or prepared for flow cytometry. To quantify the extent of binding, samples were prepared for flow cytometry analysis following established protocols[1, 27]. Briefly, cells were trypsinized and resuspended in 50 μL of PBS.

References

1. Gadok, A. K.; Busch, D. J.; Ferrati, S.; Li, B.; Smyth, H. D. C.; Stachowiak, J. C., Connectosomes for Direct Molecular Delivery to the Cellular Cytoplasm. Journal of the American Chemical Society 2016, 138 (39), 12833-12840.
2. Soares, A. R.; Martins-Marques, T.; Ribeiro-Rodrigues, T.; Ferreira, J. V.; Catarino, S.; Pinho, M. J.; Zuzarte, M.; Anjo, S. I.; Manadas, B.; Sluijter, J. P. G.; Pereira, P.; Girao, H., Gap junctional protein Cx43 is involved in the communication between extracellular vesicles and mammalian cells. Scientific Reports 2015, 5, 13.
3. Brink, P. R.; Valiunas, V.; Gordon, C.; Rosen, M. R.; Cohen, I. S., Can gap junctions deliver? Biochimica Et Biophysica Acta-Biomembranes 2012, 1818 (8), 2076-2081.
4. Kaneda, M.; Nomura, S. M.; Ichinose, S.; Kondo, S.; Nakahama, K.; Akiyoshi, K.; Morita, I., Direct formation of proteo-liposomes by in vitro synthesis and cellular cytosolic delivery with connexin-expressing liposomes. Biomaterials 2009, 30 (23-24), 3971-3977.
5. Evans, W. H.; Martin, P. E. M., Gap junctions: structure and function (Review). Molecular Membrane Biology 2002, 19 (2), 121-136.
6. Yamasaki, H.; Krutovskikh, V.; Mesnil, M.; Tanaka, T.; Zaidan-Dagli, M. L.; Omori, Y., Role of connexin (gap junction) genes in cell growth control and carcinogenesis. Comptes Rendus De L Academie Des Sciences Serie Iii-Sciences De La Vie-Life Sciences 1999, 322 (2-3), 151-159.

7. Huang, R. P.; Hossain, M. Z.; Huang, R.; Gano, J.; Fan, Y.; Boynton, A. L., Connexin 43 (cx43) enhances chemotherapy-induced apoptosis in human glioblastoma cells. International Journal of Cancer 2001, 92 (1), 130-138.

8. Garcia-Rodriguez, L.; Perez-Torras, S.; Carrio, M.; Cascante, A.; Garcia-Ribas, I.; Mazo, A.; Fillat, C., Connexin-26 Is a Key Factor Mediating Gemcitabine Bystander Effect. Molecular Cancer Therapeutics 2011, 10 (3), 505-517.

9. Mesnil, M.; Piccoli, C.; Tiraby, G.; Willecke, K.; Yamasaki, H., Bystander killing of cancer cells by herpes simplex virus thymidine kinase gene is mediated by connexins. Proceedings of the National Academy of Sciences of the United States of America 1996, 93 (5), 1831-1835.

10. Goodenough, D. A.; Paul, D. L., Gap Junctions. Cold Spring Harbor Perspectives in Biology 2009, 1 (1), 19.

11. Davis, M. E.; Chen, Z.; Shin, D. M., Nanoparticle therapeutics: an emerging treatment modality for cancer. Nature Reviews Drug Discovery 2008, 7 (9), 771-782.

12. Mamot, C.; Drummond, D. C.; Greiser, U.; Hong, K.; Kirpotin, D. B.; Marks, J. D.; Park, J. W., Epidermal growth factor receptor (EGFR)-targeted immunoliposomes mediate specific and efficient drug delivery to EGFR- and EGFRvIII-overexpressing tumor cells. Cancer Research 2003, 63 (12), 3154-3161.

13. Mamot, C.; Drummond, D. C.; Noble, C. O.; Kallab, V.; Guo, Z. X.; Hong, K. L.; Kirpotin, D. B.; Park, J. W., Epidermal growth factor receptor-targeted immunoliposomes significantly enhance the efficacy of multiple anticancer drugs in vivo. Cancer Research 2005, 65 (24), 11631-11638.

14. Park, J. W.; Hong, K. L.; Kirpotin, D. B.; Colbern, G.; Shalaby, R.; Baselga, J.; Shao, Y.; Nielsen, U. B.; Marks, J. D.; Moore, D.; Papahadjopoulos, D.; Benz, C. C., Anti-HER2 immunoliposomes: Enhanced efficacy attributable to targeted delivery. Clinical Cancer Research 2002, 8 (4), 1172-1181.

15. Gabizon, A.; Shmeeda, H.; Horowitz, A. T.; Zalipsky, S., Tumor cell targeting of liposome-entrapped drugs with phospholipid-anchored folic acid-PEG conjugates. Advanced Drug Delivery Reviews 2004, 56 (8), 1177-1192.

16. Chen, S. Y.; Zhao, X. R.; Chen, J. Y.; Chen, J.; Kuznetsova, L.; Wong, S. S.; Ojima, I., Mechanism-Based Tumor-Targeting Drug Delivery System. Validation of Efficient Vitamin Receptor-Mediated Endocytosis and Drug Release. Bioconjugate Chemistry 2010, 21 (5), 979-987.

17. Hatakeyama, H.; Akita, H.; Maruyama, K.; Suhara, T.; Harashima, H., Factors governing the in vivo tissue uptake of transferrin-coupled polyethylene glycol liposomes in vivo. International Journal of Pharmaceutics 2004, 281 (1-2), 25-33.

18. Allen, T. M., Ligand-targeted therapeutics in anticancer therapy. Nature Reviews Cancer 2002, 2 (10), 750-763.

19. Ren, Y.; Wong, S. M.; Lim, L. Y., Folic acid-conjugated protein cages of a plant virus: A novel delivery platform for doxorubicin. Bioconjugate Chemistry 2007, 18 (3), 836-843.

20. Mukthavaram, R.; Shi, G. X.; Kesari, S.; Simberg, D., Targeting and depletion of circulating leukocytes and cancer cells by lipophilic antibody-modified erythrocytes. Journal of Controlled Release 2014, 183, 146-153.

21. Zhang, W.; Yu, Z. L.; Wu, M.; Ren, J. G.; Xia, H. F.; Sa, G. L.; Zhu, J. Y.; Pang, D. W.; Zhao, Y. F.; Chen, G., Magnetic and Folate Functionalization Enables

Rapid Isolation and Enhanced Tumor-Targeting of Cell-Derived Microvesicles. Acs Nano 2017, 11 (1), 277-290.

22. Johnsen, K. B.; Gudbergsson, J. M.; Skov, M. N.; Pilgaard, L.; Moos, T.; Duroux, M., A comprehensive overview of exosomes as drug delivery vehicles - Endogenous nanocarriers for targeted cancer therapy. Biochimica Et Biophysica Acta-Reviews on Cancer 2014, 1846 (1), 75-87.

23. Alvarez-Erviti, L.; Seow, Y. Q.; Yin, H. F.; Betts, C.; Lakhal, S.; Wood, M. J. A., Delivery of siRNA to the mouse brain by systemic injection of targeted exosomes. Nature Biotechnology 2011, 29 (4), 341-U179.

24. Ohno, S.; Takanashi, M.; Sudo, K.; Ueda, S.; Ishikawa, A.; Matsuyama, N.; Fujita, K.; Mizutani, T.; Ohgi, T.; Ochiya, T.; Gotoh, N.; Kuroda, M., Systemically Injected Exosomes Targeted to EGFR Deliver Antitumor MicroRNA to Breast Cancer Cells. Molecular Therapy 2013, 21 (1), 185-191.

25. Tian, Y. H.; Li, S. P.; Song, J.; Ji, T. J.; Zhu, M. T.; Anderson, G. J.; Wei, J. Y.; Nie, G. J., A doxorubicin delivery platform using engineered natural membrane vesicle exosomes for targeted tumor therapy. Biomaterials 2014, 35 (7), 2383-2390.

26. Bronshtein, T.; Toledano, N.; Danino, D.; Pollack, S.; Machluf, M., Cell derived liposomes expressing CCR5 as a new targeted drug-delivery system for HIV infected cells. Journal of Controlled Release 2011, 151 (2), 139-148.

27. Zhao, C.; Busch, D. J.; Vershel, C. P.; Stachowiak, J. C., Multifunctional Transmembrane Protein Ligands for Cell-Specific Targeting of Plasma Membrane-Derived Vesicles. Small 2016, 12 (28), 3837-3848.

28. Peer, D.; Karp, J. M.; Hong, S.; FaroKhzad, O. C.; Margalit, R.; Langer, R., Nanocarriers as an emerging platform for cancer therapy. Nature Nanotechnology 2007, 2 (12), 751-760.

29. Kubala, M. H.; Kovtun, O.; Alexandrov, K.; Collins, B. M., Structural and thermodynamic analysis of the GFP:GFP-nanobody complex. Protein Science 2010, 19 (12), 2389-2401.

30. Sezgin, E.; Kaiser, H. J.; Baumgart, T.; Schwille, P.; Simons, K.; Levental, I., Elucidating membrane structure and protein behavior using giant plasma membrane vesicles. Nature Protocols 2012, 7 (6), 1042-1051.

31. Charras, G.; Paluch, E., Blebs lead the way: how to migrate without lamellipodia. Nature Reviews Molecular Cell Biology 2008, 9 (9), 730-736.

32. Chen, L. R.; Novicky, L.; Merzlyakov, M.; Hristov, T.; Hristova, K., Measuring the Energetics of Membrane Protein Dimerization in Mammalian Membranes. Journal of the American Chemical Society 2010, 132 (10), 3628-3635.

33. Costello, D. A.; Hsia, C. Y.; Millet, J. K.; Porri, T.; Daniel, S., Membrane Fusion-Competent Virus-Like Proteoliposomes and Proteinaceous Supported Bilayers Made Directly from Cell Plasma Membranes. Langmuir 2013, 29 (21), 6409-6419.

34. El Andaloussi, S.; Maeger, I.; Breakefield, X. O.; Wood, M. J. A., Extracellular vesicles: biology and emerging therapeutic opportunities. Nature Reviews Drug Discovery 2013, 12 (5), 348-358.

35. Simons, M.; Raposo, G., Exosomes - vesicular carriers for intercellular communication. Current Opinion in Cell Biology 2009, 21 (4), 575-581.

36. Elzarrad, M. K.; Haroon, A.; Willecke, K.; Dobrowolski, R.; Gillespie, M. N.; Al-Mehdi, A. B., Connexin-43 upregulation in micrometastases and tumor

vasculature and its role in tumor cell attachment to pulmonary endothelium. Bmc Medicine 2008, 6, 16.

37. Connors, B. W., Tales of a Dirty Drug: Carbenoxolone, Gap Junctions, and Seizures. Epilepsy Currents 2012, 12 (2), 66-68.

38. Durfee, P. N.; Lin, Y. S.; Dunphy, D. R.; Muniz, A. J.; Butler, K. S.; Humphrey, K. R.; Lokke, A. J.; Agola, J. O.; Chou, S. S.; Chen, I. M.; Wharton, W.; Townson, J. L.; Willman, C. L.; Brinker, C. J., Mesoporous Silica Nanoparticle-Supported Lipid Bilayers (Protocells) for Active Targeting and Delivery to Individual Leukemia Cells. Acs Nano 2016, 10 (9), 8325-8345.

39. Furnari, F. B.; Cloughesy, T. F.; Cavenee, W. K.; Mischel, P. S., OPINION Heterogeneity of epidermal growth factor receptor signalling networks in glioblastoma. Nature Reviews Cancer 2015, 15 (5), 302-310.

40. Scheve, C. S.; Gonzales, P. A.; Momin, N.; Stachowiak, J. C., Steric Pressure between Membrane-Bound Proteins Opposes Lipid Phase Separation. Journal of the American Chemical Society 2013, 135 (4), 1185-1188.

41. Stachowiak, J. C.; Schmid, E. M.; Ryan, C. J.; Ann, H. S.; Sasaki, D. Y.; Sherman, M. B.; Geissler, P. L.; Fletcher, D. A.; Hayden, C. C., Membrane bending by protein-protein crowding. Nature Cell Biology 2012, 14 (9), 944-+.

Chapter 4: Quantifying the Ability of Clathrin to Sense Membrane Curvature

Abstract

Clathrin-mediated endocytosis is a primary pathway of entry into the cell that impacts diverse cellular processes, including growth, division, differentiation, and the internalization of nutrients and therapeutics. Therefore, understanding the fundamental molecular mechanisms that drive clathrin coat assembly is an important problem for both fundamental and applied research. Adaptor proteins, which bind to the membrane and to clathrin, are responsible for the biochemical recruitment of clathrin to endocytic structures. However, the physical cues that influence clathrin's recruitment to the membrane remain debated. In particular, while some adaptor proteins, such as epsin and amphiphysin, bind preferentially to regions of high membrane curvature, it remains unknown whether clathrin itself possesses the ability to sense membrane curvature. To address this question, we isolated clathrin's membrane curvature sensing ability in the absence of adaptor proteins by using recombinant, histidine-tagged clathrin that is engineered to bind directly to Ni-NTA-containing membranes. To examine clathrin binding to these membranes, we used a quantitative fluorescence intensity-based approach in which vesicles were tethered to a passivated surface and incubated with clathrin at specified concentrations. Using particle detection software and single-molecule calibrations to determine the brightness of each vesicle and the brightness of the clathrin colocalized to each vesicle, we quantified the curvature of each individual vesicle as well as the corresponding number of bound clathrin triskelia. Our results demonstrate that clathrin binds preferentially to membranes of higher curvature. Specifically, when incubated with the same concentration of clathrin, vesicles with an average diameter of

25 nm recruited more than five times as many clathrin triskelia per membrane surface area in comparison to vesicles with an average diameter of 80 nm. This data was used to make a statistical model from which the curvature dependence of clathrin-lipid binding energy was extracted, providing fundamental insight into the process by which clathrin is recruited to highly curved membranes during clathrin-mediated endocytosis.

Introduction

Clathrin-mediated endocytosis (CME) is a critical internalization pathway that eukaryotic cells rely upon in order for numerous physiological processes to occur[1]. For example, CME is one of the cell's primary methods for plasma membrane receptor internalization[2, 3]. Cells also depend upon CME for the uptake of important nutrients, like cholesterol, iron, and other metabolites[1]. By controlling the uptake of these nutrients, as well as the composition of receptors at the plasma membrane, CME plays an important role in regulating signaling transduction and homeostasis, which in turn impacts a wide range of cellular functions, including growth, division, and differentiation[4-7].

Owing to clathrin-mediated endocytosis' involvement in diverse cellular processes, defects in CME have been implicated in many diseases[1]. For example, impairments in CME have been associated with numerous cancers, including leukemia, lymphoma, and breast, ovarian, lung, and renal cancers. Mutations in some of the key proteins involved in CME have also been linked to various other diseases, including metabolic disorders such as diabetes, psychiatric disorders such as schizophrenia, and neurodegenerative disorders such as Alzheimer's disease. Further, many nanoparticle-based drug delivery strategies also rely upon clathrin-mediated endocytosis for drug uptake into the cell[8]. Therefore, understanding the molecular mechanisms that drive CME is an important biological problem relevant to fundamental fields, like cell biology and biophysics, as well as to applied fields, like biotechnology and pharmaceutics.

During clathrin-mediated endocytosis, the plasma membrane is invaginated, forming a highly curved, clathrin-coated bud destined to separate from the plasma membrane and travel into the cytoplasm. This complex process of internalization can be broken into five distinct steps: (i) nucleation of the membrane bud, (ii) loading of the bud

with cargo destined for internalization, (iii) assembly of the clathrin coat, (iv) separation of the bud from the plasma membrane, and finally (v) uncoating of the trafficking vesicle[1]. For these steps to occur, a synchronized network of more than fifty distinct proteins is required[9]. For example, FCHO proteins, eps15, and intersectins are key players in bud nucleation[10-12]. Adaptor proteins including AP2, AP180, and epsin, as well as cargo-specific accessory adaptor proteins, help coordinate cargo loading and clathrin coat assembly[13-16]. Dynamin, a GTPase that is recruited to buds by proteins containing Bin/amphiphysin/Rvs (BAR) domains like amphiphysin and endophilin, is involved in vesicle scission, and vesicle uncoating is mediated by auxilin and heat shock cognate 70 (HSC70)[17-22]. However, understanding precisely how these proteins interact to drive internalization remains a challenge.

In particular, the physical cues that influence clathrin's recruitment to the buds remain debated. Studies have demonstrated that several proteins involved in clathrin-mediated endocytosis bind preferentially to regions of high membrane curvature, due to the presence of BAR domains and/or amphipathic helices in their structures[23-25]. In particular, BAR domains are thought to sense curvature due to their curved, crescent-like banana shape, while amphipathic helices are thought to sense curvature due to their enhanced insertion into membranes with lipid packing defects (these defects increase with increasing membrane curvature)[23, 25]. For example, the curvature sensing ability of the BAR domain of amphiphysin was first demonstrated using liposome sedimentation assays[23]. More recently, the curvature sensing ability of the amphipathic helices at the N-termini of both amphiphysin and endophilin was demonstrated using fluorescence-based measurements on single liposomes[24], and the curvature sensing ability of the amphipathic helix of epsin was demonstrated using fluorescence-based measurements on cylindrical liposome tethers and tubulation assays[26, 27]. In follow up studies, the curvature sensing

ability of these amphipathic helices was attributed to curvature-induced lipid-packing defects in membranes, which enable insertion of hydrophobic face of the amphipathic helices[25].

Once these proteins have assembled at highly curved membrane sites, they are able to recruit clathrin to these sites, which is thought to further reinforce curvature and drive bud formation. However, it remains unknown whether clathrin itself possesses the ability to sense membrane curvature and bind preferentially to curved structures. Therefore, understanding the inherent extent to which clathrin senses membrane curvature is important for furthering our fundamental understanding of the mechanisms that drive clathrin-mediated endocytosis.

Results and Discussion

Histidine-tagged clathrin bound to tethered vesicles

To address this question, we isolated clathrin's curvature sensing ability in the absence of adaptor proteins using recombinant, histidine-tagged clathrin triskelia that were engineered to bind directly to Ni-NTA-containing membranes[28]. Specifically, his-tagged clathrin heavy chains were mixed with equimolar concentrations of untagged clathrin light-chains in order to form soluble, monodisperse triskelia. These triskelia are identical to clathrin triskelia prepared from bovine brain, and assemble into coats that are indistinguishable from those assembled with clathrin purified from bovine brain[28]. Further, the histidine tag on the N-terminus of clathrin heavy chain (near the physiological adaptor protein binding site) enables recruitment of clathrin triskelia directly to the surfaces of Ni-NTA-DOGS membranes, in the same orientation in which clathrin triskelia are recruited to biological membranes by adaptor proteins[29, 30].

We began by designing an assay in which synthetic vesicles were tethered to a surface using biotin-neutravidin interactions (Figure 4.1a). Similar assays have been used previously to characterize the curvature sensing abilities of amphipathic helices and BAR domains, and are advantageous compared to bulk measurements on entire liposome populations because they permit measurements to occur on an individual liposome basis[31-33]. In our adaptation of this assay, glass slides were passivated using an 49:1 mixture of PEG and PEG-biotin, in order to prevent non-specific binding, while also functionalizing the surface for tethering. Following incubation of neutravidin, vesicles containing biotinylated lipid were then added to the slides at a final lipid concentration of 5 μM. In order to investigate curvature sensitivity, it was important to use vesicles that covered a range of diameters, from very highly curved vesicles roughly 30 nm in diameter, to vesicles roughly 200 nm in diameter, which are essentially planar, from the perspective of clathrin. This diameter range was achieved by tethering both sonicated and extruded vesicles.

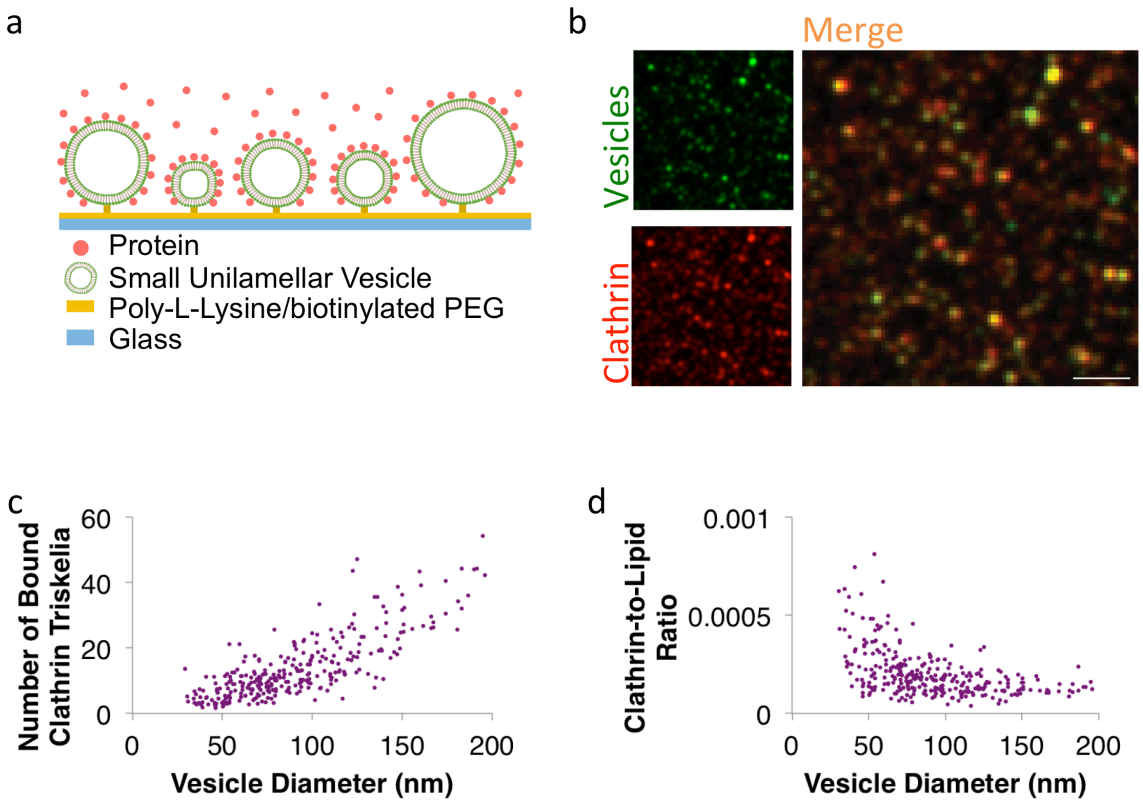

Figure 4.1: **Tethered vesicle assay allowed single liposome measurements.** (a), Schematic illustrating the tethered vesicle assay. (b), Fluorescence image showing tethered vesicles (Oregon Green) and bound clathrin (Atto 594). (c-d), Using our approach, parameters including the number of bound clathrin triskelia (c) and the clathrin-to-lipid ratio (d) were calculated for a broad range of vesicle diameters. Each point represents a single vesicle. For these studies, vesicles were extruded using a 100 nm filter and incubated with 10 nM clathrin. Scale bar 2 μm.

Next, to examine the ability of clathrin to bind to these tethered vesicles, 10 nM histidine-tagged clathrin was incubated with the tethered vesicles. Assuming that one clathrin triskelion, which contains three his-tags, binds to nine Ni-NTA lipids, this concentration provided sufficient clathrin to fully coat the vesicles based on stoichiometry, yet is several orders of magnitude lower than the micromolar concentrations of triskelia required to drive the formation of lipid-free clathrin baskets in solution[34]. Fluorescence imaging of the tethered vesicles revealed colocalization of clathrin with the vesicles, indicating that the clathrin indeed bound the vesicles (Figure 4.1b).

To quantify binding of clathrin to the tethered vesicles, we used a quantitative fluorescence intensity-based approach. Specifically, we used fluorescence intensity calibrations to quantify various parameters for each vesicle, including the vesicle diameter, the number of clathrin triskelia bound to each vesicle, and the clathrin-to-lipid ratio for each vesicle. In particular, to quantify vesicle diameter, the fluorescence intensity of each vesicle was measured, and an average vesicle brightness for the population of vesicles was calculated. This average was then adjusted to match to the average diameter of the vesicles as reported by dynamic light scattering measurements. To quantify the number of clathrin triskelia bound to each vesicle, the fluorescence intensity of the clathrin bound to each vesicle was measured and then divided by the fluorescence intensity of a single, fluorescently-labeled clathrin triskelion under identical imaging conditions. Finally, to quantify the clathrin-to-lipid ratio for each vesicle, the number of lipids in each vesicle was calculated based on the vesicle diameter, and the number of clathrin triskelia bound to each vesicle was divided by the number of lipids in each vesicle to achieve the clathrin-to-lipid ratio. Using this approach, the number of

clathrin triskelia bound to each vesicle (Figure 4.1c), as well as the clathrin-to-lipid ratio for each vesicle (Figure 4.1d), were calculated for a broad range of vesicle diameters.

Histidine-tagged clathrin assembled into coats on tethered vesicles

Having established the ability of clathrin to bind to tethered vesicles, we next investigated whether clathrin could assemble into coats on tethered vesicles, as a means of verifying the functionality of our assay. To coat the vesicles, we employed two distinct assembly strategies. In the first method, a pH drop was used to drive assembly (Figure 4.2a-b). Numerous studies have demonstrated that this is an effective method for driving clathrin assembly, due to the increased affinity of the clathrin triskelia for themselves at low pH[2, 35-38]. Specifically, the pH of the solution was dropped from pH 8.0 to pH 6.7 by adding 10% of 1M MES at pH 6.7 to the slides ten minutes after adding clathrin. The vesicles were imaged after 5 and 20 minutes at pH 6.7. For each time point, the number of triskelia and clathrin-to-lipid ratios were determined over a range of vesicle diameters as described above. As expected, the number of clathrin triskelia bound to each vesicle increased with increasing vesicle diameter, demonstrating the functionality of the assay under these conditions. Further, we observed clathrin-to-lipid ratios similar to those previously reported for complete clathrin coats, which are on average 3 triskelia bound per 1,000 lipids[39]. This agreement suggests that clathrin coat assembly was the predominant effect measured using this assay, as opposed to random clathrin aggregation.

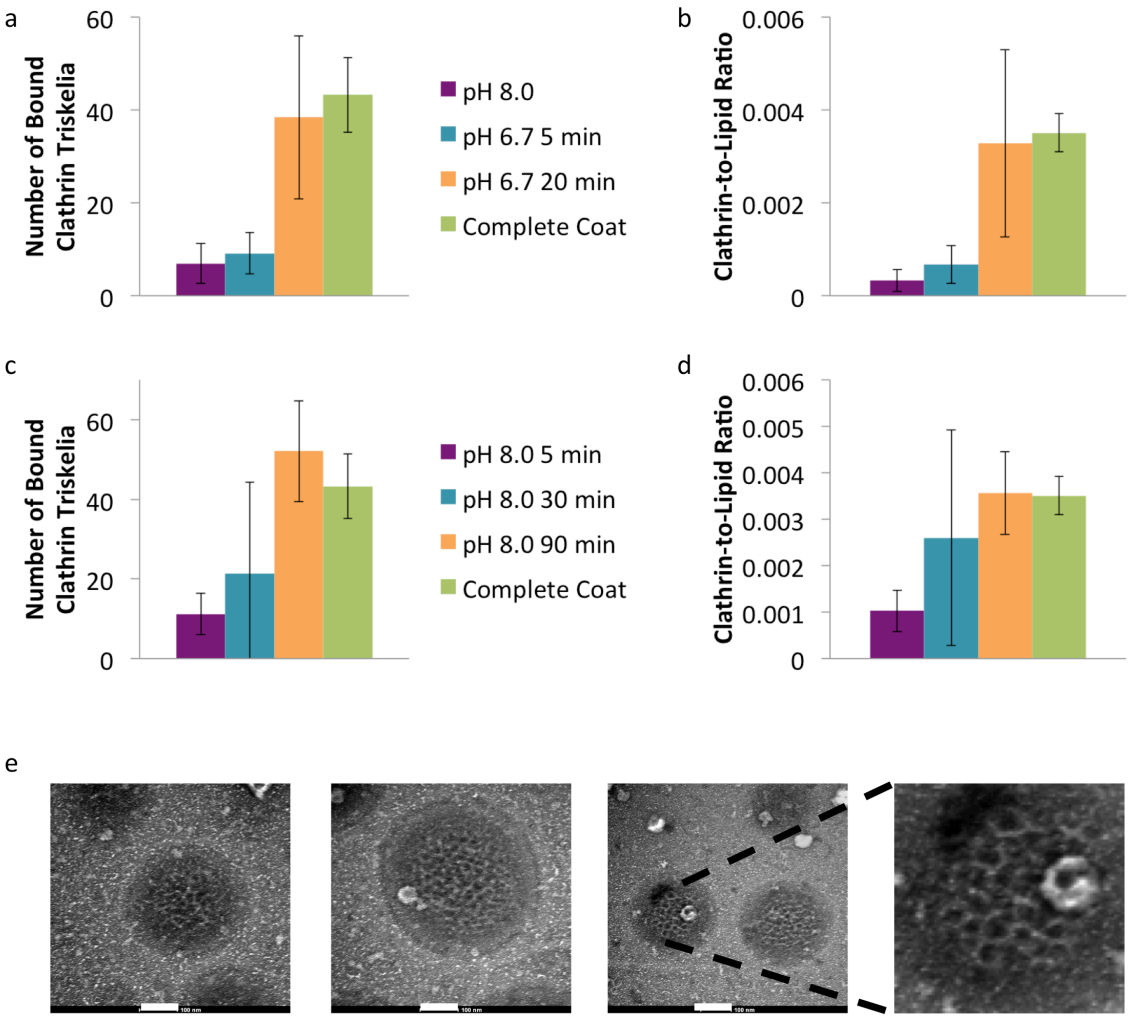

Figure 4.2: Continued on next page.

Figure 4.2: **Clathrin assembles into complete coats on tethered vesicles.** (a), The number of clathrin triskelia bound increased when the pH was dropped, and reached the value expected for a complete coat based on previous literature reports. Each bar represents the average number of bound clathrin triskelia for vesicles analyzed. Error bars represent the standard deviation of at least 300 total vesicles analyzed for each condition. (b), The clathrin-to-lipid ratio reached the value expected for a complete coat when the pH was dropped. Each barrepresents the average clathrin-to-lipid ratio for vesicles analyzed. Error bars represent the standard deviation of at least 300 total vesicles analyzed for each condition. (c), The number of clathrin triskelia bound increased over time at constant pH, and reached the value expected for a complete coat. Each bar represents the average number of bound clathrin triskelia for vesicles analyzed. Error bars represent the standard deviation of at least 300 total vesicles analyzed for each condition. (d), The clathrin-to-lipid ratio reached values expected for a complete coat after 90 minutes at constant pH. Each bar represents the average clathrin-to-lipid ratio for vesicles analyzed. Error bars represent the standard deviation of at least 300 total vesicles analyzed for each condition. (e), Negative stain transmission electron micrographs showing tethered vesicles coated in clathrin. For this study, vesicles were sonicated and incubated with 10 nM clathrin for 60 minutes. Scale bars 100 nm.

However, lowering the pH to drive clathrin assembly was at times unreliable due to the increased tendency of clathrin to aggregate at low pH. Therefore, we developed an alternative coating method which involved simply incubating clathrin with vesicles for 90 minutes at pH 8.0 (Figure 4.2c-d). Using this assembly strategy, the number of clathrin triskelia bound to each vesicle, as well as the clathrin-to-lipid ratio for individual vesicles were quantified as described above. Again, the number of triskelia bound to each vesicle increased with increasing vesicle diameter, and clathrin-to-lipid ratios were consistent with previously reported values[39], confirming that this second assembly approach was sufficient for coating the tethered vesicles.

Finally, to further verify that clathrin assembled into coats on tethered vesicles, we used negative stain transmission electron microscopy to image the tethered vesicles after incubation with clathrin using the second assembly approach (Figure 4.2e). The vesicles appeared slightly flat, and, with diameters greater than 100 nm, were somewhat larger than expected, as vesicles with an average diameter of 50 nm were used for tethering. However, these discrepancies are perhaps due to the fact that the uranyl acetate negative stain can dehydrate and distort vesicles. Nonetheless, these images clearly depict the formation of clathrin lattices, and are similar in appearance to previously published

electron microscopy images of coated vesicles[40]. Therefore, formation of clathrin coats on vesicles verified that clathrin assembled on tethered vesicles.

Histidine-tagged clathrin exhibited curvature sensitivity

After establishing the ability of clathrin to assemble on tethered vesicles, we then sought to measure the preference of clathrin for highly curved membranes. Specifically, we sought to quantify the clathrin-to-lipid ratio for each vesicle as a function of vesicle diameter, in order to evaluate clathrin's inherent curvature sensing ability. We repeated a binding assay similar to the one described above, at pH 8.0, this time incubating much lower concentrations of clathrin with the vesicles, in order to isolate clathrin's curvature sensing ability from any cooperativity that might occur as assembly begins.

Interestingly, our measurements of clathrin-to-lipid ratio suggested that clathrin binds preferentially to membranes of higher curvature (Figure 4.3a). Specifically, when incubated with the same concentration of clathrin in the same experimental well, larger clathrin-to-lipid ratios were achieved for vesicles with smaller diameters (and therefore higher curvatures). For example, vesicles with an average diameter of 25 nm recruited more than five times as many clathrin triskelia per membrane surface area in comparison to vesicles with an average diameter of 80 nm, indicating that clathrin triskelia have a similar intrinsic curvature sensing ability compared to previous reports measuring the curvature preference of the BAR domains and amphipathic helices of clathrin adaptor proteins[24, 25].

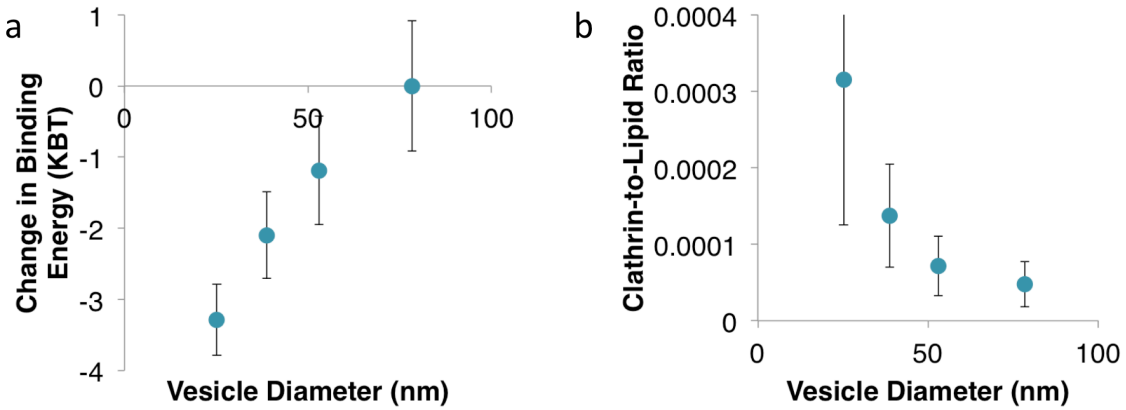

Figure 4.3: **Clathrin exhibits curvature sensitivity.** (a), The clathrin to lipid ratio increased with increasing vesicle curvature. For analysis, vesicles were divided equally into four cohorts based on diameter. Each point represents the average number of bound clathrin triskelia for vesicles within that cohort. Error bars represent the standard deviation for the vesicles within that cohort. At least 300 total vesicles analyzed for each condition. For this study, vesicles were sonicated and incubated with 100 pM clathrin. (b), Binding energy versus vesicle diameter. The change in binding energy decreased with vesicle curvature, demonstrating clathrin's curvature sensing ability.

Curvature dependence of clathrin to vesicle binding energy

Our data was input into a statistical model, from which the curvature dependence of clathrin to vesicle binding energy can be derived. Specifically, the probability of binding site occupancy as predicted by the Langmuir isotherm can be rearranged as follows to determine the change in energy that occurs when a triskelia binds to a vesicle:

$$P_{BOUND} = \frac{\left(\frac{L}{\Omega}\right)e^{-\beta\Delta E}}{1 + \left(\frac{L}{\Omega}\right)e^{-\beta\Delta E}}$$

$$\left(1 + \left(\frac{L}{\Omega}\right)e^{-\beta\Delta E}\right) * P_{BOUND} = \left(\frac{L}{\Omega}\right)e^{-\beta\Delta E}$$

$$P_{BOUND} + \left(\frac{P_{BOUND} * L}{\Omega}\right)e^{-\beta\Delta E} = \left(\frac{L}{\Omega}\right)e^{-\beta\Delta E}$$

$$\left(\frac{L}{\Omega}\right)e^{-\beta\Delta E} - \left(\frac{P_{BOUND} * L}{\Omega}\right)e^{-\beta\Delta E} = P_{BOUND}$$

$$e^{-\beta\Delta E}\left(\frac{L}{\Omega} - \frac{P_{BOUND} * L}{\Omega}\right) = P_{BOUND}$$

$$e^{-\beta\Delta E} = \frac{P_{BOUND}}{\left(\frac{L}{\Omega} - \frac{P_{BOUND} * L}{\Omega}\right)}$$

$$\beta\Delta E = \ln\left(\frac{\Omega}{L}\left(\frac{P_{Bound}}{1 - P_{Bound}}\right)\right)$$

Where P_{BOUND} is the probability that an individual binding sites on the membrane surface is occupied by a clathrin triskelion, L is the number of clathrin triskelia available per binding site, and Ω is the total number of locations in solution where triskelia can reside prior to membrane binding. To determine the relationship between binding energy and curvature, our data were analyzed in eight separate cohorts based on vesicle diameter (inversely proportional to curvature). In particular, for each cohort, the average probability of binding was determined based on the average clathrin coverage of vesicles in each cohort. The total number of possible binding sites was determined based on the average vesicle surface area for each cohort and the number of vesicles within each cohort. Finally, the number of clathrin triskelia available for each binding site was determined based on the clathrin concentration and the size and density of tethered vesicles, which were constant across all cohorts.

Analyzing the data in diameter cohorts enabled determination of the relationship between binding energy and curvature, as plotted in Figure 4.3b. We found that the change in binding energy increased (negatively) with decreasing vesicle diameter (and therefore with increasing membrane curvature), a trend that is consistent with established curvature sensors and which suggests that it is more energetically favorable for clathrin to bind to highly curved membranes[24, 25]. Further, our data demonstrate that the free energy of the system is more than 3 k_BT lower per membrane-bound triskelia when triskelia bind to the most highly curved vesicles rather than to the largest, flattest vesicles. This change in binding energy is greater than the 1 k_BT increase reported for amphipathic helices, suggesting that clathrin triskelia may possess a stronger preference for highly curved membranes than some of its adaptor proteins[25].

Conclusion

In conclusion, we have evaluated the extent to which clathrin has the inherent capacity to sense membrane curvature. Our data demonstrated that clathrin binds preferentially to membranes of high curvature. Further, using the Boltzmann distribution, we have determined how the binding energy released as clathrin binds to vesicles depends on vesicle curvature. Our ongoing work continues to map the distribution of bound clathrin triskelia over vesicles with a range of different curvatures and to improve the statistical model from which the curvature dependence of binding energy can be derived.

These findings provide fundamental insight into the process by which clathrin is recruited to highly curved membranes during clathrin-mediated endocytosis. In particular, it has previously been thought that only adaptor proteins sense curvature, while clathrin's role is simply to concentrate coated vesicle components and drive

curvature[1]. However, our findings suggest that clathrin triskelia themselves are likely involved in sensing curvature. One possible role of clathrin as a curvature sensor could be to limit assembly of clathrin-coated vesicles only to groups of membrane-bound adaptor proteins located in regions of high membrane curvature.

More broadly, our data suggests that the highly sequential model of clathrin-coated vesicle assembly, in which adaptors arrive at membranes first and are then followed by clathrin[1], could be over simplified. Specifically, our findings suggest that recruiting a critical nucleus of clathrin could be an early event that depends on membrane curvature. This speculation is consistent with the recent finding by the Kirchhausen lab, which was based on studies in live cells and showed that recruitment of clathrin is one of the earliest events to occur in the formation of a clathrin-coated vesicle[41].

Materials and Methods

Chemical reagents. DTT (dithiothreitol), TRIS (2-Amino-2-(hydroxymethyl)-1,3-propanediol), PLL (poly-L-lysine) and Atto 594 NHS-ester were purchased from Sigma-Aldrich. Neutravidin and Oregon Green 488-DHPE (Oregon Green 488 1,2-dihexadecanoyl-*sn*-glycero-3-phosphoethanolamine) were purchased from Thermo Fisher Scientific. Amine-reactive mPEG-SVA (mPEG-succinimidyl valerate) and biotin-PEG-SVA (both molecular weight 5,000 Da) were purchased from Laysan Bio (Arab, AL, USA). DP-EG10-biotin (dipalmitoyl-decaethylene glycol-biotin) was generously provided by Darryl Sasaki[42]. All other lipids were purchased from Avanti Polar Lipids (Alabaster, AL, USA), including: DOGS-NTA-Ni (1,2-dioleoyl-sn-glycero-3-[(N-(5-amino-1-carboxypentyl)iminodiacetic acid)succinyl], nickel salt) and DOPC (1,2-dioleoyl-sn-glycero-3-phosphocholine). his-Clathrin was generously provided by Eileen Lafer.

Protein labeling. Protein labeling reactions were performed in 25 mM HEPES, 150 mM NaCl, 1 mM TCEP, pH 7.2 buffer. Proteins were labeled using amine-reactive, NHS ester-functionalized dyes (Atto-Tec). The concentration of dye was adjusted experimentally to obtain the desired labeling ratio of 1:1. Reactions were performed for 20 min at room temperature, labeled protein was separated from unconjugated dye via size exclusion chromatography with Sephadex G-25 (GE Healthcare Life Sciences).

Fluorescence microscopy. A spinning disc confocal microscope (Zeiss Axio Observer Z1 with Yokagawa CSU-X1M) was used to image tethered vesicles. Laser wavelengths of 488 and 561 nm were used for excitation. Emission filters were centered at 525 nm with a 50-nm width, and 629 nm with a 62-nm width. A triple-pass dichroic mirror was used: 405/488/561 nm. The microscope objective used was a Plan-

Apochromat 100x, 1.4 numerical aperture oil immersion objective. Tethered vesicles were imaged on an EMCCD camera.

Liposome preparation. Vesicles were composed of 95.5 mol% DOPC, 2 mol% DOGS-NTA-Ni, 0.5 mol% Oregon Green 488-DHPE, and 2 mol% DP-EG10-biotin. Dried lipid films were hydrated in storage buffer (10 mM TRIS, 25mM BME, pH 8.0) and either sonicated or extruded to 100 nm.

Tethered vesicle assay. Biotinylated PLL-PEG was made according to a previous protocol (Ruiz Taylor 2001). Briefly, amine-reactive PEG and PEG-biotin was added to a 40 mg mL^{-1} mixture of PLL in 50 mM sodium tetraborate, pH 8.5, at a stoichiometric ratio of one PEG per five lysine subunits. PEG-biotin comprised either 2% of the total PEG amount. The mixture was stirred continuously for 6 h at room temperature, and subsequently buffer exchanged into PBS using Centri-Spin size exclusion columns (Princeton Separations).

Imaging wells were made by placing silicone gaskets onto ultraclean coverslips. Wells were coated for 1 h with biotinylated PLL-PEG that was diluted tenfold in experiment buffer (10 mM TRIS, 25 mM BME, 25 mM KCL, pH 8.0). After coating, the well was washed repeatedly with experiment buffer to wash out excess PLL-PEG. Neutravidin was then added to the well at a final concentration of 0.2 mg mL^{-1}, incubated for 10 min, and the well was repeatedly washed with experiment buffer.

Vesicles were then diluted to 5 μM in the imaging wells and allowed to tether to the substrate for 10 min. Untethered vesicles were removed by thorough washing of the well with experiment buffer. The same laser power and camera gain settings were used for all experiments

Determination of parameters from vesicle and protein brightness measurements. All images in the z-stacks were cropped to the center 171x171 pixels, and

the frame with the greatest mean brightness was selected for analysis. Fluorescence amplitudes of diffraction-limited puncta were obtained using cmeAnalysis particle detection software (Aguet 2013). Individual vesicles were detected by fitting two dimensional Gaussian profiles to each puncta in the lipid fluorescence channel. The standard deviation of the Gaussian was determined from the point spread function of our microscope. The brightnesses of detected puncta were reported as valid if they were diffraction-limited and had amplitudes significantly above their local fluorescence background. The program then used the centroids of the lipid fluorescent puncta to check for fluorescent puncta near the centroid in the protein fluorescence channel. To further ensure that only legitimate puncta were analyzed, we only accepted puncta whose amplitude was greater than two standard deviations above the average of all the local fluorescence background values measured for each detected puncta in the image.

We estimated vesicle size from lipid fluorescence brightness values by computing a scaling factor which centered the mean of the vesicle brightness distribution, prior to adding protein, to the intensity-weighted average vesicle size obtained from dynamic light scattering.

We estimated the number of bound proteins on each vesicle by comparing brightness values in the protein channel to the known brightness of a single molecule of his-Clathrin-Atto 594. Images of single molecules of his-Clathrin-Atto 594 were obtained by adding a dilute concentration of protein to an imaging well on an ultraclean coverslip, and imaging in a similar manner as described for the tethered vesicles. A longer camera exposure time was necessary to image single molecules. A linear correction for exposure time was therefore applied to the single molecule brightness value before comparing with brightnesses of membrane-bound protein.

Electron microscopy. Vesicles for electron microscopy were tethered directly onto glow-discharged, 300 square mesh, carbon-coated grids and stained with 2% uranyl acetate (Electron Microscopy Sciences; Hatfield, PA, USA). Images were collected on a Tecnai Spirit BioTwin T12 electron microscope (Tecnai; Hillsboro, OR, USA).

References

1. McMahon, H. T.; Boucrot, E., Molecular mechanism and physiological functions of clathrin-mediated endocytosis. Nature Reviews Molecular Cell Biology 2011, 12 (8), 517-533.
2. Pearse, B. M. F., COATED VESICLES FROM HUMAN-PLACENTA CARRY FERRITIN, TRANSFERRIN, AND IMMUNOGLOBULIN-G. Proceedings of the National Academy of Sciences of the United States of America-Biological Sciences 1982, 79 (2), 451-455.
3. Anderson, R. G. W.; Brown, M. S.; Goldstein, J. L., Role of the coated endocytic vesicle in the uptake of receptor-bound low density lipoprotein in human fibroblasts. Cell 1977, 10 (3), 351-364.
4. Vanneste, S.; Friml, J., Auxin: A Trigger for Change in Plant Development. Cell 2009, 136 (6), 1005-1016.
5. Sorkin, A.; von Zastrow, M., Endocytosis and signalling: intertwining molecular networks. Nature Reviews Molecular Cell Biology 2009, 10 (9), 609-622.
6. Scita, G.; Di Fiore, P. P., The endocytic matrix. Nature 2010, 463 (7280), 464-473.
7. Haucke, V.; Neher, E.; Sigrist, S. J., Protein scaffolds in the coupling of synaptic exocytosis and endocytosis. Nature Reviews Neuroscience 2011, 12 (3), 127-138.
8. Sahay, G.; Alakhova, D. Y.; Kabanov, A. V., Endocytosis of nanomedicines. Journal of Controlled Release 2010, 145 (3), 182-195.
9. McPherson, P. S.; Kay, B. K.; Hussain, N. K., Signaling on the endocytic pathway. Traffic 2001, 2 (6), 375-384.

10. Stimpson, H. E. M.; Toret, C. P.; Cheng, A. T.; Pauly, B. S.; Drubin, D. G., Early-Arriving Syp1p and Ede1p Function in Endocytic Site Placement and Formation in Budding Yeast. Molecular Biology of the Cell 2009, 20 (22), 4640-4651.

11. Henne, W. M.; Boucrot, E.; Meinecke, M.; Evergren, E.; Vallis, Y.; Mittal, R.; McMahon, H. T., FCHo Proteins Are Nucleators of Clathrin-Mediated Endocytosis. Science 2010, 328 (5983), 1281-1284.

12. Reider, A.; Barker, S. L.; Mishra, S. K.; Im, Y. J.; Maldonado-Baez, L.; Hurley, J. H.; Traub, L. M.; Wendland, B., Syp1 is a conserved endocytic adaptor that contains domains involved in cargo selection and membrane tubulation. Embo Journal 2009, 28 (20), 3103-3116.

13. Collins, B. M.; McCoy, A. J.; Kent, H. M.; Evans, P. R.; Owen, D. J., Molecular architecture and functional model of the endocytic AP2 complex. Cell 2002, 109 (4), 523-535.

14. Ford, M. G. J.; Mills, I. G.; Peter, B. J.; Vallis, Y.; Praefcke, G. J. K.; Evans, P. R.; McMahon, H. T., Curvature of clathrin-coated pits driven by epsin. Nature 2002, 419 (6905), 361-366.

15. Ford, M. G. J.; Pearse, B. M. F.; Higgins, M. K.; Vallis, Y.; Owen, D. J.; Gibson, A.; Hopkins, C. R.; Evans, P. R.; McMahon, H. T., Simultaneous binding of PtdIns(4,5)P-2 and clathrin by AP180 in the nucleation of clathrin lattices on membranes. Science 2001, 291 (5506), 1051-1055.

16. Robinson, M. S., Adaptable adaptors for coated vesicles. Trends in Cell Biology 2004, 14 (4), 167-174.

17. Kosaka, T.; Ikeda, K., REVERSIBLE BLOCKAGE OF MEMBRANE RETRIEVAL AND ENDOCYTOSIS IN THE GARLAND CELL OF THE TEMPERATURE-SENSITIVE MUTANT OF DROSOPHILA-

MELANOGASTER, SHIBIRETS1. Journal of Cell Biology 1983, 97 (2), 499-507.

18. Wigge, P.; Kohler, K.; Vallis, Y.; Doyle, C. A.; Owen, D.; Hunt, S. P.; McMahon, H. T., Amphiphysin heterodimers: Potential role in clathrin-mediated endocytosis. Molecular Biology of the Cell 1997, 8 (10), 2003-2015.

19. Sundborger, A.; Soderblom, C.; Vorontsova, O.; Evergren, E.; Hinshaw, J. E.; Shupliakov, O., An endophilin-dynamin complex promotes budding of clathrin-coated vesicles during synaptic vesicle recycling. Journal of Cell Science 2011, 124 (1), 133-143.

20. Ferguson, S.; Raimondi, A.; Paradise, S.; Shen, H. Y.; Mesaki, K.; Ferguson, A.; Destaing, O.; Ko, G.; Takasaki, J.; Cremona, O.; O'Toole, E.; De Camilli, P., Coordinated Actions of Actin and BAR Proteins Upstream of Dynamin at Endocytic Clathrin-Coated Pits. Developmental Cell 2009, 17 (6), 811-822.

21. Schlossman, D. M.; Schmid, S. L.; Braell, W. A.; Rothman, J. E., AN ENZYME THAT REMOVES CLATHRIN COATS - PURIFICATION OF AN UNCOATING ATPASE. Journal of Cell Biology 1984, 99 (2), 723-733.

22. Ungewickell, E.; Ungewickell, H.; Holstein, S. E. H.; Lindner, R.; Prasad, K.; Barouch, W.; Martin, B.; Greene, L. E.; Eisenberg, E., ROLE OF AUXILIN IN UNCOATING CLATHRIN-COATED VESICLES. Nature 1995, 378 (6557), 632-635.

23. Peter, B. J.; Kent, H. M.; Mills, I. G.; Vallis, Y.; Butler, P. J. G.; Evans, P. R.; McMahon, H. T., BAR domains as sensors of membrane curvature: The amphiphysin BAR structure. Science 2004, 303 (5657), 495-499.

24. Bhatia, V. K.; Madsen, K. L.; Bolinger, P. Y.; Kunding, A.; Hedegard, P.; Gether, U.; Stamou, D., Amphipathic motifs in BAR domains are essential for membrane curvature sensing. Embo Journal 2009, 28 (21), 3303-3314.

25. Hatzakis, N. S.; Bhatia, V. K.; Larsen, J.; Madsen, K. L.; Bolinger, P. Y.; Kunding, A. H.; Castillo, J.; Gether, U.; Hedegard, P.; Stamou, D., How curved membranes recruit amphipathic helices and protein anchoring motifs. Nature Chemical Biology 2009, 5 (11), 835-841.

26. Capraro, B. R.; Yoon, Y.; Cho, W.; Baumgart, T., Curvature Sensing by the Epsin N-Terminal Homology Domain Measured on Cylindrical Lipid Membrane Tethers. Journal of the American Chemical Society 2010, 132 (4), 1200-+.

27. Holkar, S. S.; Kamerkar, S. C.; Pucadyil, T. J., Spatial Control of Epsin-induced Clathrin Assembly by Membrane Curvature. Journal of Biological Chemistry 2015, 290 (23), 14267-14276.

28. Sousa, R.; Liao, H. S.; Cuellar, J.; Jin, S. P.; Valpuesta, J. M.; Jin, A. J.; Lafer, E. M., Clathrin-coat disassembly illuminates the mechanisms of Hsp70 force generation. Nature Structural & Molecular Biology 2016, 23 (9), 821-829.

29. Zhuo, Y.; Ilangovan, U.; Schirf, V.; Demeler, B.; Sousa, R.; Hinck, A. P.; Lafer, E. M., Dynamic Interactions between Clathrin and Locally Structured Elements in a Disordered Protein Mediate Clathrin Lattice Assembly. Journal of Molecular Biology 2010, 404 (2), 274-290.

30. Wakeham, D. E.; Ybe, J. A.; Brodsky, F. M.; Hwang, P. K., Molecular structures of proteins involved in vesicle coat formation. Traffic 2000, 1 (5), 393-398.

31. Stamou, D.; Duschl, C.; Delamarche, E.; Vogel, H., Self-assembled microarrays of attoliter molecular vessels. Angewandte Chemie-International Edition 2003, 42 (45), 5580-5583.

32. Ruiz-Taylor, L. A.; Martin, T. L.; Zaugg, F. G.; Witte, K.; Indermuhle, P.; Nock, S.; Wagner, P., Monolayers of derivatized poly(L-lysine)-grafted poly(ethylene glycol) on metal oxides as a class of biomolecular interfaces. Proceedings of the National Academy of Sciences of the United States of America 2001, 98 (3), 852-857.

33. Elbert, D. L.; Hubbell, J. A., Self-assembly and steric stabilization at heterogeneous, biological surfaces using adsorbing block copolymers. Chemistry & Biology 1998, 5 (3), 177-183.

34. Hao, W. H.; Luo, Z.; Zheng, L.; Prasad, K.; Lafer, E. M., AP180 and AP-2 interact directly in a complex that cooperatively assembles clathrin. Journal of Biological Chemistry 1999, 274 (32), 22785-22794.

35. Wakeham, D. E.; Chen, C. Y.; Greene, B.; Hwang, P. K.; Brodsky, F. M., Clathrin self-assembly involves coordinated weak interactions favorable for cellular regulation. Embo Journal 2003, 22 (19), 4980-4990.

36. Fotin, A.; Cheng, Y. F.; Sliz, P.; Grigorieff, N.; Harrison, S. C.; Kirchhausen, T.; Walz, T., Molecular model for a complete clathrin lattice from electron cryomicroscopy. Nature 2004, 432 (7017), 573-579.

37. Nandi, P. K.; Edelhoch, H., THE EFFECTS OF LYOTROPIC (HOFMEISTER) SALTS ON THE STABILITY OF CLATHRIN COAT STRUCTURE IN COATED VESICLES AND BASKETS. Journal of Biological Chemistry 1984, 259 (18), 1290-1296.

38. Heuser, J., EFFECTS OF CYTOPLASMIC ACIDIFICATION ON CLATHRIN LATTICE MORPHOLOGY. Journal of Cell Biology 1989, 108 (2), 401-411.

39. Cheng, Y. F.; Boll, W.; Kirchhausen, T.; Harrison, S. C.; Walz, T., Cryo-electron tomography of clathrin-coated vesicles: Structural implications for coat assembly. Journal of Molecular Biology 2007, 365 (3), 892-899.

40. Dannhauser, P. N.; Ungewickell, E. J., Reconstitution of clathrin-coated bud and vesicle formation with minimal components. Nature Cell Biology 2012, 14 (6), 634-+.

41. Cocucci, E.; Aguet, F.; Boulant, S.; Kirchhausen, T., The First Five Seconds in the Life of a Clathrin-Coated Pit. Cell 2012, 150 (3), 495-507.

42. Torchilin, V. P., Recent advances with liposomes as pharmaceutical carriers. Nature Reviews Drug Discovery 2005, 4 (2), 145-160.

Chapter 5: Conclusion

Ultimately, in my thesis work I have addressed both the need to (i) introduce new methods of therapeutic delivery that overcome the limitations of existing mechanisms, and the need to (ii) understand the existing mechanisms of therapeutic uptake at a molecular level.

Towards introducing new methods of therapeutic delivery that overcome the limitations of existing mechanisms, I have developed targeted Connectosomes, cell-derived lipid vesicle materials that contain embedded connexons and are capable of forming functional gap junctions with cells. By opening direct routes to the cytoplasm, these materials reduced the therapeutically effective dose (LD50) of doxorubicin for target cells by more than an order of magnitude in comparison to the unencapsulated drug, and by several orders of magnitude in comparison to conventional liposomal doxorubicin. Further, through interactions of embedded multi-functional, multi-domain transmembrane targeting proteins that target cell-specific receptors, these materials achieved targeted delivery of molecular cargo directly into the cytoplasm of specific populations of target cells.

Illustrating the therapeutic importance of direct access to the cell cytoplasm, my work in this area represents a key step towards achieving efficient therapeutic delivery independently of endocytosis. In the future, targeted Connectosomes could be used to increase the effectiveness of diverse therapeutics. Likely next steps for the Connectosomes include adapting the technology to facilitate delivery of diverse, membrane impermeable therapeutics, including siRNA and peptides. Additionally, in order to realize the translational potential of the Connectosomes, many steps must also be taken in order to scale-up production of these materials, and to characterize their *in vivo*

behaviors such as circulation time, tumor penetration, and stability. While there are still many challenges to overcome, the contribution of my work has been to inspire the field by highlighting the potential of gap junctions as delivery route that is entirely untapped by current therapeutics.

Towards furthering our fundamental understanding of the mechanisms of therapeutic uptake at the molecular level, I have also investigated the curvature sensing abilities of clathrin, a key protein involved in clathrin-mediated endocytosis. In particular, my findings demonstrate that clathrin binds preferentially to highly curved membranes. Although it has previously been thought that clathrin is involved only in the later stages of endocytosis, my results demonstrate clathrin's inherent curvature-sensing ability and suggest a possible explanation for clathrin's early participation in endocytic vesicle formation. Therefore, my work in this field represents a key step in furthering our basic biophysical understanding of the mechanisms that drive clathrin-mediated internalization of nanoparticles and other molecular cargo.

In sum, this work represents key steps towards improving the success of nanoparticle-based drug delivery strategies from both applied and fundamental standpoints.

Bibliography

Allen, M. J.; Gemel, J.; Beyer, E. C.; Lal, R., Atomic force microscopy of Connexin40 gap junction hemichannels reveals calcium-dependent three-dimensional molecular topography and open-closed conformations of both the extracellular and cytoplasmic faces. The Journal of biological chemistry 2011, 286 (25), 22139-46.

Allen, T. M., Ligand-targeted therapeutics in anticancer therapy. Nature Reviews Cancer 2002, 2 (10), 750-763.

Alvarez-Erviti, L.; Seow, Y. Q.; Yin, H. F.; Betts, C.; Lakhal, S.; Wood, M. J. A., Delivery of siRNA to the mouse brain by systemic injection of targeted exosomes. Nature Biotechnology 2011, 29 (4), 341-U179.

Anderson, R. G. W.; Brown, M. S.; Goldstein, J. L., Role of the coated endocytic vesicle in the uptake of receptor-bound low density lipoprotein in human fibroblasts. Cell 1977, 10 (3), 351-364.

Ashley, C. E.; Carnes, E. C.; Phillips, G. K.; Padilla, D.; Durfee, P. N.; Brown, P. A.; Hanna, T. N.; Liu, J. W.; Phillips, B.; Carter, M. B.; Carroll, N. J.; Jiang, X. M.; Dunphy, D. R.; Willman, C. L.; Petsev, D. N.; Evans, D. G.; Parikh, A. N.; Chackerian, B.; Wharton, W.; Peabody, D. S.; Brinker, C. J., The targeted delivery of multicomponent cargos to cancer cells by nanoporous particle-supported lipid bilayers. Nature Materials 2011, 10 (5), 389-397.

Bareford, L. A.; Swaan, P. W., Endocytic mechanisms for targeted drug delivery. Advanced Drug Delivery Reviews 2007, 59 (8), 748-758.

Barenholz, Y., Doxil (R) - The first FDA-approved nano-drug: Lessons learned. Journal of Controlled Release 2012, 160 (2), 117-134.

Barenholz, Y., Liposome application: problems and prospects. Current Opinion in Colloid & Interface Science 2001, 6 (1), 66-77.

Bhatia, V. K.; Madsen, K. L.; Bolinger, P. Y.; Kunding, A.; Hedegard, P.; Gether, U.; Stamou, D., Amphipathic motifs in BAR domains are essential for membrane curvature sensing. Embo Journal 2009, 28 (21), 3303-3314.

Brink, P. R.; Valiunas, V.; Gordon, C.; Rosen, M. R.; Cohen, I. S., Can gap junctions deliver? Biochimica Et Biophysica Acta-Biomembranes 2012, 1818 (8), 2076-2081.

Bronshtein, T.; Toledano, N.; Danino, D.; Pollack, S.; Machluf, M., Cell derived liposomes expressing CCR5 as a new targeted drug-delivery system for HIV infected cells. Journal of Controlled Release 2011, 151 (2), 139-148.

Caldorera-Moore, M.; Guimard, N.; Shi, L.; Roy, K., Designer nanoparticles: incorporating size, shape and triggered release into nanoscale drug carriers. Expert Opin Drug Deliv 2010, 7 (4), 479-495.

Capraro, B. R.; Yoon, Y.; Cho, W.; Baumgart, T., Curvature Sensing by the Epsin N-Terminal Homology Domain Measured on Cylindrical Lipid Membrane Tethers. Journal of the American Chemical Society 2010, 132 (4), 1200-+.

Charras, G.; Paluch, E., Blebs lead the way: how to migrate without lamellipodia. Nature Reviews Molecular Cell Biology 2008, 9 (9), 730-736.

Chen, L.; Novicky, L.; Merzlyakov, M.; Hristov, T.; Hristova, K., Measuring the energetics of membrane protein dimerization in mammalian membranes. Journal of the American Chemical Society 2010, 132 (10), 3628-35.

Chen, S. Y.; Zhao, X. R.; Chen, J. Y.; Chen, J.; Kuznetsova, L.; Wong, S. S.; Ojima, I., Mechanism-Based Tumor-Targeting Drug Delivery System. Validation of

Efficient Vitamin Receptor-Mediated Endocytosis and Drug Release. Bioconjugate Chemistry 2010, 21 (5), 979-987.

Cheng, Y. F.; Boll, W.; Kirchhausen, T.; Harrison, S. C.; Walz, T., Cryo-electron tomography of clathrin-coated vesicles: Structural implications for coat assembly. Journal of Molecular Biology 2007, 365 (3), 892-899.

Cocucci, E.; Aguet, F.; Boulant, S.; Kirchhausen, T., The First Five Seconds in the Life of a Clathrin-Coated Pit. Cell 2012, 150 (3), 495-507.

Collins, B. M.; McCoy, A. J.; Kent, H. M.; Evans, P. R.; Owen, D. J., Molecular architecture and functional model of the endocytic AP2 complex. Cell 2002, 109 (4), 523-535.

Connors, B. W., Tales of a Dirty Drug: Carbenoxolone, Gap Junctions, and Seizures. Epilepsy Currents 2012, 12 (2), 66-68.

Costello, D. A.; Hsia, C. Y.; Millet, J. K.; Porri, T.; Daniel, S., Membrane fusion-competent virus-like proteoliposomes and proteinaceous supported bilayers made directly from cell plasma membranes. Langmuir : the ACS journal of surfaces and colloids 2013, 29 (21), 6409-19.

Damaraju, V. L.; Damaraju, S.; Young, J. D.; Baldwin, S. A.; Mackey, J.; Sawyer, M. B.; Cass, C. E., Nucleoside anticancer drugs: the role of nucleoside transporters in resistance to cancer chemotherapy. Oncogene 2003, 22 (47), 7524-7536.

Dannhauser, P. N.; Ungewickell, E. J., Reconstitution of clathrin-coated bud and vesicle formation with minimal components. Nature Cell Biology 2012, 14 (6), 634-+.

Davis, M. E.; Chen, Z.; Shin, D. M., Nanoparticle therapeutics: an emerging treatment modality for cancer. Nature Reviews Drug Discovery 2008, 7 (9), 771-782.

Durand, R. E.; Olive, P. L., FLOW-CYTOMETRY STUDIES OF INTRACELLULAR ADRIAMYCIN IN SINGLE CELLS-INVITRO. Cancer Research 1981, 41 (9), 3489-3494.

Durfee, P. N.; Lin, Y. S.; Dunphy, D. R.; Muniz, A. J.; Butler, K. S.; Humphrey, K. R.; Lokke, A. J.; Agola, J. O.; Chou, S. S.; Chen, I. M.; Wharton, W.; Townson, J. L.; Willman, C. L.; Brinker, C. J., Mesoporous Silica Nanoparticle-Supported Lipid Bilayers (Protocells) for Active Targeting and Delivery to Individual Leukemia Cells. Acs Nano 2016, 10 (9), 8325-8345.

El Andaloussi, S.; Maeger, I.; Breakefield, X. O.; Wood, M. J. A., Extracellular vesicles: biology and emerging therapeutic opportunities. Nature Reviews Drug Discovery 2013, 12 (5), 348-358.

El-Sayed, A.; Futaki, S.; Harashima, H., Delivery of Macromolecules Using Arginine-Rich Cell-Penetrating Peptides: Ways to Overcome Endosomal Entrapment. Aaps Journal 2009, 11 (1), 13-22.

Elbert, D. L.; Hubbell, J. A., Self-assembly and steric stabilization at heterogeneous, biological surfaces using adsorbing block copolymers. Chemistry & Biology 1998, 5 (3), 177-183.

Elzarrad, M. K.; Haroon, A.; Willecke, K.; Dobrowolski, R.; Gillespie, M. N.; Al-Mehdi, A. B., Connexin-43 upregulation in micrometastases and tumor vasculature and its role in tumor cell attachment to pulmonary endothelium. BMC Med 2008, 6, 20.

Erazo-Oliveras, A.; Muthukrishnan, N.; Baker, R.; Wang, T.-Y.; Pellois, J.-P., Improving the endosomal escape of cell-penetrating peptides and their cargos: strategies and challenges. Pharmaceuticals (Basel, Switzerland) 2012, 5 (11), 1177-209.

Evans, W. H.; Martin, P. E. M., Gap junctions: structure and function (Review). Molecular Membrane Biology 2002, 19 (2), 121-136.

Ewer, M. S.; Ewer, S. M., Cardiotoxicity of anticancer treatments. Nature reviews. Cardiology 2015, 12 (9), 547-58.

Eytan, G. D., Mechanism of multidrug resistance in relation to passive membrane permeation. Biomedicine & Pharmacotherapy 2005, 59 (3), 90-97.

Ferguson, S.; Raimondi, A.; Paradise, S.; Shen, H. Y.; Mesaki, K.; Ferguson, A.; Destaing, O.; Ko, G.; Takasaki, J.; Cremona, O.; O'Toole, E.; De Camilli, P., Coordinated Actions of Actin and BAR Proteins Upstream of Dynamin at Endocytic Clathrin-Coated Pits. Developmental Cell 2009, 17 (6), 811-822.

Ford, M. G. J.; Pearse, B. M. F.; Higgins, M. K.; Vallis, Y.; Owen, D. J.; Gibson, A.; Hopkins, C. R.; Evans, P. R.; McMahon, H. T., Simultaneous binding of PtdIns(4,5)P-2 and clathrin by AP180 in the nucleation of clathrin lattices on membranes. Science 2001, 291 (5506), 1051-1055.

Fotin, A.; Cheng, Y. F.; Sliz, P.; Grigorieff, N.; Harrison, S. C.; Kirchhausen, T.; Walz, T., Molecular model for a complete clathrin lattice from electron cryomicroscopy. Nature 2004, 432 (7017), 573-579.

Furnari, F. B.; Cloughesy, T. F.; Cavenee, W. K.; Mischel, P. S., OPINION Heterogeneity of epidermal growth factor receptor signalling networks in glioblastoma. Nature Reviews Cancer 2015, 15 (5), 302-310.

Gabizon, A.; Shmeeda, H.; Horowitz, A. T.; Zalipsky, S., Tumor cell targeting of liposome-entrapped drugs with phospholipid-anchored folic acid-PEG conjugates. Advanced Drug Delivery Reviews 2004, 56 (8), 1177-1192.

Gadok, A. K.; Busch, D. J.; Ferrati, S.; Li, B.; Smyth, H. D. C.; Stachowiak, J. C., Connectosomes for Direct Molecular Delivery to the Cellular Cytoplasm. Journal of the American Chemical Society 2016, 138 (39), 12833-12840.

Ganta, S.; Devalapally, H.; Shahiwala, A.; Amiji, M., A review of stimuli-responsive nanocarriers for drug and gene delivery. Journal of Controlled Release 2008, 126 (3), 187-204.

Garcia-Rodriguez, L.; Perez-Torras, S.; Carrio, M.; Cascante, A.; Garcia-Ribas, I.; Mazo, A.; Fillat, C., Connexin-26 Is a Key Factor Mediating Gemcitabine Bystander Effect. Molecular Cancer Therapeutics 2011, 10 (3), 505-517.

Gilleron, J.; Querbes, W.; Zeigerer, A.; Borodovsky, A.; Marsico, G.; Schubert, U.; Manygoats, K.; Seifert, S.; Andree, C.; Stoter, M.; Epstein-Barash, H.; Zhang, L. G.; Koteliansky, V.; Fitzgerald, K.; Fava, E.; Bickle, M.; Kalaidzidis, Y.; Akinc, A.; Maier, M.; Zerial, M., Image-based analysis of lipid nanoparticle-mediated siRNA delivery, intracellular trafficking and endosomal escape. Nature Biotechnology 2013, 31 (7), 638-U102.

Goodenough, D. A.; Paul, D. L., Gap Junctions. Cold Spring Harbor Perspectives in Biology 2009, 1 (1), 19.

Gottesman, M. M.; Fojo, T.; Bates, S. E., Multidrug resistance in cancer: role of ATP-dependent transporters. Nat Rev Cancer 2002, 2 (1), 48-58.

Hada, S.; Sato, H.; Virgona, N.; Hagiwara, H.; Saito, T.; Suzuki, K.; Asano, R.; Yano, T., Connexin 32 expression reduces malignant phenotype in human A549 adenocarcinoma cells: Implication of Src involvement. Oncol Rep 2006, 16 (5), 1149-54.

Hao, W. H.; Luo, Z.; Zheng, L.; Prasad, K.; Lafer, E. M., AP180 and AP-2 interact directly in a complex that cooperatively assembles clathrin. Journal of Biological Chemistry 1999, 274 (32), 22785-22794.

Harris, A. L., Emerging issues of connexin channels: biophysics fills the gap. Quarterly Reviews of Biophysics 2001, 34 (3), 325-472.

Hatakeyama, H.; Akita, H.; Maruyama, K.; Suhara, T.; Harashima, H., Factors governing the in vivo tissue uptake of transferrin-coupled polyethylene glycol liposomes in vivo. International Journal of Pharmaceutics 2004, 281 (1-2), 25-33.

Hatzakis, N. S.; Bhatia, V. K.; Larsen, J.; Madsen, K. L.; Bolinger, P. Y.; Kunding, A. H.; Castillo, J.; Gether, U.; Hedegard, P.; Stamou, D., How curved membranes recruit amphipathic helices and protein anchoring motifs. Nature Chemical Biology 2009, 5 (11), 835-841.

Haucke, V.; Neher, E.; Sigrist, S. J., Protein scaffolds in the coupling of synaptic exocytosis and endocytosis. Nature Reviews Neuroscience 2011, 12 (3), 127-138.

Henne, W. M.; Boucrot, E.; Meinecke, M.; Evergren, E.; Vallis, Y.; Mittal, R.; McMahon, H. T., FCHo Proteins Are Nucleators of Clathrin-Mediated Endocytosis. Science 2010, 328 (5983), 1281-1284.

Heuser, J., EFFECTS OF CYTOPLASMIC ACIDIFICATION ON CLATHRIN LATTICE MORPHOLOGY. Journal of Cell Biology 1989, 108 (2), 401-411.

Holkar, S. S.; Kamerkar, S. C.; Pucadyil, T. J., Spatial Control of Epsin-induced Clathrin Assembly by Membrane Curvature. Journal of Biological Chemistry 2015, 290 (23), 14267-14276.

Horowitz, A. T.; Barenholz, Y.; Gabizon, A. A., INVITRO CYTOTOXICITY OF LIPOSOME-ENCAPSULATED DOXORUBICIN - DEPENDENCE ON LIPOSOME COMPOSITION AND DRUG RELEASE. Biochimica Et Biophysica Acta 1992, 1109 (2), 203-209.

Huang, R. P.; Hossain, M. Z.; Huang, R.; Gano, J.; Fan, Y.; Boynton, A. L., Connexin 43 (cx43) enhances chemotherapy-induced apoptosis in human glioblastoma cells. International Journal of Cancer 2001, 92 (1), 130-138.

Hughes, L. D.; Rawle, R. J.; Boxer, S. G., Choose your label wisely: water-soluble fluorophores often interact with lipid bilayers. PLoS One 2014, 9 (2), e87649.

Hyndman, L.; Lemoine, J. L.; Huang, L.; Porteous, D. J.; Boyd, A. C.; Nan, X. S., HIV-1 Tat protein transduction domain peptide facilitates gene transfer in combination with cationic liposomes. Journal of Controlled Release 2004, 99 (3), 435-444.

Johnsen, K. B.; Gudbergsson, J. M.; Skov, M. N.; Pilgaard, L.; Moos, T.; Duroux, M., A comprehensive overview of exosomes as drug delivery vehicles - Endogenous nanocarriers for targeted cancer therapy. Biochimica Et Biophysica Acta-Reviews on Cancer 2014, 1846 (1), 75-87.

Kamba, A. S.; Ismail, M.; Ibrahim, T. A.; Zakaria, Z. A.; Gusau, L. H., In vitro ultrastructural changes of MCF-7 for metastasise bone cancer and induction of apoptosis via mitochondrial cytochrome C released by CaCO3/Dox nanocrystals. Biomed Res Int 2014, 2014, 391869.

Kaneda, M.; Nomura, S. M.; Ichinose, S.; Kondo, S.; Nakahama, K.; Akiyoshi, K.; Morita, I., Direct formation of proteo-liposomes by in vitro synthesis and cellular cytosolic delivery with connexin-expressing liposomes. Biomaterials 2009, 30 (23-24), 3971-3977.

Kirpotin, D. B.; Drummond, D. C.; Shao, Y.; Shalaby, M. R.; Hong, K.; Nielsen, U. B.; Marks, J. D.; Benz, C. C.; Park, J. W., Antibody targeting of long-circulating lipidic nanoparticles does not increase tumor localization but does increase internalization in animal models. Cancer Res 2006, 66 (13), 6732-40.

Kosaka, T.; Ikeda, K., REVERSIBLE BLOCKAGE OF MEMBRANE RETRIEVAL AND ENDOCYTOSIS IN THE GARLAND CELL OF THE TEMPERATURE-SENSITIVE MUTANT OF DROSOPHILA-MELANOGASTER, SHIBIRETS1. Journal of Cell Biology 1983, 97 (2), 499-507.

Kubala, M. H.; Kovtun, O.; Alexandrov, K.; Collins, B. M., Structural and thermodynamic analysis of the GFP:GFP-nanobody complex. Protein Science 2010, 19 (12), 2389-2401.

Lee, E. S.; Na, K.; Bae, Y. H., Doxorubicin loaded pH-sensitive polymeric micelles for reversal of resistant MCF-7 tumor. Journal of Controlled Release 2005, 103 (2), 405-418.

Li, M.; Tao, Y.; Shu, Y.; LaRochelle, J. R.; Steinauer, A.; Thompson, D.; Schepartz, A.; Chen, Z. Y.; Liu, D. R., Discovery and characterization of a peptide that enhances endosomal escape of delivered proteins in vitro and in vivo. Journal of the American Chemical Society 2015, 137 (44), 14084-93.

Lipinski, C. A.; Lombardo, F.; Dominy, B. W.; Feeney, P. J., Experimental and computational approaches to estimate solubility and permeability in drug discovery and development settings. Advanced Drug Delivery Reviews 1997, 23 (1-3), 3-25.

Maeda, H.; Wu, J.; Sawa, T.; Matsumura, Y.; Hori, K., Tumor vascular permeability and the EPR effect in macromolecular therapeutics: a review. Journal of Controlled Release 2000, 65 (1-2), 271-284.

Mamot, C.; Drummond, D. C.; Noble, C. O.; Kallab, V.; Guo, Z. X.; Hong, K. L.; Kirpotin, D. B.; Park, J. W., Epidermal growth factor receptor-targeted immunoliposomes significantly enhance the efficacy of multiple anticancer drugs in vivo. Cancer Research 2005, 65 (24), 11631-11638.

McMahon, H. T.; Boucrot, E., Molecular mechanism and physiological functions of clathrin-mediated endocytosis. Nature Reviews Molecular Cell Biology 2011, 12 (8), 517-533.

McPherson, P. S.; Kay, B. K.; Hussain, N. K., Signaling on the endocytic pathway. Traffic 2001, 2 (6), 375-384.

Mese, G.; Richard, G.; White, T. W., Gap junctions: Basic structure and function. Journal of Investigative Dermatology 2007, 127 (11), 2516-2524.

Mesnil, M.; Piccoli, C.; Tiraby, G.; Willecke, K.; Yamasaki, H., Bystander killing of cancer cells by herpes simplex virus thymidine kinase gene is mediated by connexins. Proceedings of the National Academy of Sciences of the United States of America 1996, 93 (5), 1831-1835.

Mitragotri, S.; Burke, P. A.; Langer, R., Overcoming the challenges in administering biopharmaceuticals: formulation and delivery strategies. Nature Reviews Drug Discovery 2014, 13 (9), 655-672.

Mukthavaram, R.; Shi, G. X.; Kesari, S.; Simberg, D., Targeting and depletion of circulating leukocytes and cancer cells by lipophilic antibody-modified erythrocytes. Journal of Controlled Release 2014, 183, 146-153.

Muller, D. J.; Hand, G. M.; Engel, A.; Sosinsky, G. E., Conformational changes in surface structures of isolated connexin 26 gap junctions. Embo Journal 2002, 21 (14), 3598-3607.

Mura, S.; Nicolas, J.; Couvreur, P., Stimuli-responsive nanocarriers for drug delivery. Nature Materials 2013, 12 (11), 991-1003.

Murthy, N.; Robichaud, J. R.; Tirrell, D. A.; Stayton, P. S.; Hoffman, A. S., The design and synthesis of polymers for eukaryotic membrane disruption. Journal of Controlled Release 1999, 61 (1-2), 137-143.

Nandi, P. K.; Edelhoch, H., THE EFFECTS OF LYOTROPIC (HOFMEISTER) SALTS ON THE STABILITY OF CLATHRIN COAT STRUCTURE IN COATED VESICLES AND BASKETS. Journal of Biological Chemistry 1984, 259 (18), 1290-1296.

Neijssen, J.; Herberts, C.; Drijfhout, J. W.; Reits, E.; Janssen, L.; Neefjes, J., Cross-presentation by intercellular peptide transfer through gap junctions. Nature 2005, 434 (7029), 83-88.

Nurcahyanti, A. D.; Wink, M., L-Canavanine potentiates the cytotoxicity of doxorubicin and cisplatin in arginine deprived human cancer cells. PeerJ 2016, 4, e1542.

Ohno, S.-i.; Takanashi, M.; Sudo, K.; Ueda, S.; Ishikawa, A.; Matsuyama, N.; Fujita, K.; Mizutani, T.; Ohgi, T.; Ochiya, T.; Gotoh, N.; Kuroda, M., Systemically Injected Exosomes Targeted to EGFR Deliver Antitumor MicroRNA to Breast Cancer Cells. Molecular Therapy 2013, 21 (1), 185-191.

Overington, J. P.; Al-Lazikani, B.; Hopkins, A. L., Opinion - How many drug targets are there? Nature Reviews Drug Discovery 2006, 5 (12), 993-996.

Park, J. H.; Gu, L.; von Maltzahn, G.; Ruoslahti, E.; Bhatia, S. N.; Sailor, M. J., Biodegradable luminescent porous silicon nanoparticles for in vivo applications. Nature Materials 2009, 8 (4), 331-336.

Park, J. W.; Hong, K. L.; Kirpotin, D. B.; Colbern, G.; Shalaby, R.; Baselga, J.; Shao, Y.; Nielsen, U. B.; Marks, J. D.; Moore, D.; Papahadjopoulos, D.; Benz, C. C., Anti-HER2 immunoliposomes: Enhanced efficacy attributable to targeted delivery. Clinical Cancer Research 2002, 8 (4), 1172-1181.

Pearse, B. M. F., COATED VESICLES FROM HUMAN-PLACENTA CARRY FERRITIN, TRANSFERRIN, AND IMMUNOGLOBULIN-G. Proceedings of the National Academy of Sciences of the United States of America-Biological Sciences 1982, 79 (2), 451-455.

Peer, D.; Karp, J. M.; Hong, S.; FaroKhzad, O. C.; Margalit, R.; Langer, R., Nanocarriers as an emerging platform for cancer therapy. Nature Nanotechnology 2007, 2 (12), 751-760.

Peter, B. J.; Kent, H. M.; Mills, I. G.; Vallis, Y.; Butler, P. J. G.; Evans, P. R.; McMahon, H. T., BAR domains as sensors of membrane curvature: The amphiphysin BAR structure. Science 2004, 303 (5657), 495-499.

Phillips, M. A.; Gran, M. L.; Peppas, N. A., Targeted nanodelivery of drugs and diagnostics. Nano Today 2010, 5 (2), 143-159.

Preus, D.; Johnson, R.; Sheridan, J.; Meyer, R., ANALYSIS OF GAP-JUNCTIONS AND FORMATION PLAQUES BETWEEN REAGGREGATING NOVIKOFF HEPATOMA-CELLS. Journal of Ultrastructure Research 1981, 77 (3), 263-276.

Qin, H.; Shao, Q.; Curtis, H.; Galipeau, J.; Belliveau, D. J.; Wang, T.; Alaoui-Jamali, M. A.; Laird, D. W., Retroviral delivery of connexin genes to human breast tumor cells inhibits in vivo tumor growth by a mechanism that is independent of significant gap junctional intercellular communication. The Journal of biological chemistry 2002, 277 (32), 29132-8.

Reider, A.; Barker, S. L.; Mishra, S. K.; Im, Y. J.; Maldonado-Baez, L.; Hurley, J. H.; Traub, L. M.; Wendland, B., Syp1 is a conserved endocytic adaptor that contains domains involved in cargo selection and membrane tubulation. Embo Journal 2009, 28 (20), 3103-3116.

Ren, Y.; Wong, S. M.; Lim, L. Y., Folic acid-conjugated protein cages of a plant virus: A novel delivery platform for doxorubicin. Bioconjugate Chemistry 2007, 18 (3), 836-843.

Robinson, M. S., Adaptable adaptors for coated vesicles. Trends in Cell Biology 2004, 14 (4), 167-174.

Ruiz-Taylor, L. A.; Martin, T. L.; Zaugg, F. G.; Witte, K.; Indermuhle, P.; Nock, S.; Wagner, P., Monolayers of derivatized poly(L-lysine)-grafted poly(ethylene glycol)

on metal oxides as a class of biomolecular interfaces. Proceedings of the National Academy of Sciences of the United States of America 2001, 98 (3), 852-857.

S, E. L. A.; Mager, I.; Breakefield, X. O.; Wood, M. J., Extracellular vesicles: biology and emerging therapeutic opportunities. Nature reviews. Drug discovery 2013, 12 (5), 347-57.

Safra, T.; Muggia, F.; Jeffers, S.; Tsao-Wei, D. D.; Groshen, S.; Lyass, O.; Henderson, R.; Berry, G.; Gabizon, A., Pegylated liposomal doxorubicin (doxil): Reduced clinical cardiotoxicity in patients reaching or exceeding cumulative doses of 500 mg/m(2). Annals of Oncology 2000, 11 (8), 1029-1033.

Sahay, G.; Alakhova, D. Y.; Kabanov, A. V., Endocytosis of nanomedicines. Journal of Controlled Release 2010, 145 (3), 182-195.

Sakhtianchi, R.; Minchin, R. F.; Lee, K. B.; Alkilany, A. M.; Serpooshan, V.; Mahmoudi, M., Exocytosis of nanoparticles from cells: Role in cellular retention and toxicity. Advances in Colloid and Interface Science 2013, 201, 18-29.

Scheve, C. S.; Gonzales, P. A.; Momin, N.; Stachowiak, J. C., Steric Pressure between Membrane-Bound Proteins Opposes Lipid Phase Separation. Journal of the American Chemical Society 2013, 135 (4), 1185-1188.

Schlossman, D. M.; Schmid, S. L.; Braell, W. A.; Rothman, J. E., AN ENZYME THAT REMOVES CLATHRIN COATS - PURIFICATION OF AN UNCOATING ATPASE. Journal of Cell Biology 1984, 99 (2), 723-733.

Scita, G.; Di Fiore, P. P., The endocytic matrix. Nature 2010, 463 (7280), 464-473.

Segretain, D.; Falk, M. A., Regulation of connexin biosynthesis, assembly, gap junction formation, and removal. Biochim. Biophys. Acta-Biomembr. 2004, 1662 (1-2), 3-21.

Sezgin, E.; Kaiser, H.-J.; Baumgart, T.; Schwille, P.; Simons, K.; Levental, I., Elucidating membrane structure and protein behavior using giant plasma membrane vesicles. Nature Protocols 2012, 7 (6), 1042-1051.

Simons, M.; Raposo, G., Exosomes--vesicular carriers for intercellular communication. Current opinion in cell biology 2009, 21 (4), 575-81.

Soares, A. R.; Martins-Marques, T.; Ribeiro-Rodrigues, T.; Ferreira, J. V.; Catarino, S.; Pinho, M. J.; Zuzarte, M.; Anjo, S. I.; Manadas, B.; Sluijter, J. P. G.; Pereira, P.; Girao, H., Gap junctional protein Cx43 is involved in the communication between extracellular vesicles and mammalian cells. Scientific Reports 2015, 5, 13.

Sorkin, A.; von Zastrow, M., Endocytosis and signalling: intertwining molecular networks. Nature Reviews Molecular Cell Biology 2009, 10 (9), 609-622.

Sousa, R.; Liao, H. S.; Cuellar, J.; Jin, S. P.; Valpuesta, J. M.; Jin, A. J.; Lafer, E. M., Clathrin-coat disassembly illuminates the mechanisms of Hsp70 force generation. Nature Structural & Molecular Biology 2016, 23 (9), 821-829.

Stachowiak, J. C.; Schmid, E. M.; Ryan, C. J.; Ann, H. S.; Sasaki, D. Y.; Sherman, M. B.; Geissler, P. L.; Fletcher, D. A.; Hayden, C. C., Membrane bending by protein-protein crowding. Nature Cell Biology 2012, 14 (9), 944-+.

Stamou, D.; Duschl, C.; Delamarche, E.; Vogel, H., Self-assembled microarrays of attoliter molecular vessels. Angewandte Chemie-International Edition 2003, 42 (45), 5580-5583.

Stimpson, H. E. M.; Toret, C. P.; Cheng, A. T.; Pauly, B. S.; Drubin, D. G., Early-Arriving Syp1p and Ede1p Function in Endocytic Site Placement and Formation in Budding Yeast. Molecular Biology of the Cell 2009, 20 (22), 4640-4651.

Sundborger, A.; Soderblom, C.; Vorontsova, O.; Evergren, E.; Hinshaw, J. E.; Shupliakov, O., An endophilin-dynamin complex promotes budding of clathrin-coated

vesicles during synaptic vesicle recycling. Journal of Cell Science 2011, 124 (1), 133-143.

Thevenin, D.; An, M.; Engelman, D. M., pHLIP-Mediated Translocation of Membrane-Impermeable Molecules into Cells. Chemistry & Biology 2009, 16 (7), 754-762.

Thimm, J.; Mechler, A.; Lin, H.; Rhee, S.; Lal, R., Calcium-dependent open/closed conformations and interfacial energy maps of reconstituted hemichannels. Journal of Biological Chemistry 2005, 280 (11), 10646-10654.

Tian, Y. H.; Li, S. P.; Song, J.; Ji, T. J.; Zhu, M. T.; Anderson, G. J.; Wei, J. Y.; Nie, G. J., A doxorubicin delivery platform using engineered natural membrane vesicle exosomes for targeted tumor therapy. Biomaterials 2014, 35 (7), 2383-2390.

Torchilin, V. P., Recent advances with liposomes as pharmaceutical carriers. Nature Reviews Drug Discovery 2005, 4 (2), 145-160.

Ungewickell, E.; Ungewickell, H.; Holstein, S. E. H.; Lindner, R.; Prasad, K.; Barouch, W.; Martin, B.; Greene, L. E.; Eisenberg, E., ROLE OF AUXILIN IN UNCOATING CLATHRIN-COATED VESICLES. Nature 1995, 378 (6557), 632-635.

Vanneste, S.; Friml, J., Auxin: A Trigger for Change in Plant Development. Cell 2009, 136 (6), 1005-1016.

Wadia, J. S.; Stan, R. V.; Dowdy, S. F., Transducible TAT-HA fusogenic peptide enhances escape of TAT-fusion proteins after lipid raft macropinocytosis. Nature Medicine 2004, 10 (3), 310-315.

Wakeham, D. E.; Ybe, J. A.; Brodsky, F. M.; Hwang, P. K., Molecular structures of proteins involved in vesicle coat formation. Traffic 2000, 1 (5), 393-398.

Wang, S. G.; Wu, Y. L.; Guo, R.; Huang, Y. P.; Wen, S. H.; Shen, M. W.; Wang, J. H.; Shi, X. Y., Laponite Nanodisks as an Efficient Platform for Doxorubicin Delivery to Cancer Cells. Langmuir 2013, 29 (16), 5030-5036.

Weber, P. A.; Chang, H. C.; Spaeth, K. E.; Nitsche, J. M.; Nicholson, B. J., The permeability of gap junction channels to probes of different size is dependent on connexin composition and permeant-pore affinities. Biophysical Journal 2004, 87 (2), 958-973.

Wigge, P.; Kohler, K.; Vallis, Y.; Doyle, C. A.; Owen, D.; Hunt, S. P.; McMahon, H. T., Amphiphysin heterodimers: Potential role in clathrin-mediated endocytosis. Molecular Biology of the Cell 1997, 8 (10), 2003-2015.

Yamasaki, H.; Krutovskikh, V.; Mesnil, M.; Tanaka, T.; Zaidan-Dagli, M. L.; Omori, Y., Role of connexin (gap junction) genes in cell growth control and carcinogenesis. Comptes Rendus De L Academie Des Sciences Serie Iii-Sciences De La Vie-Life Sciences 1999, 322 (2-3), 151-159.

Yanes, R. E.; Tarn, D.; Hwang, A. A.; Ferris, D. P.; Sherman, S. P.; Thomas, C. R.; Lu, J.; Pyle, A. D.; Zink, J. I.; Tamanoi, F., Involvement of lysosomal exocytosis in the excretion of mesoporous silica nanoparticles and enhancement of the drug delivery effect by exocytosis inhibition. Small 2013, 9 (5), 697-704.

Zhang, W.; Yu, Z. L.; Wu, M.; Ren, J. G.; Xia, H. F.; Sa, G. L.; Zhu, J. Y.; Pang, D. W.; Zhao, Y. F.; Chen, G., Magnetic and Folate Functionalization Enables Rapid Isolation and Enhanced Tumor-Targeting of Cell-Derived Microvesicles. Acs Nano 2017, 11 (1), 277-290.

Zhao, C.; Busch, D. J.; Vershel, C. P.; Stachowiak, J. C., Multifunctional Transmembrane Protein Ligands for Cell-Specific Targeting of Plasma Membrane-Derived Vesicles. Small 2016, 12 (28), 3837-48.

Zhuo, Y.; Ilangovan, U.; Schirf, V.; Demeler, B.; Sousa, R.; Hinck, A. P.; Lafer, E. M., Dynamic Interactions between Clathrin and Locally Structured Elements in a Disordered Protein Mediate Clathrin Lattice Assembly. Journal of Molecular Biology 2010, 404 (2), 274-290.